2017

Influence of Conditioning Period on the Displacement Response of Nonlinear Single-Degree-of-Freedom Structural Systems

Jonathan P. Williams
Lehigh University

Influence of Conditioning Period on the Displacement Response of Nonlinear Single-Degree-of-Freedom Structural Systems

by

Jonathan P. Williams, P.E.

A Thesis

Presented to the Graduate and Research Committee

of Lehigh University

in Candidacy for the Degree of

Master of Science

in

Structural Engineering

Lehigh University

September 2017

This thesis is accepted and approved in partial fulfillment of the requirements for the Master of Science.

July 13, 2017

Date

Dr. Richard Sause
Thesis Advisor

Dr. Panayiotis Diplas
Chairperson of the Department

Acknowledgements

I am extremely grateful to my research advisor Dr. Richard Sause for his time and patience. His guidance and input have been essential to the completion of the present work.

I would also like to thank my friends and family for supporting me through this journey; with a special note of gratitude to John Paglione for his assistance in managing my business while I devoted time towards my research.

The present work is dedicated to Virginia Williams who taught me patience, curiosity, and that there is always more to be learned; and to Helen Wanke, without her help I would not have progressed this far in my academic pursuits.

CONTENTS

List of Figures

NOTATION

f_{el}	elastic strength
f_y	yield strength
k_i	initial stiffness of the system
m	mass of the system
M_{seis}	magnitude earthquake
$\bar{M}_{seis}$	mean magnitude earthquake
R_{seis}	site to source distance
$\bar{R}_{seis}$	mean site to source distance
R	strength reduction factor
S_a	spectral pseudo-acceleration
S_d	spectral displacement
$\tilde{S}_d$	median spectral displacement
T_{cms}	conditioning period
T_n	natural period of the structure
T_o	peak conditioning period
u_o	peak displacement
u_y	yield displacement
V_{s30}	shear wave velocity in top 30 m
Y	intensity measure of interest
α	post yielding stiffness ratio
β	energy dissipation ratio
ζ	damping ratio
λ_o	peak conditioning period ratio
ε	epsilon
$\bar{\varepsilon}$	mean epsilon
ε_{seis}	random error for ground motions
μ	ductility demand
$\tilde{\mu}$	median ductility demand
μ_o	maximum ductility demand
$\tilde{\mu}_o$	peak median ductility demand

ABSTRACT

This research explores the use of the Conditional Mean Spectrum for selecting and conditioning ground motion records for the seismic analysis of nonlinear systems with an emphasis on self-centering systems. Self-centering systems are an innovative type of seismic lateral force-resisting system which can reduce the post-earthquake damage sustained by building structures. Self-centering systems may experience greater lateral displacements than conventional systems, resulting in more significant period elongation. The period elongation may cause self-centering systems to be more sensitive to ground motions selected and conditioned on periods other than the initial natural period. Specifically, this study focuses on the influence of conditioning period with respect to the displacement-ductility demands on self-centering and conventional systems. During the study, nonlinear response spectra for 25 different single-degree-of-freedom models were evaluated over a range of 60 natural periods. Conditional Mean Spectra were constructed for ten logarithmically spaced conditioning periods. Twenty ground motions were selected and amplitude scaled to match each of these ten Conditional Mean Spectra.

The results show that conditioning periods greater than the initial natural period of the structure produced the largest ductility demands. A conditioning period ratio was defined as the ratio of the conditioning period which produces the largest ductility demand to the initial natural period. The results show that the conditioning period ratio is strongly dependent on the strength reduction factor and energy dissipation, and approximately independent of the initial natural period. The effects of variation of the post-yielding stiffness are not considered. For a given strength reduction factor and energy dissipation, the conditioning period ratio appears to be constant. Conventional bilinear elasto-plastic systems exhibited a period ratio close to unity for strength

reduction factors greater than 2. Although the results suggest a relationship between the conditioning period and the nonlinear characteristics of self-centering and conventional systems, further study is required due to the limited number of conditioning periods considered in the present study.

INTRODUCTION

The seismic hazard for the site of a structure is frequently quantified based upon a pseudo-acceleration response spectrum (spectral acceleration) with a certain probability of exceedance. In current design provisions, the spectral acceleration used for design is based on a Uniform Seismic Hazard Spectrum (UHS). The UHS identifies the pseudo-acceleration at each period with a given probability of exceedance in a specified period of time. The UHS thus provides the spectral acceleration with uniform probability over the range of periods; however it does not represent the response to individual ground motion records.

Response history analyses and site specific ground motion procedures are important tools for analysis of innovative earthquake-resistant structural systems. Selecting and conditioning ground motions (i.e., scaling) to represent a given level of seismic hazard for a given site and structure can lead to more accurately predicting the response for the stated level of seismic hazard. Correctly selecting and conditioning records is critical to the accurate analysis of innovative systems.

As noted, the UHS provides the pseudo-acceleration response with a constant probability of exceedance for all periods. The pseudo-acceleration response to an individual earthquake record is not consistent with the UHS at every period. Typically the pseudo-acceleration response spectrum for an individual ground motion has peaks only at certain periods. Therefore a UHS may be an overly conservative target spectrum for selecting and conditioning ground motions for a given site and structure. Baker [1] begins to address this concern by proposing the Conditional Mean Spectrum (CMS) as an alternative to the UHS for ground motion selection and conditioning. The CMS has a similar value as the UHS at a specified period of interest, denoted as the "conditioning period", while trending below the UHS and toward the median spectrum away from this period [1]. Crucial to properly using the CMS as the basis for selecting ground motions is the selection of an appropriate conditioning period. The current study aims to assess the effect of different conditioning periods on the nonlinear response of single-degree-of-freedom (SDOF) structures. In particular, the study focuses on "self-centering" SDOF structures.

Self-centering structures are a special class of earthquake-resistant systems that aim to reduce post-earthquake structural damage in the form of residual drift [2]. A self-centering system typically dissipates less energy than a bilinear elasto-plastic system, however, a self-centering system with comparable initial period can be identified that has equal or better performance than bilinear elasto-plastic system by varying the self-centering system parameters [3] [4]. Past research [5] found when selecting ground motions that are consistent with a target CMS, in some cases the ground motions based on a CMS with a conditioning period larger than the initial natural period of the structure produced greater displacement demands. While others have investigated the effect of the conditioning period, they have focused on ways to broaden the CMS, or the effect the

conditioning period has on structural reliability [6] [7]. The primary focus of the current study is to examine the effect of the conditioning period for selecting ground motion records as it relates to the displacement ductility demands for self-centering systems.

BACKGROUND

SEISMIC HAZARD ANALYSIS

The seismic hazard can be quantified using seismic intensity measures such as the peak ground acceleration, peak ground velocity, and pseudo-acceleration. The United States Geological Survey (USGS) defines the seismic hazard as the level of ground shaking or motion for a given probability of exceedance in a given time period, and further identifies this time period to be 50 years [8]. Seismic hazard analysis (SHA) determines the intensity of earthquake induced ground motion at a particular site. This analysis aggregates the effects of seismic events of various magnitudes from earthquake sources at different distances from a site, while taking different earthquake sources into account [5]. The seismic hazard maps developed by the USGS are based on detailed probabilistic seismic hazard analyses for the entire United States [9]. Maps have been developed for the peak ground acceleration and for the pseudo-acceleration (or spectral acceleration) corresponding to natural periods of 0.2 seconds and 1.0 seconds [8].

GROUND MOTION PREDICTION EQUATIONS

Understanding ground motions is fundamental to gaining insight into the response of a structure to an earthquake [9]. Crucial to this understanding is the ability to estimate a response quantity based on the geological and seismological characteristics of a site. A Ground Motion Prediction Equation (GMPE) is an empirically derived function

that provides a probabilistic estimate of a seismic intensity measure at a particular site with given seismic characteristics. Common input parameters may include magnitude, distance, and fault mechanism. GMPEs are usually logarithmic, and are expressed as follows:

$$\ln Y = C_1 + C_2\, M_{seis} - C_3 \ln R_{seis} - C_4 R_{seis} + \varepsilon_{seis} \qquad \textbf{EQUATION 1}$$

Here, Y is the intensity measure; while M_{seis}, R_{seis}, and ε_{seis} are the magnitude, distance, and random error in the intensity respectively. In Equation 1, C_1, C_2 , C_3, and C_4 denote the model parameters. GMPEs are developed based on historical data for a specific region [9], and are required in order to conduct a Probabilistic Seismic Hazard Analysis (PSHA). For the western North American region, the USGS has used four GMPEs, which are named according to the researchers which developed them; Abrahamson & Silva, Boore et al, Sadigh et al, and Campbell & Bozorgnia [9] [8].

Each principal input parameter required by a GMPE describes a characteristic of the site specific seismic hazard. Earthquake magnitude is used to characterize the severity of an earthquake at the source (e.g. at a location on a known fault). The "moment magnitude" is related to the energy released by an earthquake and is often used as a GMPE input parameter. The distance from the site to the source is an important GMPE input parameter, which characterizes the reduction of ground motion intensity as seismic waves radiate away from the earthquake source. Faults may be considered as either point sources or finite sources. Large earthquakes are better characterized using finite sources because they have greater rupture areas that are not well represented by point sources. Two common distance measures for finite sources are the Joyner-Boore distance and the closest distance to the fault rupture plane. The Joyner Boore distance is the closest

horizontal distance to the fault rupture plane and is easy to estimate for future earthquakes [9]. The closest distance to the rupture plane is not as easy to estimate, but may be inferred from properties of the fault mechanism [9]. It has been noted by past research that inelastic displacement demands are not sensitive to the distance parameter in GMPEs [10]. Site soil conditions are critical in evaluating the seismic hazard since soft soils tend to amplify the ground shaking. Current design standards permit site soil conditions to be considered through the use of GMPEs that are representative of local and regional geology [11]. Local soil conditions can be characterized by various parameters, however, the shear-wave velocity and soil depth to bedrock are preferred because they are quantitative descriptions of subsurface conditions [9]. The site classes described in the International Building Code [12], and by the NEHRP (National Earthquake Hazard Reduction Program) Recommended Seismic Provisions for New Buildings and Other Structures [13] are based on the average shear wave velocity in the top 30 meters of soil, denoted as V_{s30} [9].

PROBABILISTIC SEISMIC HAZARD ANALYSIS

In earthquake engineering, response history analyses are usually used for three different assessments, namely: scenario-based, intensity-based, and risk-based assessments. Often the earthquake hazard is characterized by a ground motion intensity measure with an annual rate of exceedance, or a return period. Defining the hazard in this way is referred to as risk-based assessment [14]. Probabilistic seismic hazard analysis is a risk-based assessment and considered to be the most comprehensive of the methods [15].

UNIFORM HAZARD SPECTRA

Response spectra are used to describe the response of SDOF structures as a function of the natural period, T_n. Elastic pseudo-acceleration response spectra (spectral

acceleration) are usually prescribed by design standards and codes [16]. In critical cases, the spectral accelerations are determined by a site specific seismic hazard analysis [16]. The design spectra in current building codes are based on and similar to a UHS. A UHS identifies spectral values, often the spectral accelerations, which have a uniform probability of exceedance (POE) over a range of periods. For example the USGS UHS with 2% POE in 50 years is similar to the Maximum Considered Earthquake outlined in the American Society of Civil Engineers (ASCE) Minimum Design Loads For Buildings and Other Structures (ASCE 7-10) [1] [11]. For a given site, various magnitudes and distances contribute to the seismic hazard at the site. The UHS is an upper bound or envelope of the structural response for these various magnitudes and distances, and does not represent the response across the range of periods for any specific ground motion. Some consider the traditional UHS to be overly conservative as a target spectrum for selecting a set of ground motions to represent the seismic hazard for a given site and structure, arguing that the spectral accelerations at different T_n in the UHS are caused by different earthquake events [1]. In the present study, the UHS and median spectra were calculated for a sample site, an example of which can be seen in Figure 1. The study focused on selecting ground motions that are consistent with several different target CMS.

CONDITIONAL MEAN SPECTRUM

Prior research has investigated the Conditional Mean Spectrum (CMS) for use in selecting ground motion records. The CMS, as defined by Baker [1], provides a target spectral acceleration value (S_a) for each T_n conditional on the S_a value at a specified conditioning period, T_{cms}. Baker asserts the CMS is easier to compile than the UHS and only requires existing GMPEs, PSHA results, and two other equations [1]. When constructing the CMS based on PSHA results, mean values of M_{seis}, R_{seis}, and ε_{seis} from

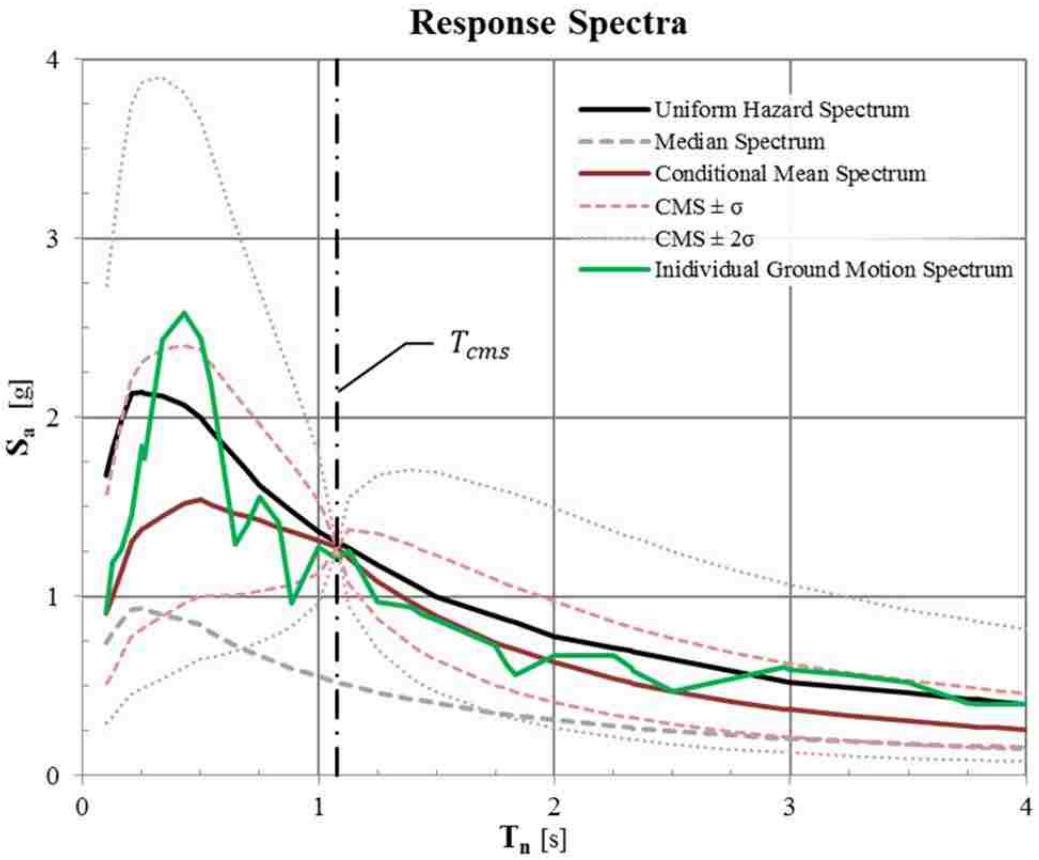

FIGURE 1 *– Comparison of different response spectra*

the disaggregation are used to obtain the target value of S_a at T_n. The principal advantage of the CMS is the consistency between the PSHA and the ground motion selection [1]. As shown in Figure 1 and mentioned earlier, the CMS has an S_a value that is similar to the UHS at T_{cms}, and trends below the UHS and toward the median spectrum at T_n away from T_{cms}. This shape of the CMS represents the average shape of response spectra associated with earthquake input (magnitude and distance) that produces the target value of S_a at the specified T_{cms}, and ground motions consistent with the CMS are representative of the site specific seismic hazard as defined at T_{cms} [1] [7]. The CMS incorporates the effect of the epsilon parameter, ε, which represents the number of standard deviations an S_a value deviates from the predicted median value [1].

There are a few limitations of the CMS as proposed by Baker in [1]. One limitation was that it did not include the variability of spectra for a given T_{cms} [17] [18]; however, more recent work has focused on selecting a set ground motions where the mean and variance of the set match a target spectrum [19], such as the CMS, and the corresponding conditional variance [17]. Also, Baker explicitly notes that the CMS should be constructed and evaluated for all periods of interest. In the case of nonlinear systems, multiple CMS should be calculated for a range of T_{cms} [1]. There is a tradeoff between the two approaches. The UHS is more conservative but also more convenient; the CMS is not as conservative but requires additional analyses when multiple CMS are used [1]. If the response of a nonlinear structure is primarily driven by an earthquake input at a period other than T_{cms} , the ground motions selected for a CMS may produce low and inappropriate responses [1]. Multiple CMS should be considered if a multi-degree-of-freedom structure is sensitive to the response at various modes or if the T_n value to be used as T_{cms} is uncertain. Although the CMS can provide a better representation of the hazard, it becomes cumbersome if $T_{cms}$is unknown, or is not easy to estimate [1].

T_{cms} should be selected to produce the largest response. For a linear elastic SDOF system, or near linear elastic SDOF system, T_{cms} should equal the period T_n of the system. Guidelines for selecting T_{cms} for nonlinear self-centering systems do not exist. Due to the highly nonlinear behavior of self-centering systems, these structures go through greater period elongation than conventional bilinear elasto-plastic systems, and their response may be especially sensitive to T_{cms} [20]. Other research has explored the problem of constructing multiple CMS and the effects of T_{cms} on nonlinear seismic response of structures; however, these studies have been limited and do not directly

investigate the effect of T_{cms} and the selection of ground motions consistent with the corresponding CMS on the response of self-centering systems [6].

GROUND MOTION SELECTION & CONDITIONING METHOD

Ground motions can be characterized by various parameters depending on the application. One common application is nonlinear response history analyses. The significant variations between different ground motion records are due to many factors including magnitude, distance, and fault mechanism [9], as well as inherent randomness. Ground motions are often selected based on the response spectrum value at the fundamental natural period of a structure, as it is the period corresponding to the largest response for a linear elastic system, and is expected to be the period of largest response for a nonlinear system [5].

Individual ground motions are often selected so that their pseudo-acceleration response spectrum matches a target response spectrum at a specified T_n or over a specified range of periods. In practice ASCE 7-10 requires the average response spectrum for a set of ground motions selected for response history analyses to be not less than the design spectrum for periods ranging from 0.2 T_n to 1.5 T_n. To select ground motions with spectra that match the CMS, a period range should be identified [1]. The procedures by which appropriate ground motions are identified and conditioned, or scaled, should take into account the potential for nonlinear structural response [11].

The provisions of ASCE 7-10 for ground motion selection require a period range of 0.2T_n to 1.5 T_n to be considered, however, for highly nonlinear structures the response may be sensitive to ground motion components at periods greater than 1.5 T_n [11]. Therefore, ASCE requires ground motions used in response history analyses be selected from events having magnitude, distances, and sources appropriate for the site [11] [21].

Where a set of seven or more ground motions are used in analysis, the mean nonlinear response can be taken as the structural response, otherwise the maximum nonlinear response should be used [11].

The Sum of the Squared Errors (SSE) is an effective method for determining how well the spectrum for a ground motion matches a target spectrum [1]. The SSE can be calculated for each individual ground motion under consideration and the records with the smallest SSE are those that best match the target spectrum, in this case, the CMS [1].

Buildings designed based on amplitude-scaled ground motions have been shown to be comparable to those based on other conditioning methods such as, spectral matching [22]. A common and straightforward method of ground motion conditioning is to scale each record so the response spectrum matches the target spectrum at the conditioning period [1] [14].

ASCE 7-10 requires a ground motion record to be scaled so the corresponding response spectrum approximately matches the target spectrum over the period range [11]. Another scaling method which is consistent with the requirements of ASCE 7-10 is to scale the ground motion so the average response spectrum over the period range matches the average of the target spectrum over the same period range [11]. Scaling the ground motion so the response spectrum matches the CMS at the conditioning period does not significantly impact the consistency of the ground motion with the CMS, so Baker recommends this method since it is the simpler method [1].

BACKGROUND ON SELF-CENTERING SYSTEMS

Self-centering (SC) systems are a new type of lateral force-resisting system which has virtually no residual drift following a seismic event [2]. The appeal of these

systems is the potentially low level of post-earthquake structural damage allowing for immediate use of the structure following an earthquake. By definition, the lateral displacement response of a self-centering system oscillates around zero displacement, unlike the baseline offset of the displacement response that may occur for conventional bilinear elasto-plastic (BEP) systems. The development of SC systems poses new challenges to engineers. Response history analyses have shown that the softening and associated period elongation of SC systems limits the acceleration response; however, SC systems may have greater lateral displacement response amplitude compared to conventional systems [5] [20]. The displacement response of conventional systems can include permanent residual drift requiring expensive repairs [5] [20]. While the SC systems may have greater displacement and ductility response, they are expected to have relatively little residual drift or post-earthquake damage [20].

The lateral displacement demand for SC systems is often greater than for similar BEP systems [4] [20]. Self-centering systems with low levels of hysteretic energy dissipation typically exhibit large lateral displacement responses. The energy dissipation ratio, β, corresponds to the ratio of the area enclosed by the hysteresis loop of an SC system relative that of a BEP system with the same initial properties subjected to the same peak displacement [20]. The post-yielding stiffness ratio, α, is the ratio of the system lateral stiffness beyond the point of yield to the initial stiffness, as illustrated in Figure 2. Increasing β from 0 to 12.5% or more can reduce the displacement demands; however the equal displacement principle should not be applied to SC systems with small values of α and β. To prevent excessive displacements demands a β value of 12.5% is considered to be the minimum [5].

In general, the displacement ductility demand is strongly dependent on the period of the structure for short periods but is approximately period independent at long periods [20]. Ductility demand is the ratio of the maximum displacement of the system, u_o, to the yield displacement of the system, u_y, which are shown in Figure *2*. The ductility demand for SC systems is controlled by the parameters α, β, and strength reduction factor, R. The ductility demands for self-centering systems have been shown to increase with increasing R values [20]. For a given R value, ductility demands similar to those of conventional systems can be achieved by varying the parameters α and β. Generally increasing α or β can reduce the ductility demand, however, increasing α is more effective for SC systems with large R values (low strength) than it is for SC systems with small R values (high strength) [5].

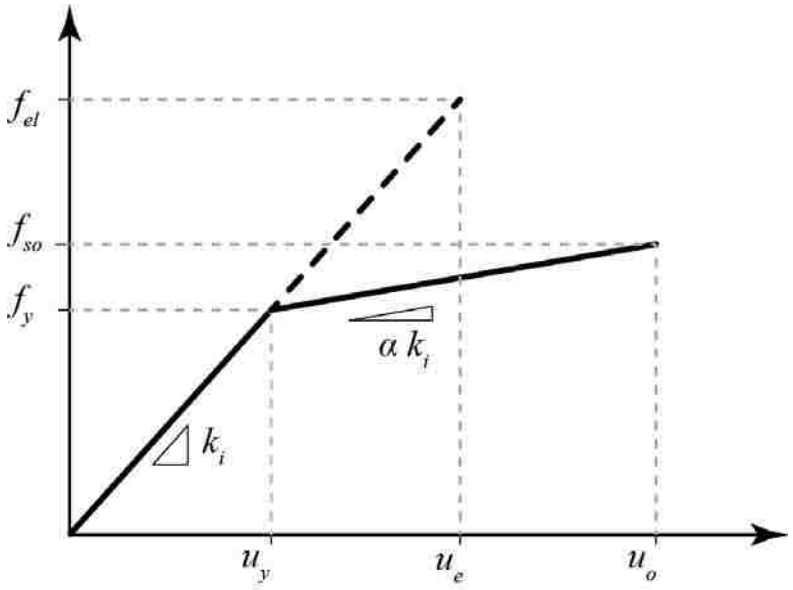

FIGURE 2 – *Force versus displacement diagram showing yield strength formulation based on elastic strength*

INDIVIDUAL RESPONSE SPECTRA

A response spectrum describes the peak response of an SDOF system, over a range of periods, subjected to a given ground motion [23] [9]. The response quantities

may be based on the elastic response, or the nonlinear (inelastic) response of SDOF models [9]. While elastic response spectra only require the natural period, T_n, and damping ratio, ζ; nonlinear response spectra require a complete definition of the force-deformation relationship [9]. The yield strength of the system, f_y, is an important property in this relationship [20] (See Figure 2). The strength reduction factor, R, is defined as the ratio of the force associated with peak displacement of a structure if the structure were to remain elastic, f_{el}, relative to f_y as shown in Figure 2 [16]. In seismic design practice the yield strength of a structure, f_y, is often determined by reducing the elastic strength by a specified R value as follows [20] [2]:

$$f_y = \frac{f_{el}}{R}$$

EQUATION 2

Low R (e.g., not greater than 2.0) values correspond to systems with high lateral strength, which exhibit similar behavior to linear elastic systems [20]. Many previous research studies of nonlinear response spectra determined the elastic strength and the corresponding yield strength for SDOF systems based on individual ground motion spectra. Seo and Sause [20] determined the yield strength from a smooth spectrum like those commonly used in seismic design provisions.

Current design standards expect structures to exhibit inelastic response during the design earthquake [20]. As conventional systems yield and move into the inelastic range, the system sustains structural damage and often permanent residual lateral displacements [20]. As noted previously SC systems are expected to have little permanent residual displacement.

In buildings, a significant amount of both structural and nonstructural damage from severe earthquakes is the result of lateral displacements [24]. Consequently displacement demand is a response quantity associated with damage, and is often used to evaluate structural performance [16]. For a given R value the ductility ratio, μ, is a convenient, normalized response parameter for nonlinear systems. μ is the ratio of the maximum nonlinear displacement to the yield displacement [2]. A ratio of 1.0 or less indicates the response has remained linear elastic [9]. The ductility ratio is expressed as follows:

$$\mu = \frac{u_o}{u_y} \qquad \textbf{EQUATION 3}$$

where u_o and u_y are the peak displacement and yield displacement of the system, respectively [2]. Prior studies have shown the effect of α on μ is dependent upon T_n. Seo and Sause [20] found for periods less than 0.5 sec, a small increase in α can significantly reduce μ, while at periods longer than 0.5 sec the impact of α on μ is nearly independent of period [20]. Furthermore, it was found that increasing β reduces μ, and the effect is relatively uniform over the period range evaluated [20].

Analysis Methods

The seismological and geological properties of the site of a structure depend upon the physical location of a site, including the proximity to active faults. The seismic hazard depends on the site-to-source distance, fault type, site soil conditions, and other factors. As noted earlier, design standards often use approximate methods to characterize the seismic hazard, whereas the CMS is based on site-specific seismic hazard analysis procedures.

SITE SELECTION FOR STUDY

For the current study certain site characteristics are preferable. A site where similar events govern the hazard over the period range of interest helps to reduce the variability introduced by properties of the seismic event, which is beneficial since the focus of the study is on the effects of the conditioning period, T_{cms}, and not the seismic event. A site which has a strong peak in the CMS at each T_{cms} is desirable so trends in the results will be more readily observed. When reviewing potential sites for the study, it was observed that for sites where the hazard is governed by a single fault, the spectral acceleration often has less dispersion. Consequently, the UHS and the median spectrum (for a characteristic earthquake magnitude and distance) for the site are closer together over the period range of interest. For sites near multiple less active faults with one dominant fault, the CMS tends to have a stronger peak. Finally, a site with unique or uncommon characteristics is less desirable.

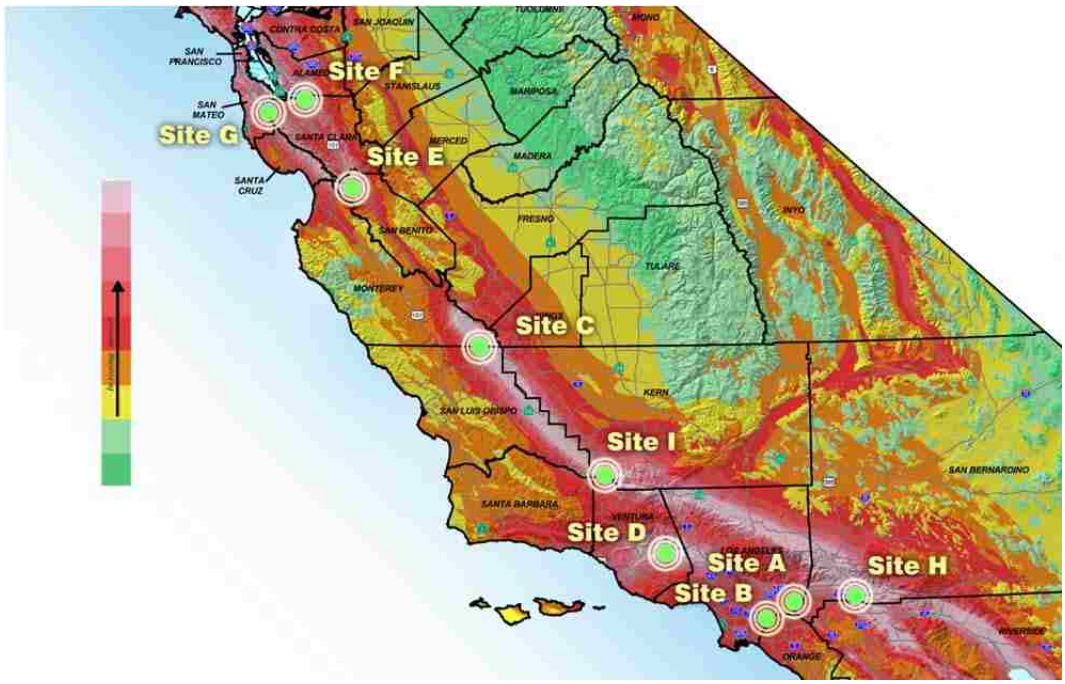

FIGURE 3 – *Earthquake Shaking Potential Map showing preliminary site locations*

Several preliminary sites were selected by reviewing shake maps and interactive fault maps published by the California Division of Mines & Geology (CDMG). The preliminary sites are shown on the shake map in Figure 3 which classifies regions by severity of the ground motion during an earthquake. These preliminary sites were selected because they have high potential for damaging ground motions and are in close proximity to active faults. An initial probabilistic seismic hazard analysis was conducted for each preliminary site using the USGS online tool [25]. Ultimately Site G, Emerald Hills, was identified as a site with the seismic hazard controlled by similar seismic events across the period range of interest, and was selected for the current study.

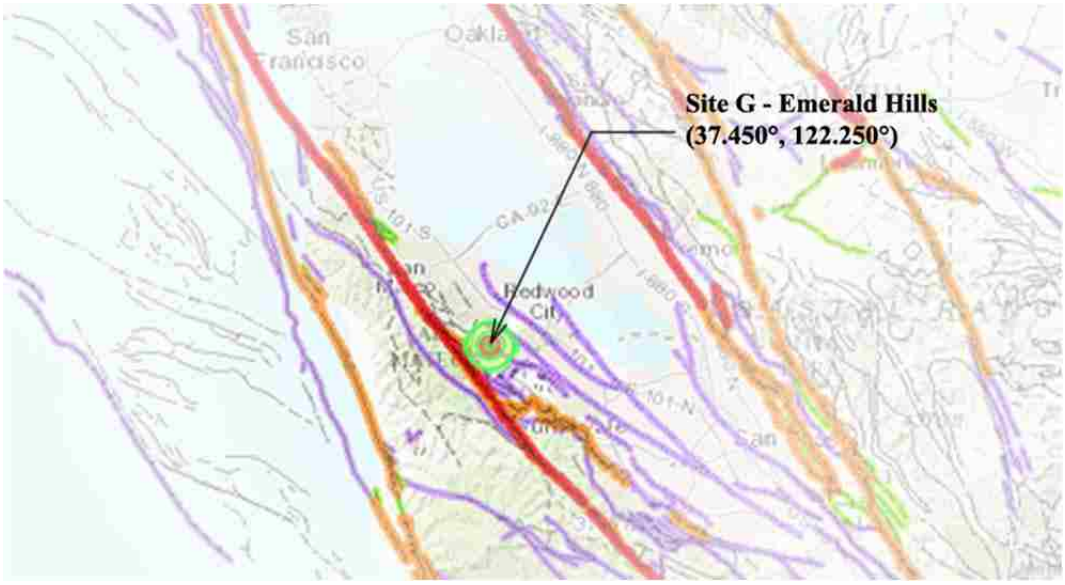

FIGURE 4 *–Fault map of sample site location used in the current study*

SITE SPECIFIC SEISMIC HAZARD

The initial probabilistic seismic hazard analysis was used to evaluate the contribution of each GMPE toward the total seismic hazard of the site, since only one GMPE is used to construct the CMS. The Campbell & Bozorgnia 2008 GMPE was selected for use in the remainder of the study based on its contribution to the overall

hazard, and its validity across the period range of interest. Additionally, this GMPE provides S_a values corresponding to an individual horizontal ground motion component, which is the seismic intensity measure used in the current study. Although updated versions of the Campbell & Bozorgnia model are available, the 2008 version was used for consistency with the work by Baker since the correlation function by Baker is based on data corresponding to the Campbell & Bozorgnia 2008 GMPE [1].

A probabilistic seismic hazard analysis was carried out using OpenSHA [26] analysis tools, specifically the Hazard Spectrum Calculator and Hazard Curve Calculator, for all available periods. OpenSHA can perform PSHA at only at only a few discrete periods. The discrete periods are shown in Table 1. For other conditioning periods, linear interpolation was used. The UHS was calculated for a 2% probability of exceedance in 50 years. The spectral acceleration from the UHS at each discrete period was then used to disaggregate the seismic hazard at each discrete period. The seismic hazard disaggregation at each discrete period is shown in Table 1 and Appendix I. At each discrete period, the following characteristic (i.e., mean) values for the site were obtained from the disaggregated hazard data: the mean earthquake magnitude, $\bar{M}_{seis}$, the mean site-to-source distance, $\bar{R}_{seis}$, and the mean epsilon, $\bar{\varepsilon}$, which is a measure of the difference between the spectral acceleration from the UHS (i.e., the hazard) at the period and the median spectral acceleration from the GMPE for the M_{seis} and R_{seis}. A larger $\bar{\varepsilon}$ will produce a CMS with a stronger peak.

CONSTRUCTING CONDITIONAL MEAN SPECTRUM FOR SITE

For each T_{cms}, a CMS was constructed following procedures outlined by Baker [1] using the $\bar{M}_{seis}$, $\bar{R}_{seis}$, and $\bar{\varepsilon}$, values obtained from the PSHA described above. As mentioned above, the PSHA was carried out at only the discrete periods listed in Table 1.

Ten conditioning periods, denoted T_{cms}, were selected with logarithmic spacing over the period range of interest, 0.5 seconds to 5.0 seconds, where T_{cms} = 0.500s, 0.646s, 0.834s, 1.077s, 1.391s, 1.797s, 2.321s, 2.997s, 3.871s, and 5.000s. The values of $\bar{M}_{seis}$, $\bar{R}_{seis}$, and $\bar{\varepsilon}$ at T_{cms} were obtained by interpolating the data in Table 1.

TABLE 1 *– OpenSHA disaggregation for discrete periods of the sample site*

T_n	S_a	$\bar{M}_{seis}$	$\bar{R}_{seis}$	$\bar{\varepsilon}$
0.01	0.900	7.5331	3.0266	1.3891
0.02	0.920	7.5331	3.0270	1.3900
0.03	1.000	7.5319	3.0397	1.4024
0.05	1.220	7.5250	3.1099	1.4113
0.08	1.463	7.4972	3.4076	1.4545
0.10	1.680	7.4735	3.6486	1.4877
0.15	1.940	7.4616	3.8243	1.5103
0.20	2.130	7.5092	3.4599	1.4547
0.25	2.140	7.5309	3.2442	1.4217
0.30	2.130	7.5383	3.1586	1.4086
0.40	2.100	7.5462	3.0262	1.3894
0.50	2.000	7.5889	3.0085	1.3870
0.75	1.620	7.6562	3.0363	1.3691
1.00	1.360	7.7039	3.0681	1.3452
1.50	1.000	7.7575	3.0989	1.3130
2.00	0.780	7.7844	3.1145	1.2860
3.00	0.520	7.8039	3.1245	1.2606
4.00	0.400	7.8124	3.1285	1.2534
5.00	0.350	7.8079	3.1400	1.2553
7.50	0.260	7.8416	3.1544	1.2077
10.00	0.210	7.8541	3.1694	1.1839

The Conditional Selection Algorithm provided by Baker [27] constructs the CMS, selects corresponding ground motion records, and determines the scale factor for each ground motion record using a MatLab [28] script. This MatLab script utilizes the correlation function from Baker [1], and outputs the median spectrum (for the given M_{seis}, R_{seis}), standard deviation spectrum (for the given M_{seis}, R_{seis}), the CMS (for the given M_{seis} R_{seis} and ε), and the conditional standard deviation spectrum (for the given M_{seis}, R_{seis}, and ε, and using Baker's correlation function). The Conditional Selection

Algorithm provided by Baker [27] was adapted to function with other MatLab scripts developed specifically for the current study.

GROUND MOTION SELECTION & CONDITIONING

The Conditional Selection Algorithm provided by Baker uses the Monte-Carlo method to simulate random earthquake spectra. A set of simulated spectra are generated and then ground motions are selected which best match these spectra. In addition to matching the ground motions to the CMS the algorithm also matches the conditional standard deviation. The greedy improvement method of optimization is then used to refine the results [17].

The Conditional Selection Algorithm amplitude scales the individual ground motions so that the spectral acceleration at T_{cms}, matches the CMS value at T_{cms}. The ground motion scale factor, denoted SF_{GM} is determined using Equation 4 where Sa_{GM} and Sa_{CMS} are the spectral accelerations of the individual ground motion and target CMS respectively as shown in Figure 5.

$$SF_{GM} = \frac{Sa_{CMS}(T_{CMS})}{Sa_{GM}(T_{CMS})} \qquad \text{EQUATION 4}$$

In the current study, SF_{GM} is limited to be no more than a factor of four, as follows:

$$0.25 \leq SF_{GM} \leq 4.0$$

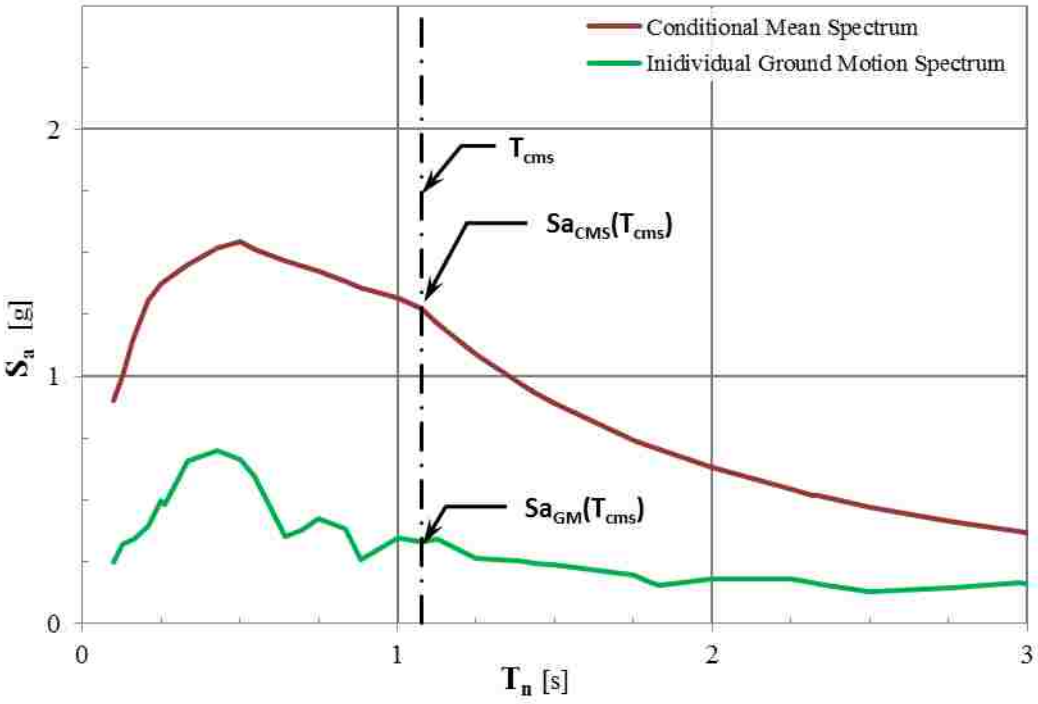

Figure 5 – *Scaling method for individual ground motions to match CMS at T_{cms}*

Using the Conditional Selection Algorithm, 10 sets of 20 ground motions were generated for each value of T_{cms} (given previously as 0.500s, 0.646s, 0.834s, 1.077s, 1.391s, 1.797s, 2.321s, 2.997s, 3.871s, and 5.000s), which are, as noted earlier, logarithmically spaced over the period range of interest of 0.5 seconds to 5.0 seconds.

Appendix II describes the ground motion sets in more detail. For each ground motion set, the appendix lists $\bar{M}_{seis}$, $\bar{R}_{seis}$, and $\bar{\varepsilon}$. For each ground motion in the set, the record sequence number (RSN), the magnitude, M_{seis}, the distance from the recording site to the source, R_{seis}, the horizontal ground motion component direction, "Component", and the ground motion scale factor (SF_{GM}) are listed. The RSN is a unique identifier for each ground motion record in the PEER NGA West 2 Database [29].

SDOF ANALYSIS

SDOF analyses were carried out for a variety of systems to evaluate the impact of the T_{cms} value used to construct a CMS and associated ground motion set, on the nonlinear structural response. Nonlinear dynamic analyses of the SDOF systems were conducted using the Newmark Beta Method with Newton Raphson Iteration. For simplicity, a unit mass was assumed for each SDOF system. The natural period of each SDOF system was calculated based on the initial stiffness. The natural periods range from 0.10 to 10.0 seconds and are linearly spaced. In addition, SDOF systems with natural periods equal to the values of T_{cms} were included in the study. The SDOF systems were assigned 5% initial stiffness proportional viscous damping to model the inherent damping of the system

Figure 6 shows that the SDOF systems had various hysteretic force-deformation models, including linear elastic ('LIN'), bilinear elastic ('BEL'), bilinear elasto-plastic ('BEP'), and self-centering ('SC') models. All systems, except linear elastic, were assigned a post-yielding stiffness ratio, α, of 5%. Self-centering systems were given an energy dissipation ratio, β, of 12.5% or 25%.

The yield strength of each SDOF system was determined systematically. As noted earlier, the strength reduction factor, R, can be defined as the ratio of the elastic strength, f_{el}, relative to the yield strength, f_y, of the inelastic system.

$$\mathrm{R} = \frac{f_{el}}{f_y} \qquad \textbf{EQUATION 5}$$

Alternatively f_y can be calculated from f_{el}, for a specified R value, as follows:

$$f_y = \frac{f_{el}}{R} \qquad \textbf{EQUATION 6}$$

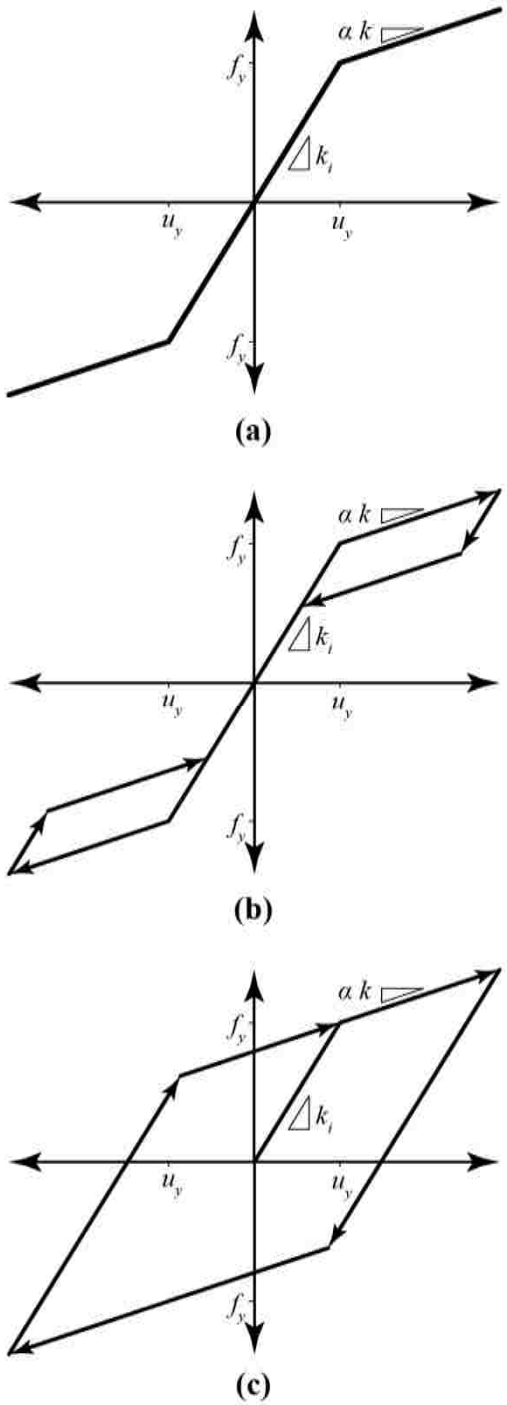

FIGURE 6 – *Force Deformation Models for (a) Bilinear Elastic System, (b) Self-Centering System, (c) Bilinear Elasto-Plastic System*

where f_{el} is the spring force that develops in a linear elastic system (with the same natural period and 5% damping ratio) at the point of peak displacement based on the

median spectral acceleration for the ground motion set. Thus, f_{el} can be expressed as follows:

$$f_{el} = Sa_{med} \cdot m \qquad \textbf{EQUATION 7}$$

Since the SDOF systems have a unit mass, Equation 7 simplifies to:

$$f_{el} = Sa_{med} \qquad \textbf{EQUATION 8}$$

and f_y can then be determined as:

$$f_y = \frac{Sa_{med}}{R} \qquad \textbf{EQUATION 9}$$

Systems with R values of 2, 4, 6, 8, and 10 were studied. Nonlinear response histories were determined for each ground motion, each SDOF system (T_n and force deformation model), and each R value using MatLab. The results were output in the format of nonlinear response spectra.

RESULTS

The analyses generated 5,000 nonlinear response spectra, which correspond to 25 nonlinear SDOF systems subjected to 10 ground motion sets of 20 records each. Details of the ground motion sets used in the present study may be found in Appendix II. Examining the displacement demand of different systems it is evident that, due to its higher energy dissipation capacity, the BEP system generally has the lowest displacement demand, as shown in Figure 7. A BEP system can be thought of as an SC system having a β value of 100%. For a true SC system, β must be less than 50%. Considering an SC system with decreasing levels of energy dissipation, the special case of an SC system with a β value of zero corresponds to a BEL system. This is an important concept; a BEL system being an SC system with β = 0%, and a BEP system being an SC system with β

=100%. The response of an SC system is expected to be bounded by the response of the corresponding BEP and BEL systems.

Figure 7 shows the median nonlinear displacement response, $\tilde{S}_d$, for various SDOF systems, for the ground motion set conditioned on T_{cms} = 2.321s. Figure 8 shows the nonlinear displacement response, S_d, for various SDOF systems for an individual ground motion of the set. The SDOF systems shown in these figures have R = 6. It can be observed that the response of the two SC systems, SC-12 and SC-25, are bounded by the response of the BEL and BEP systems over most of the period range. While the results for the individual ground motion exhibits some irregularities, the median spectra are generally consistent with this expected behavior.

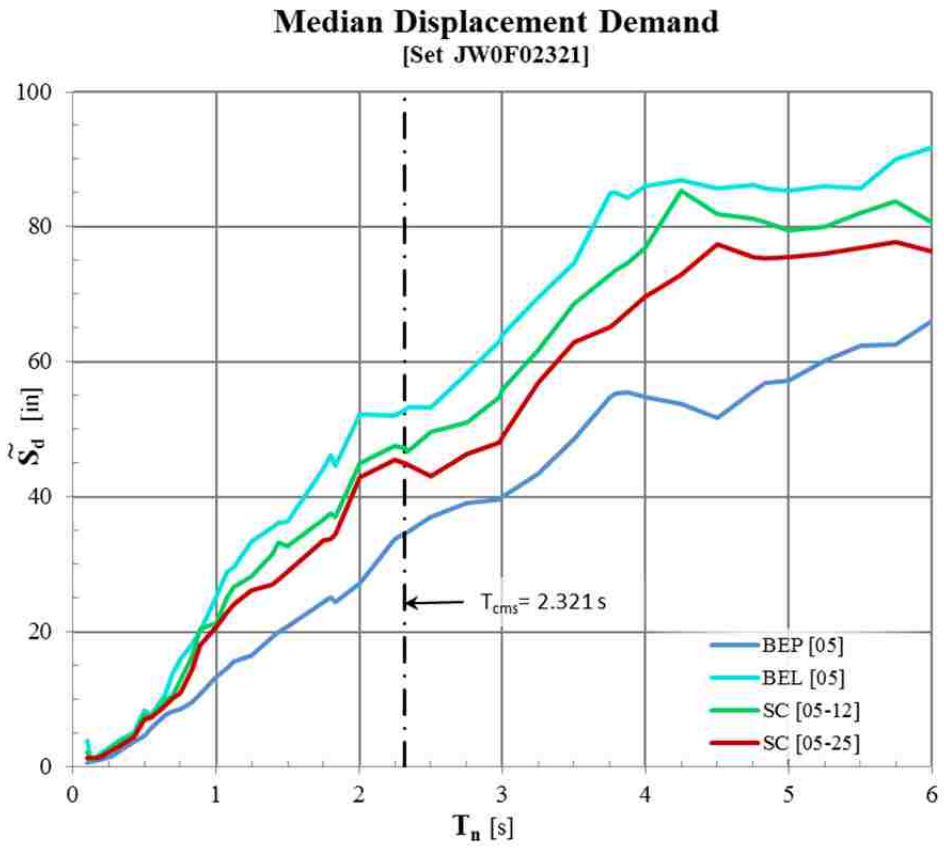

FIGURE 7 – *Median displacement demand comparison of inelastic systems for suite of ground motions*

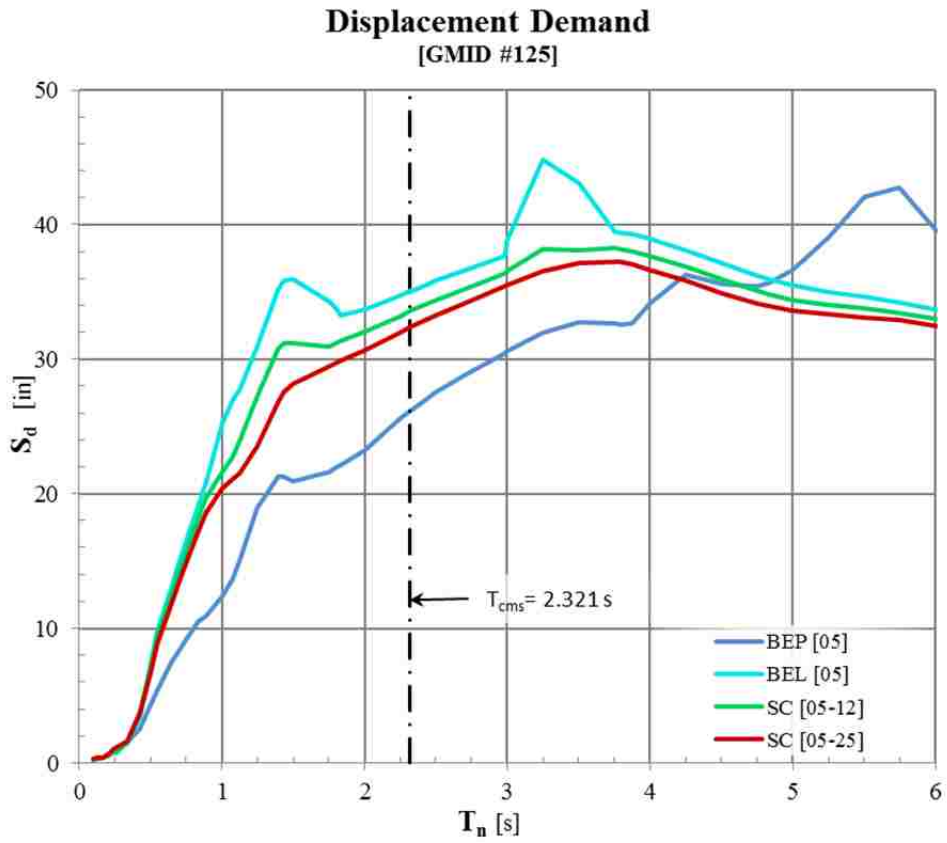

FIGURE 8 – *Displacement demand comparison of inelastic systems for individual ground motion*

An alternative to the nonlinear displacement, the ductility ratio μ, is an efficient normalized parameter for evaluating the performance of nonlinear systems. The analysis results shown in Figures 9, 10, and 11 revealed local maxima in μ at periods other than, T_{cms} confirming observations by others [5]. For systems with high lateral strength (e.g., R = 2) the peak μ occurs at, or near, T_{cms} for all systems. As the R value increases the local maxima can be observed at periods shorter than T_{cms}.

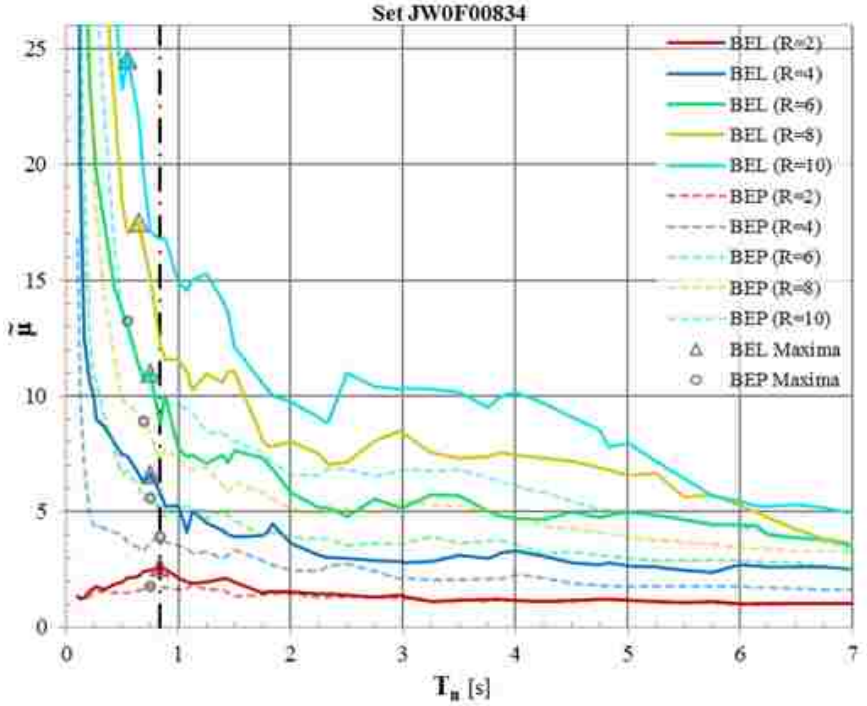

FIGURE 9 – *Median ductility ratio for Ground Motion Set JW0F00834 conditioned at Tcms = 0.834 s*

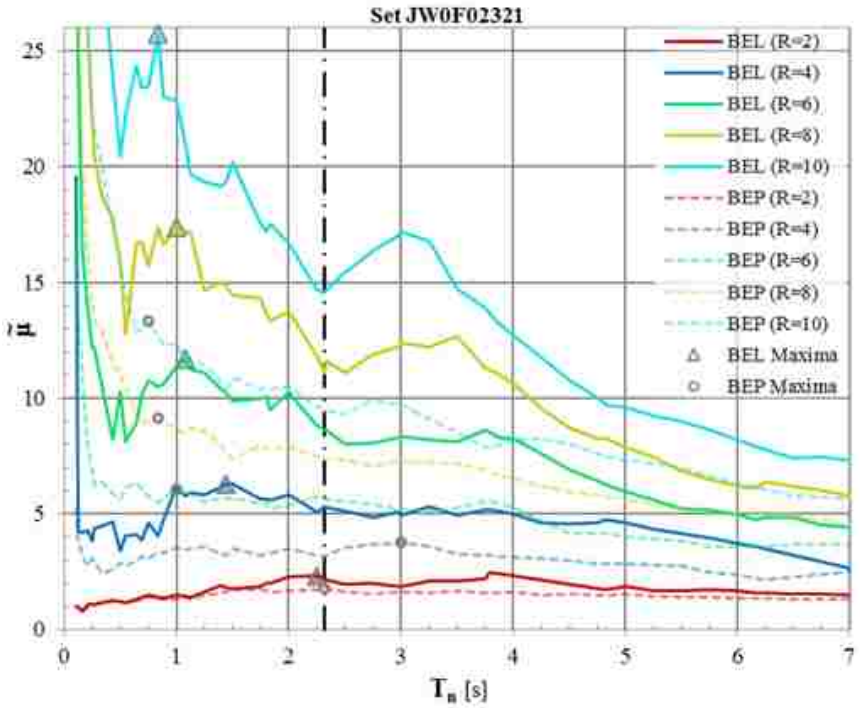

FIGURE 10 – *Median ductility ratio for Ground Motion Set JW0F02321 conditioned at Tcms = 2.321 s*

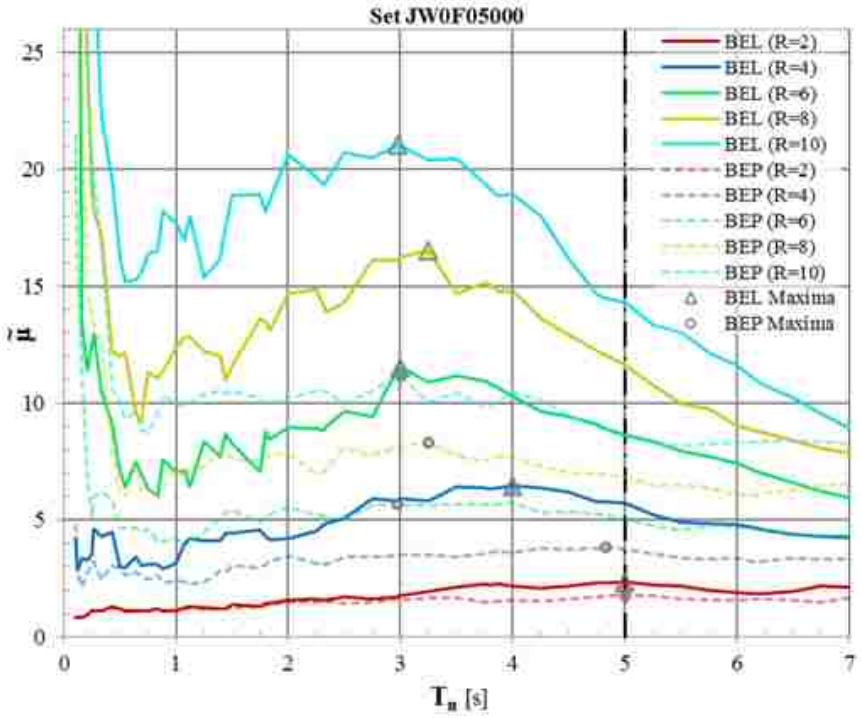

FIGURE 11 – *Median ductility ratio for Ground Motion Set JW0F05000 conditioned at Tcms = 5.000 s*

Comparisons of the BEL and BEP systems are shown in Figures 9, 10, and 11 for conditioning periods of 0.834 s, 2.321 s, and 5.000 s respectively[1]. The figures depict the median ductility ratio, $\tilde{\mu}$, for each set of ground motions over the range of R values considered. Systems with high lateral strength, low R values, have a local maximum occurring near T_{cms} for all models. The BEP systems generally exhibit a decreasing $\tilde{\mu}$ with increasing T_n, with any local maxima near T_{cms}. This trend was consistent for BEP systems for all R values. For BEL systems, $\tilde{\mu}$ is larger than for BEP systems due to reduced energy dissipation. This relative increase in $\tilde{\mu}$ is greater in the short and intermediate period range and less significant in the long period range. The BEL systems, shown in Figure 11**,** have local maxima occurring at periods less than the T_{cms}.

[1] A complete set of plots for all systems and ground motion sets can be found in Appendix III.

This trend is present in the SC systems as well, the results of which can be found in Appendix III.

Additionally, with increasing R values, the period at the local maximum in $\tilde{\mu}$ decreases. Upon closer inspection, the BEP systems have small deviations in similar locations to these local maxima, however, those exhibited by the SC and BEL systems are of greater significance. The magnitude of the maximums increases with increasing R value as well.

The maximum $\tilde{\mu}$ at T_n less than T_{cms} is of particular interest for ground motion selection, as it indicates uncertainty regarding the period that should be used for T_{cms}. Recall that linear SDOF systems will have responses similar to the CMS, with local maxima at T_{cms}. Nonlinear systems with small R values and low levels of nonlinear response can be expected to have their peak response for ground motions conditioned at T_n. With increasing nonlinearity, significant period elongation may cause a larger response to occur for ground motions conditioned at a period (T_{cms}) larger than T_n. Highly nonlinear structures, such as self-centering systems, will have greater response to input at longer periods. Noted earlier, multiple CMS should be constructed for the periods to which the structure is sensitive, and the results of the present study indicate for SC systems these periods are greater than T_n. The largest $\tilde{\mu}$ for the ground motion sets considered, or the absolute peak median ductility ratio at each period, $\tilde{\mu}_o$ can be expressed as:

$$\tilde{\mu}_o = max\left(\tilde{\mu}_{(T_n)}\right) \qquad \textbf{EQUATION 10}$$

Comparing $\tilde{\mu}$ for various systems subjected to different ground motion sets, it is evident that $\tilde{\mu}_o$ is usually caused by a ground motion set with T_{cms} that is greater than T_n. Comparisons of $\tilde{\mu}$ over the range of conditioning periods are shown in Figures 12 a, b,

and c for the BEP, SC-12, and BEL models respectively. The $\tilde{\mu}$ values shown are for models with R = 6.

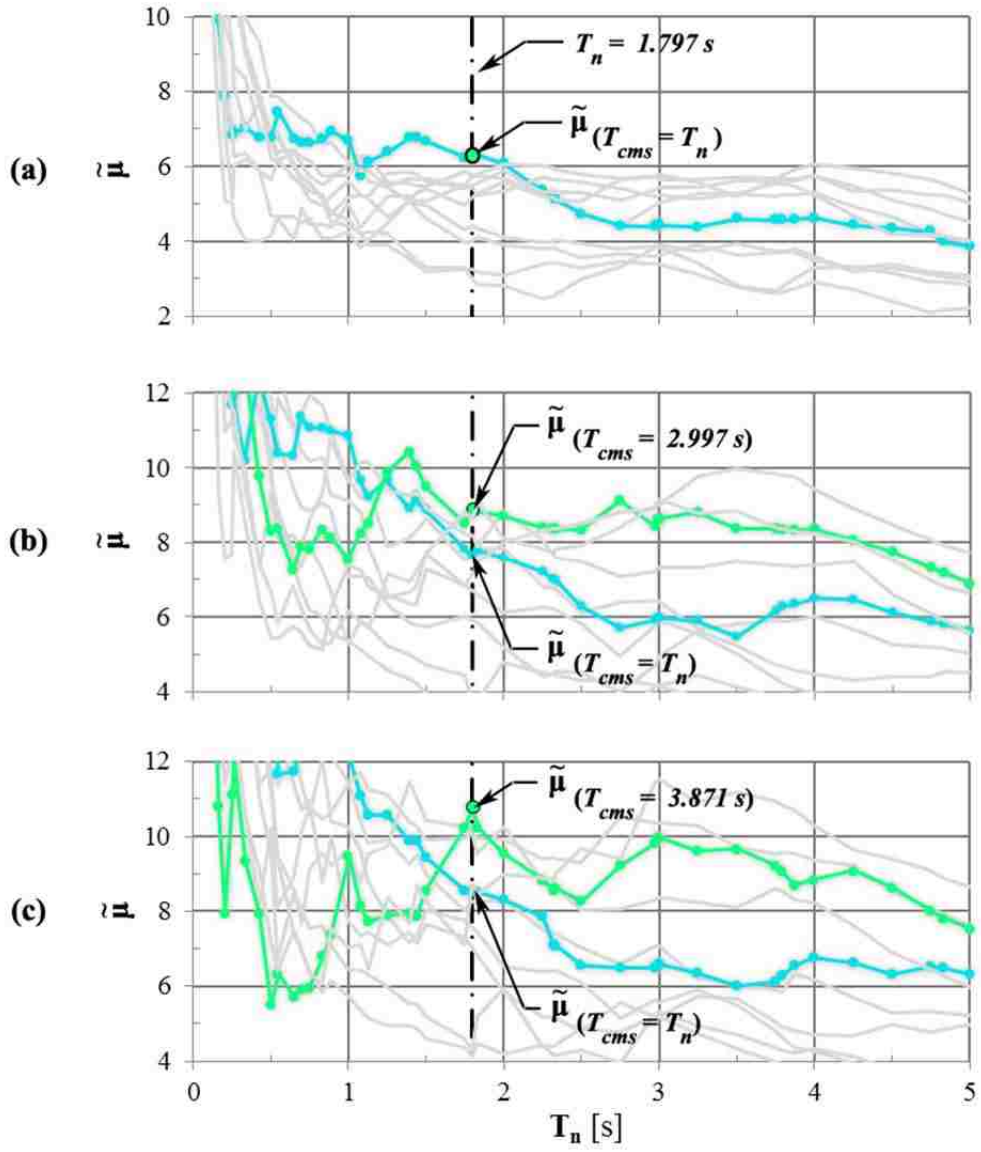

FIGURE 12 – *Peak displacement ductility comparison*
(a) BEP (α=5%) , (b) SC (α=5%, β=12.5%), (c) BEL (α=5%)

Consider an example system with T_n= 1.797s. For the BEP system, $\tilde{\mu}_o$ is caused by the ground motion set with T_{cms}= T_n= 1.797s. For the comparable SC-12 system, $\tilde{\mu}_o$ is caused by the ground motion set with T_{cms}= 2.997s, and not the set with T_{cms}= T_n. Similarly, for the BEL system, $\tilde{\mu}_o$ is caused by a ground motion set with T_{cms} greater than T_n. The $\tilde{\mu}_o$ for this system is caused by the set with T_{cms}= 3.871s. Considering these results further, it is useful to determine the value of T_{cms} which causes $\tilde{\mu}_o$, defined as T_o, as follows:

$$T_o = T_{cms}(\tilde{\mu}_o) \qquad \textbf{EQUATION 11}$$

The importance of nonlinear response on the value of T_o can be observed by plotting T_o against the T_n. The relationship is shown for the ten values of T_{cms} for the BEL, SC-12,

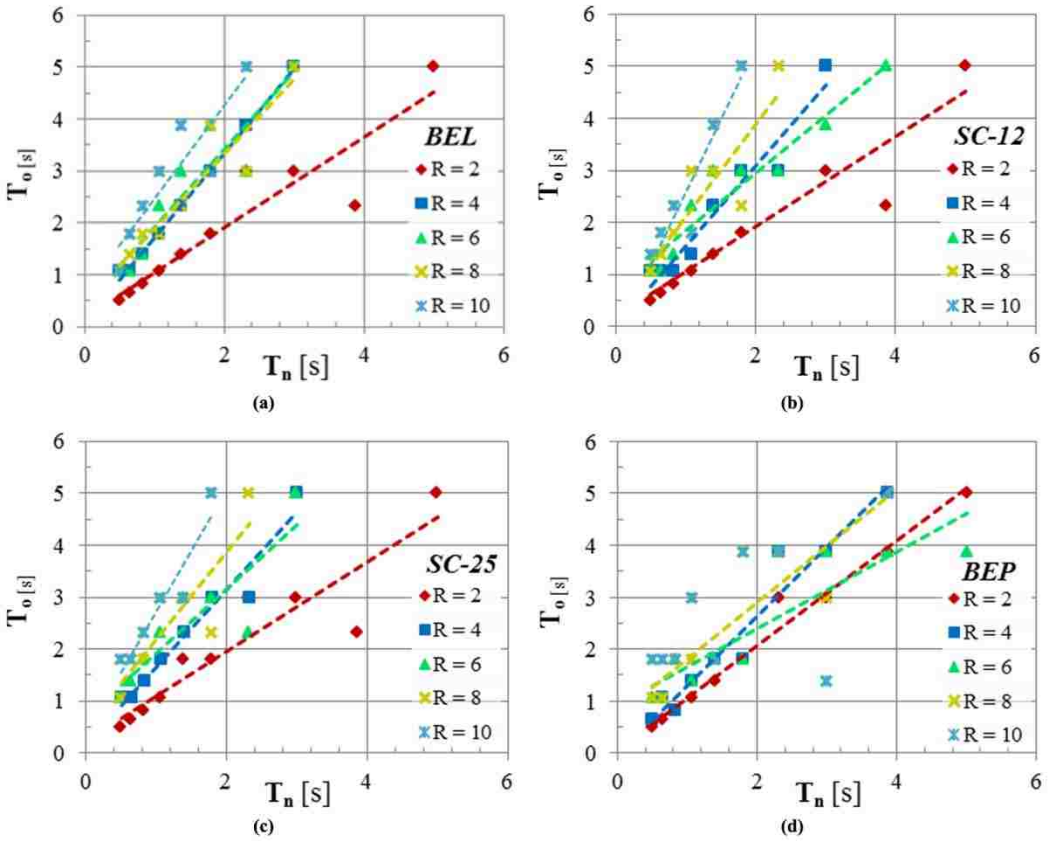

FIGURE 13 – *Peak conditioning period, T_o, versus intial natural period, T_n, for* ***(a)*** *BEL (α = 5%)* ***(b)*** *SC (α = 5%, β = 12.5%)* ***(c)*** *SC (α = 5%, β = 25%)* ***(d)*** *BEP (α = 5%)*

SC-25, and BEP systems in Figures 13 a, b, c, and d respectively. The results shown in Figure 13 only include the first value of T_o= 5.0s for each series, as it was the upper limit of T_{cms} values considered in the study. The results indicate that the value of T_{cms} has a significant impact on the ductility demand of the system.

The results shown in Figure 13 indicate an approximately linear relationship between T_o and T_n, as demonstrated by the trendlines. An exception is seen for the BEP system, where the trend is less clear for R = 10, (Figure 13d) where the trendline has been omitted. Trendlines with a slope of unity indicate that using a ground motion set conditioned on T_{cms}= T_n should give an appropriate estimate for the expected value of the ductility ratio for a given hazard level. Trendlines with slopes greater than unity indicate the extent to which T_{cms} for the ground motion set should exceed T_n to properly estimate the expected value of the ductility ratio for a given hazard level. The results shown in Figure 13 show that as R increases, for all systems, the slopes of the trendlines tend to increase. The exception is for the BEP system where a distinct trend for R = 6, 8, and 10, as R increases, is less clear for the current data set. The trendline for a BEP system with R = 10 has been omitted since the resulting data is seemingly random. Furthermore, for systems with R = 2, the slopes of the trendlines are approximately equal to unity indicating it is appropriate to use T_{cms}= T_n. For all systems with R > 2, the slope of the trendlines are greater than unity, and it is therefore not appropriate to use T_{cms}= T_n. As the energy dissipation ratio, β, decreases, T_{cms} should be increasingly larger than T_n, as shown by the steeper trendlines. The plots terminate at a T_o value of 5.0s, which is the largest T_{cms} considered in the present study.

As a specific example, consider a structure with T_n= 2.0s. Based on the results in Figure 13, when selecting ground motions for a BEL or SC system it would be more

appropriate to construct a CMS and the corresponding ground motion set based on $T_{cms} \approx 3.0\ s$ for R = 4.0 and $T_{cms} \approx 5.0\ s$ for R = 10.0, rather than using $T_{cms} = T_n$.

In reviewing the data summarized in Figure 13 the relationship appears roughly linear, so the ratio of T_o to T_n may be a convenient way to characterize the relationship. The ratio of T_o to T_n is defined as λ_o, and is written as follows:

$$\lambda_o = \frac{T_o}{T_n} \qquad \textbf{EQUATION 12}$$

The variation of λ_o is plotted versus R using a standard box and whisker plot in Figure 14 for the systems considered. The box and whisker plot highlights the median, upper quartile, lower quartile, and extreme values of each dataset. For BEL and SC systems, λ_o is relatively constant for a specified R value. Figure 14 shows the variability of λ_o for a given R of the SDOF system. The plots on the left show all conditioning periods; while the plots on the right include only up to the first T_n values where T_o = 5.0s due to the limited number of T_{cms} considered. The noticeable reduction in scatter, illustrated by the reduced space between the median and the quartile marks, between the two plots demonstrates the need for additional T_{cms} to be evaluated. Ultimately the results of the study indicate the greatest displacement ductility demand is usually caused by a ground motion set conditioned on a T_{cms} greater than T_n for structures with highly nonlinear behavior. T_o is shown to vary with lateral strength (R) and energy dissipation.

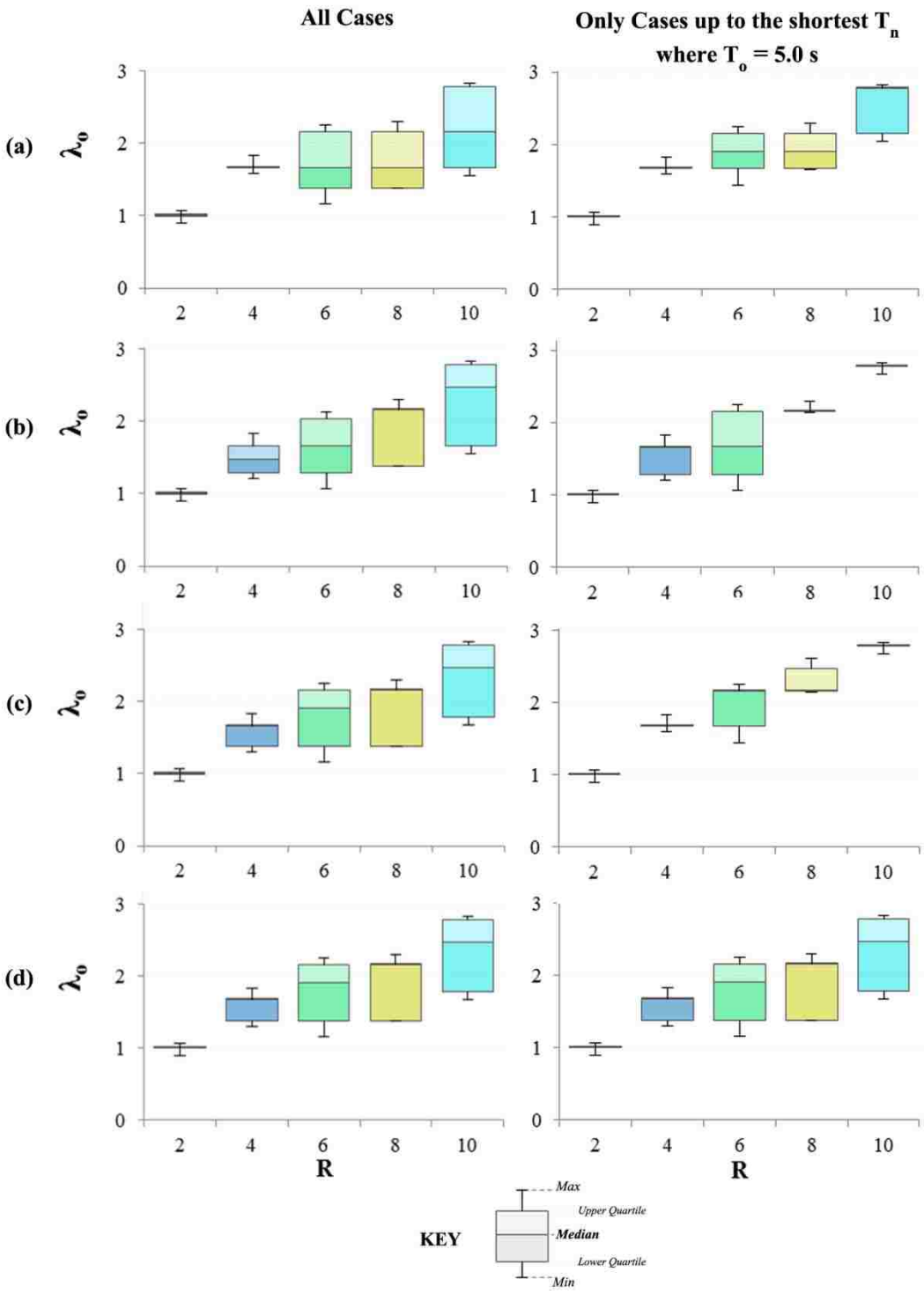

FIGURE 14 *–Variation in period ratio, λ_o, values by R value for (a) BEL (α = 5%) (b) SC-12 (α = 5%, β = 12.5%) (c) SC-25 (α = 5%, β = 25%) (d) BEP (α = 5%)*

Conclusions

Self-centering (SC) systems are a class of lateral systems which aims to reduce post-earthquake damage in the form of residual drift. Due to the limited energy dissipation capacity inherent in these systems, SC systems may experience greater lateral displacements than conventional systems. The larger displacements may result in greater period elongation, which causes them to be more sensitive to ground motions selected and conditioned for a conditioning period, T_{cms}, longer than T_n. For this study, nonlinear response spectra for 25 different single-degree-of-freedom models were constructed over a range of 60 initial periods. Conditional Mean Spectra (CMS) were constructed for ten logarithmically spaced T_{cms} values. Twenty ground motions were selected and amplitude scaled to match each target CMS. A total of 5,000 nonlinear response spectra were calculated, with an additional 200 linear elastic response spectra.

The results of the study found that ground motion sets with T_{cms} greater than T_n produced the largest ductility demand. The value of T_{cms} resulting in the largest ductility demand for each value of T_n was denoted T_o.The period elongation experienced by highly nonlinear structures creates sensitivity to ground motion sets conditioned at larger T_{cms} values. Based on the results of the study, the conditioning period ratio, $\lambda_o = \frac{T_o}{T_n}$, was found to be primarily dependent on lateral strength (R) and energy dissipation. The effects of post-yielding stiffness ratio, α, were not evaluated. The study showed that for systems with high lateral strength (R not greater than 2.0), $\lambda_o$is approximately equal to 1.0. λ_o increases with increasing R value and decreasing energy dissipation. For a given R value and energy dissipation ratio, $\lambda_o$appears to be relatively constant, and T_o appears to be directly proportional to T_n. For SC systems with low R

values, T_o is approximately equal to T_n. Conventional BEP systems exhibited λ_o values close to 1.0 except at large R values.

There are limitations to the results of the current study. The CMS and the corresponding ground motion set, was developed for only ten values of T_{cms}; the limitations of having only ten T_{cms} up to only 5.0s can be observed from Figure 13. With additional conditioning periods, especially at periods longer than 5.0s, a more complete relationships, between T_n, T_{cms}, and T_o could be observed over a wider range of periods.

Future work should further investigate the effects of T_{cms} on displacement ductility. CMS should be constructed for a greater number T_{cms} and corresponding ground motions sets should be compiled. Other single-degree-of-freedom systems should be analyzed for additional values of R and β; as well as for the effects of post-yielding stiffness α. The additional results could be used to develop a relationship for estimating the most appropriate T_{cms} for a given structure.

References

[1] J. W. Baker, "Conditional Mean Spectrum: Tool for Ground Motion Selection," *Journal of Structural Engineering,* pp. 322-33, March 2011.

[2] C.-Y. Seo, "Influence of Ground Motion Characteristics and Structural Parameters on Seismic Responses of SDOF Systems," Lehigh University, Bethlehem, 2005.

[3] C. Christopoulos, A. Filiatrault and B. Folz, "Seismic Response of Self-Centering Hysteretic SDOF Systems," *Earthquake Engineering & Structural Dynamics,* vol. 21, no. 5, pp. 131-1150, 2002.

[4] S. Zhu and Y. Zhang, "Seismic Anlaysis of Concentrically Braced Frame Systems with Self-Centering Friction Damping Braces," *Journal of Structural Engineering,* vol. 134, no. 1, pp. 121-131, 2008.

[5] N. B. Chancellor, Seismic Design and Performance of Self-Centering Concentrically-Braced Frames, Bethlehem, Pennsylvania: Lehigh University, 2014.

[6] B. Carlton and N. Abrahamson, "Issues and approaches for implementing conditional mean spectra in practice," *Bulletin of the Seismological Society of America,* vol. 104, no. 1, pp. 503-512, 2014.

[7] J. W. Baker, T. Lin and C. B. Haselton, "Ground Motion Selection for Performance-Based Engineering: Effect of Target Spectrum and Conditioning Period," in

Performance-Based Seismic Engineering: Vision of an Earthquake Resilient Society, 2014, pp. 423-434.

[8] USGS, "Earthquake Hazards 101," United States Geological Survey, [Online]. Available: http://earthquake.usgs.gov/hazards/about/basics.php. [Accessed 9 June 2015].

[9] Y. Bozorgnia and K. W. Campbell, "Engineering characterization of ground motion," in *Earthquake Engineering: From Engineering Seismology to Performance-Based Engineering*, Y. Bozorgnia and V. V. Bertero, Eds., CRC Press, 2004.

[10] E. Miranda, "Inelastic Displacement Ratios for Structures on Firm Sites," *Journal of Structural Engineering,* vol. 126, no. 10, pp. 1150-1159, 2000.

[11] ASCE (American Society of Civil Engineers), Minimum Design Loads for Buildings and Other Structures, Reston, Virginia: American Society of Civil Engineers, 2010.

[12] 2012 International Building Code, Country Club Hills, IL: International Code Council, Inc., 2012.

[13] NEHRP Recommended Seismic Provisions for New Buildings and Other Structures, Washington, D.C.: Building Seismic Safety Council, 2009.

[14] N. S. Kwong, A. K. Chopra and R. K. McGuire, "A framework for the evaluation of ground motion selection and modification procedures," *Earthquake Engineering &*

Structural Dynamics, vol. 5, pp. 795-815, 2015.

[15] N. S. Kwong, A. K. Chopra and R. K. McGuire, "A ground motion selection procedure for enforcing hazard consistency and estimating seismic demand hazard curves," *Earthquake Engineering & Structural Dynamics,* vol. 44, no. 14, pp. 2467-2487, 2015.

[16] T. Vidic, P. Fajfar and M. Fischinger, "Consistent Inelastic Design Spectra: Strength and Displacement," *Earthquake Engineering & Structural Dynamics,* vol. 23, no. 5, pp. 507-521, 1994.

[17] N. Jayaram, T. Lin and J. W. Baker, "A Computationally Efficient Ground-Motion Selection Algorithm for Matching a Target Response Spectrum Mean and Variance," *Earthquake Spectra,* vol. 27, no. 3, pp. 797-815, August 2011.

[18] N. S. Kwong and A. K. Chopra, "Evaluation of the exact conditional spectrum and generalized conditional intensity measure methods for ground motion selection," *Earthquake Engineering & Structural Dynamics,* vol. 45, no. 5, pp. 757-777, 2015.

[19] S. J. Ha and S. W. Han, "An efficient method for selecting and scaling ground motions matching target response spectrum mean and variance," *Earthquake Engineering & Structural Dynamics,* vol. 45, no. 8, p. 1381, 2016.

[20] C.-Y. Seo and R. Sause, "Ductility Demands on Self-Centering Systems under Earthquake Loading," *ACI Structural Journal,* pp. 275-285, March-April 2005.

[21] R. B. Zimmerman, J. W. Baker, J. D. Hooper, S. Bono, C. B. Haselton, A. Engel, R.

O. Hamburger, A. Celikbas and A. Jalalian, "Response History Analysis for the Design of New Buildings in the NEHRP Provisions and ASCE/SEI 7 Standard: Part III-Example Applications Illustrating the Recommended Methodology," *Earthquake Spectra,* vol. 33, no. 2, pp. 419-447, May 2017.

[22] J. W. Baker, C. B. Haselton, N. Luco, J. P. Stewart and R. B. Zimmerman, "Updated ground motion spectral matching requirements in the 2015 NEHRP recommended seismic provisions," in *6th International Conference on Earthqake Geotechnical Engineering*, 2015.

[23] A. K. Chopra, Dynamics of Structures, Third ed., Upper Saddle River, New Jersey: Pearson Prentice Hall, 2007.

[24] E. Miranda and J. Ruiz-García, "Evaluation of Approximate Methods to Estimate Maximum Inelastic Displacement Demand," *Earthquake Engineering & Structural Dynamics,* vol. 31, no. 3, pp. 539-560, 2002.

[25] "USGS Interactive Deaggregation Tools," United States Geological Survey, 2008. [Online]. Available: http://geohazards.usgs.gov/deaggint/2008. [Accessed 29 March 2016].

[26] E. H. Field, T. H. Jordan and C. A. Cornell, "OpenSHA: A Developing Community-Modeling Environment for Seismic Hazard Analysis," *Seismological Research Letters,* vol. 74, no. 4, pp. 406-419, 2003.

[27] J. W. Baker, N. Jayaram and T. Lin, "Software for selecting earthquake ground motions to match a target conditional spectrum," Baker Research Group, [Online].

Available: http://web.stanford.edu/~bakerjw/gm_selection.html. [Accessed 18 September 2015].

[28] *MATLAB Release 2015b,* Natick, Massachusetts: The Mathworks, Inc, 2015.

[29] T. D. Ancheta , R. B. Darragh, J. P. Stewart, E. Seyhan, W. J. Silva, B. S. Chiou, K. E. Wooddell, R. W. Graves, A. R. Kottke, D. M. Boore, T. Kishida and J. L. Donahue, "PEER 2013/03 - PEER NGA-West2 Database," Pacific Earthquake Engineering Research Center, Berkeley, 2013.

Appendix I Site Hazard Disaggregation

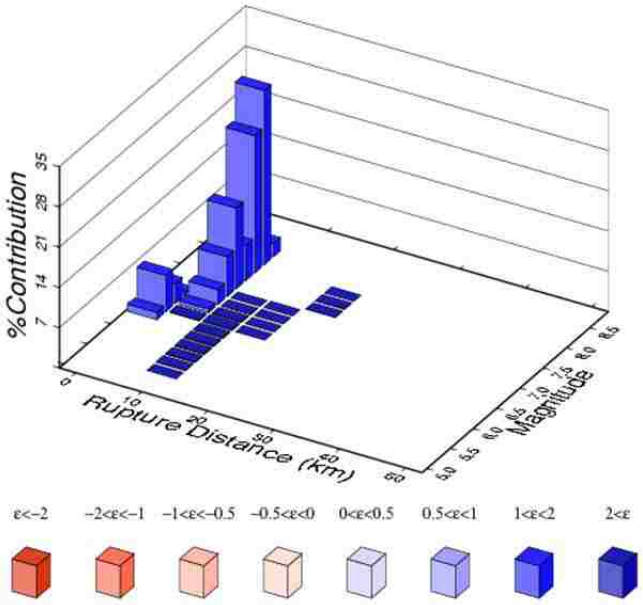

T_n = 0.01 s

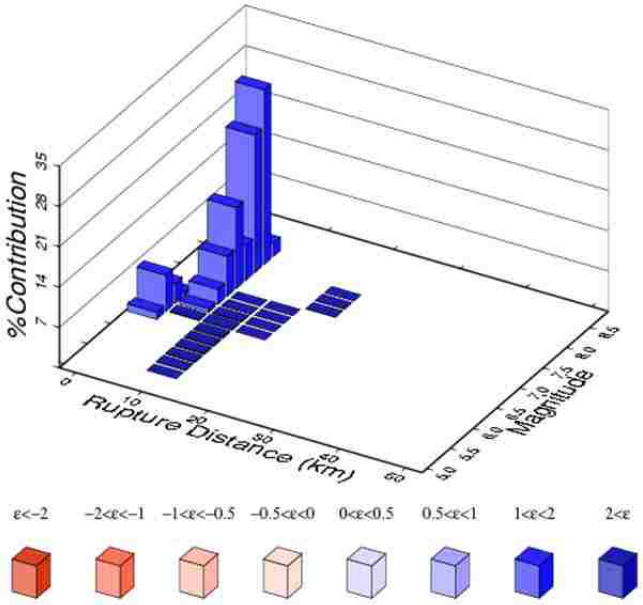

T_n = 0.02 s

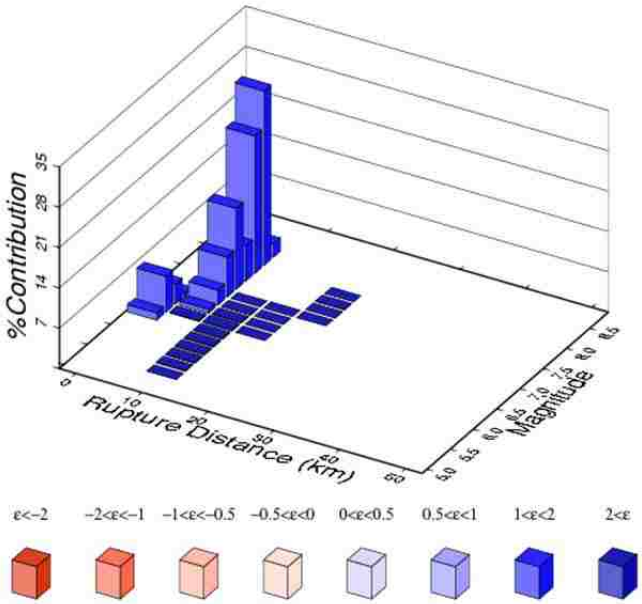

T_n = 0.03 s

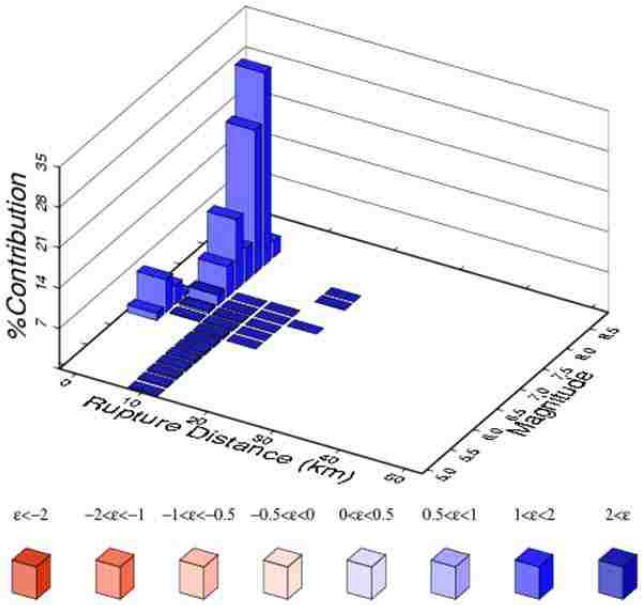

T_n = 0.04 s

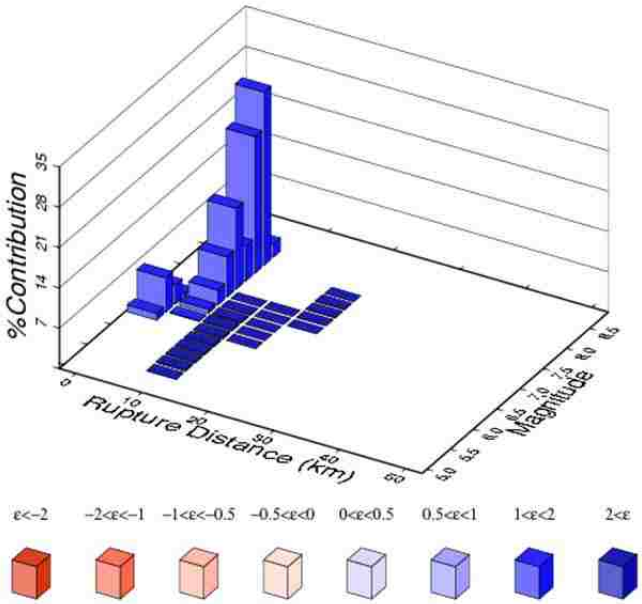

T_n = 0.05 s

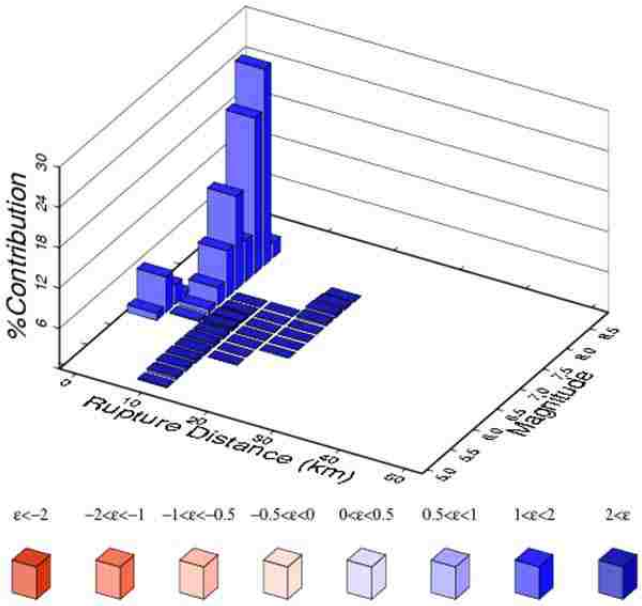

T_n = 0.07 s

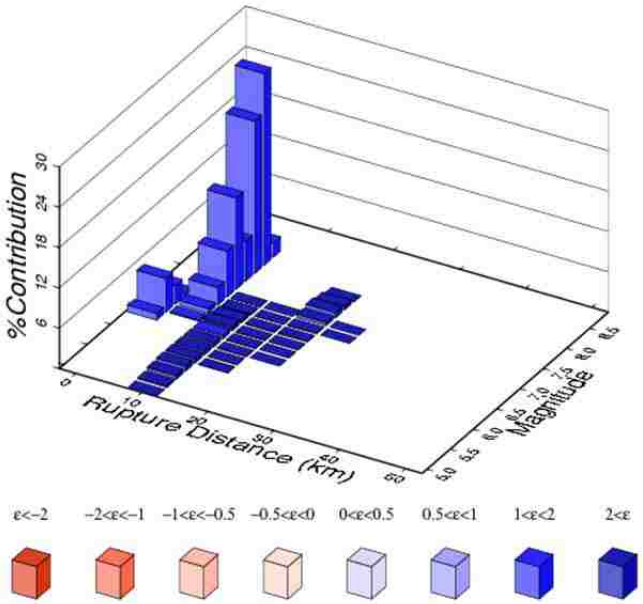

T_n = 0.10 s

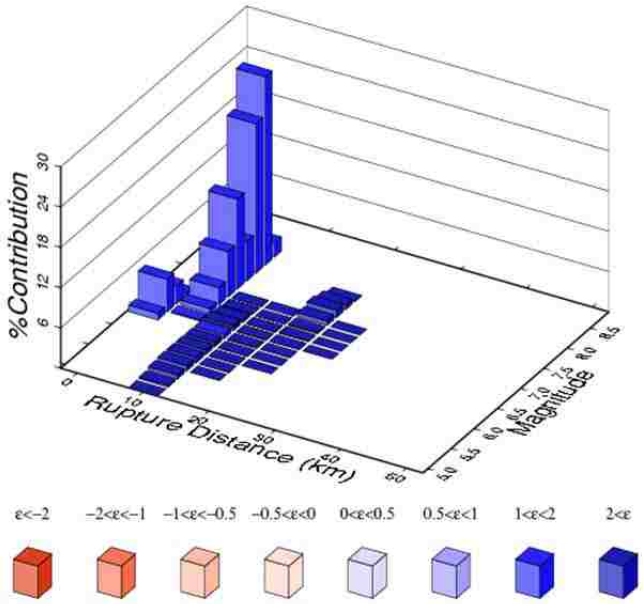

T_n = 0.15 s

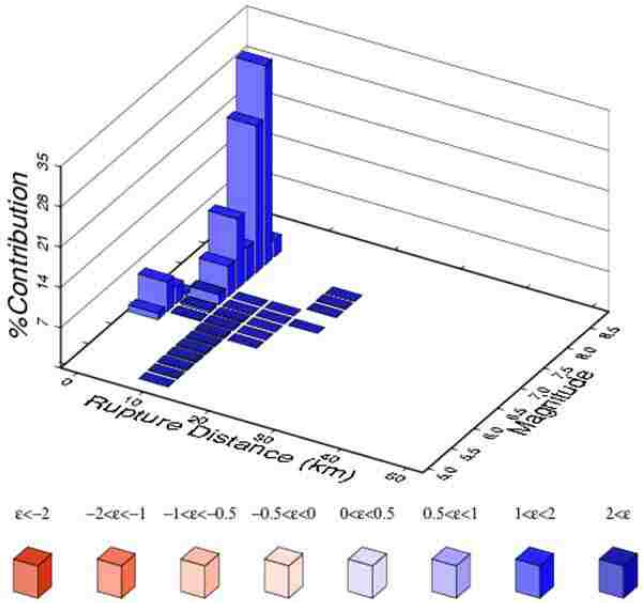

T_n = 0.20 s

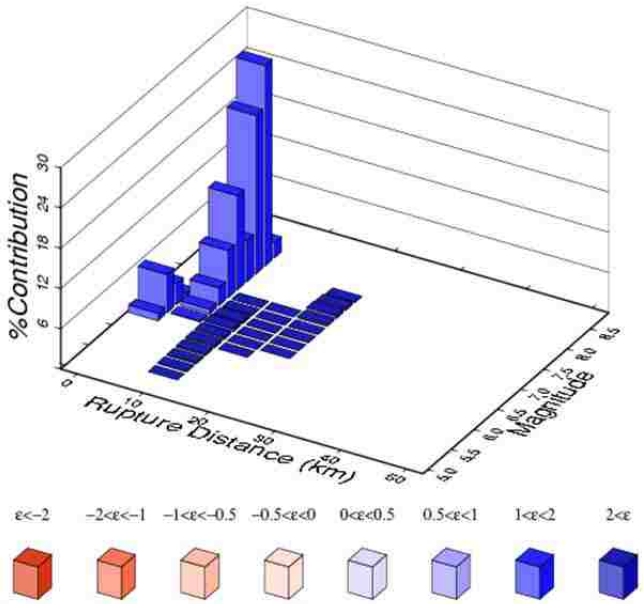

T_n = 0.25 s

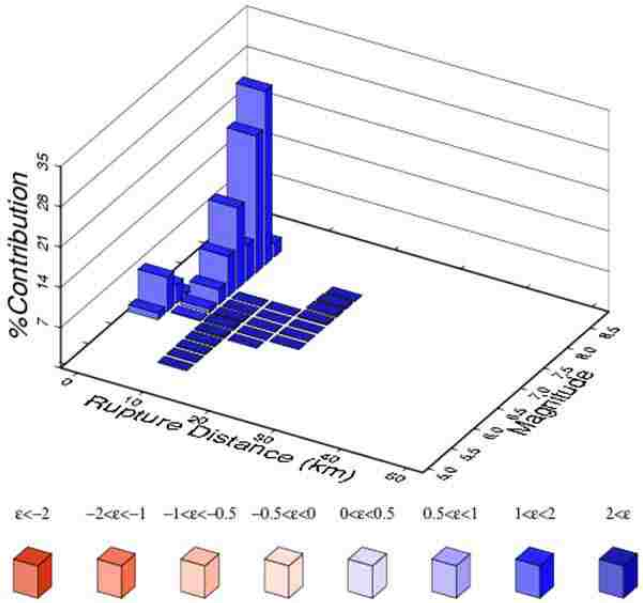

T_n = 0.30 s

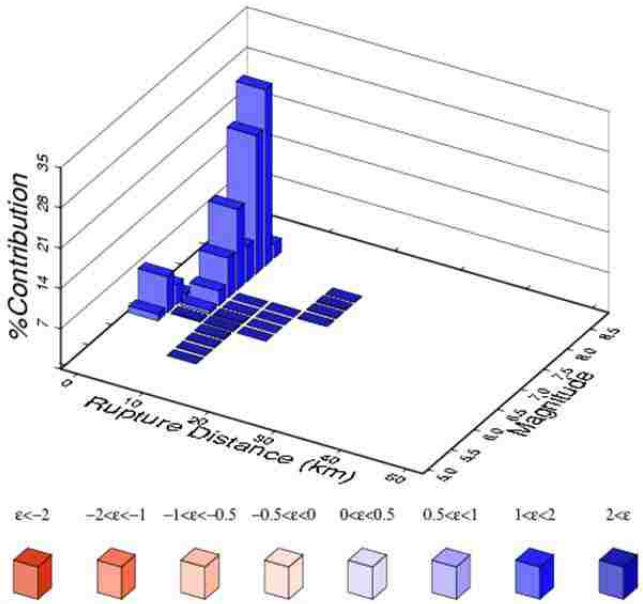

T_n = 0.40 s

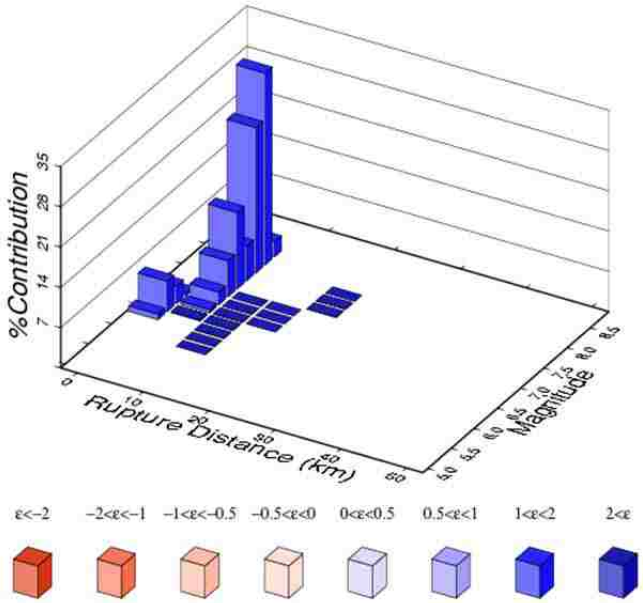

T_n = 0.50 s

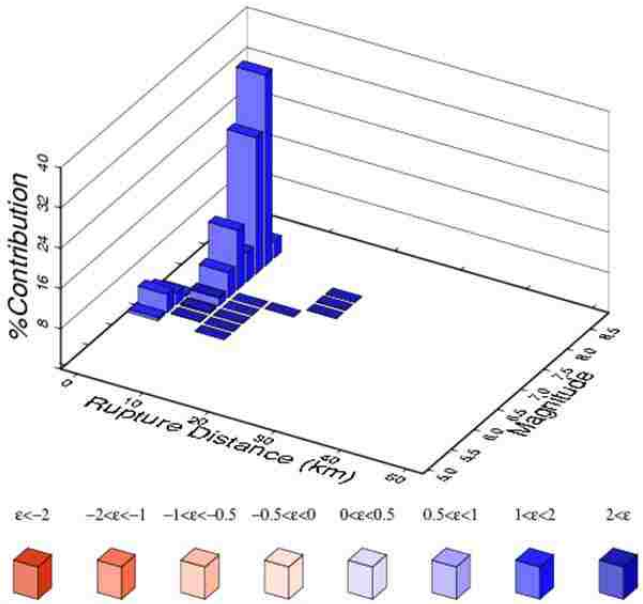

T_n = 0.75 s

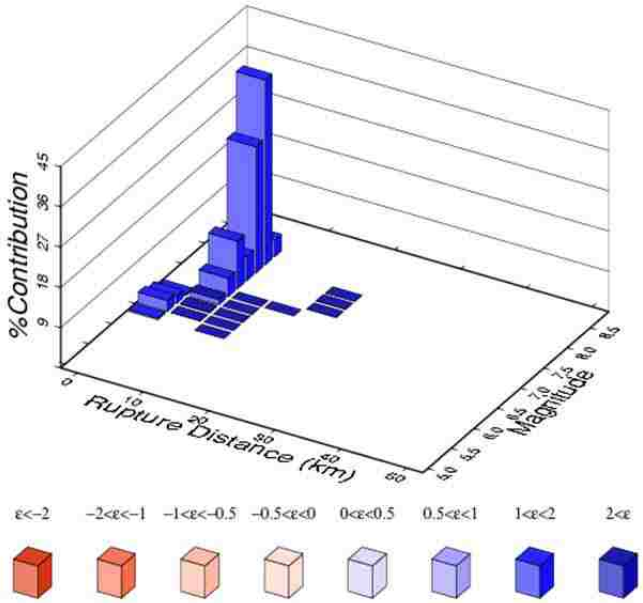

T_n = 1.00 s

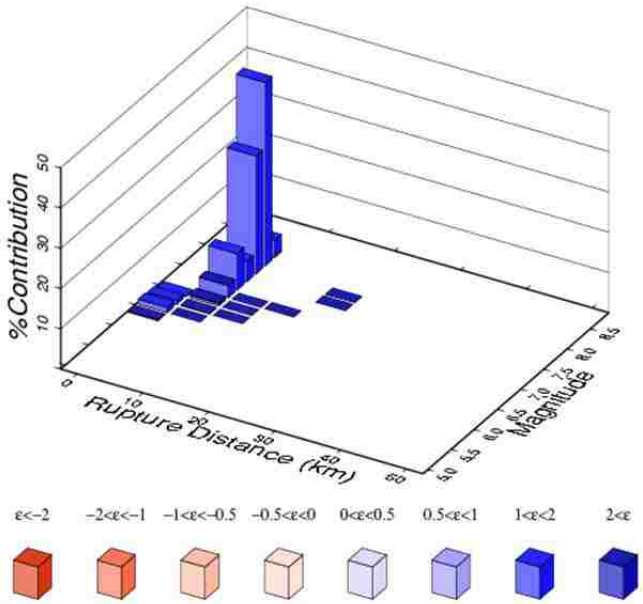

T_n = 1.50 s

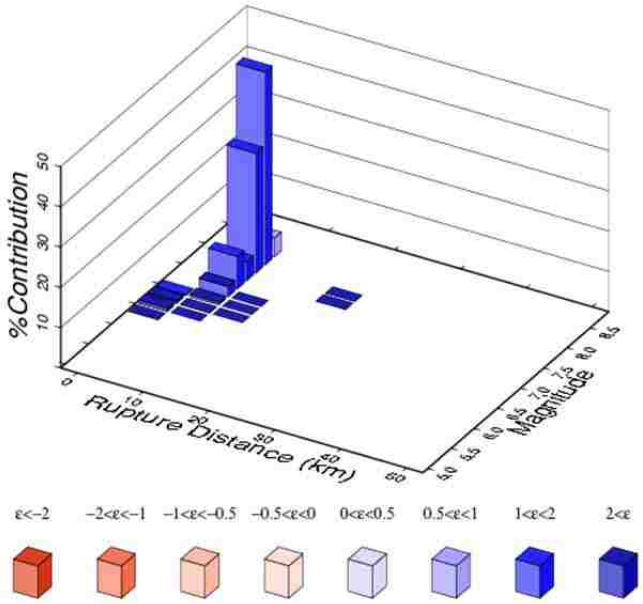

T_n = 2.00 s

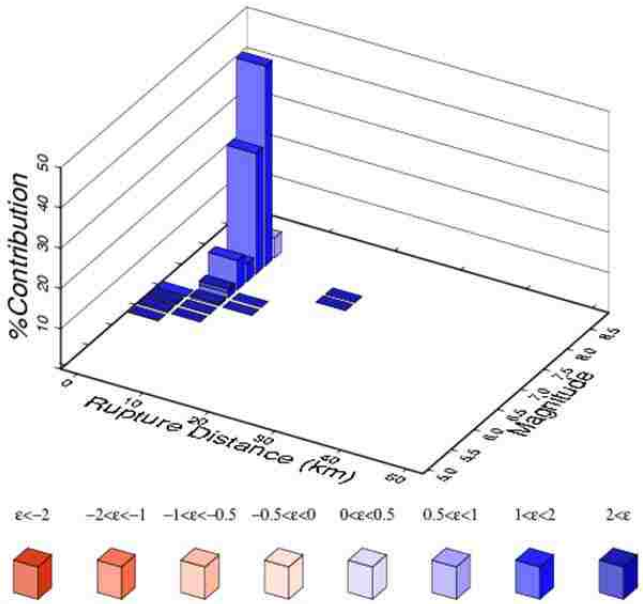

T_n = 3.00 s

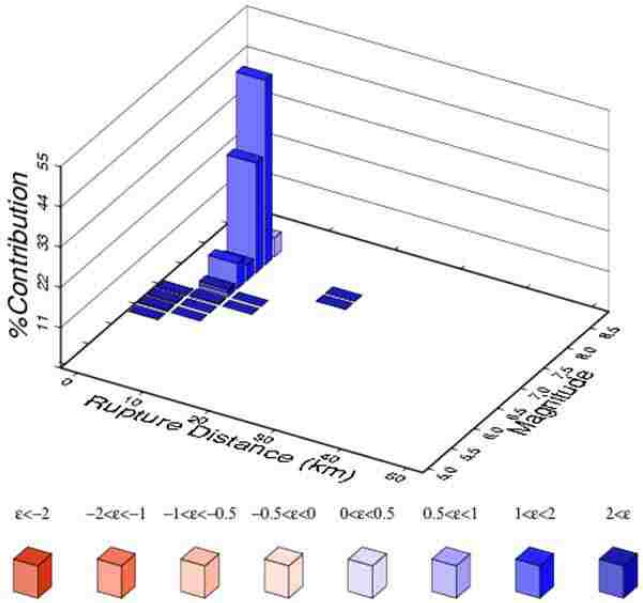

T_n = 4.00 s

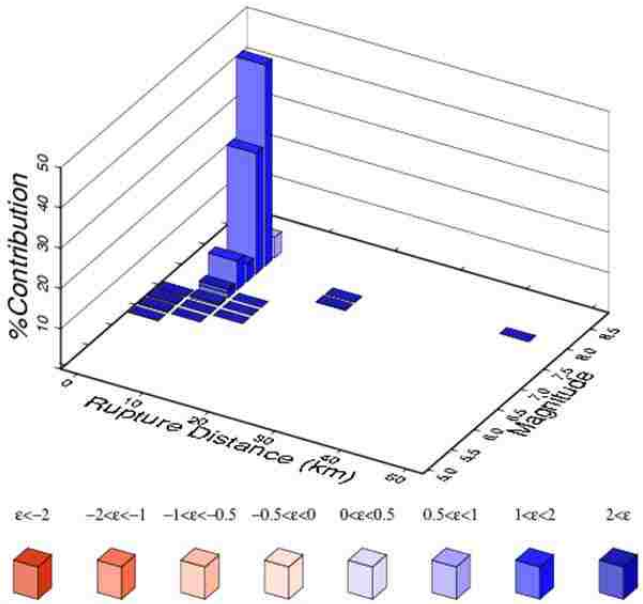

T_n = 5.00 s

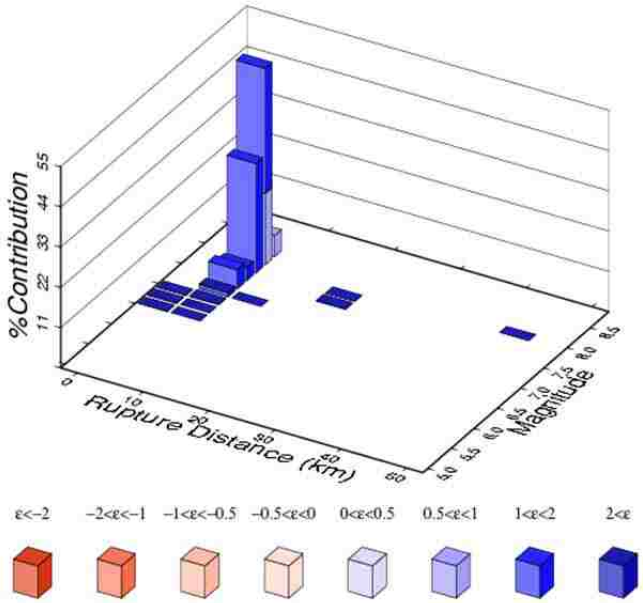

T_n = 7.50 s

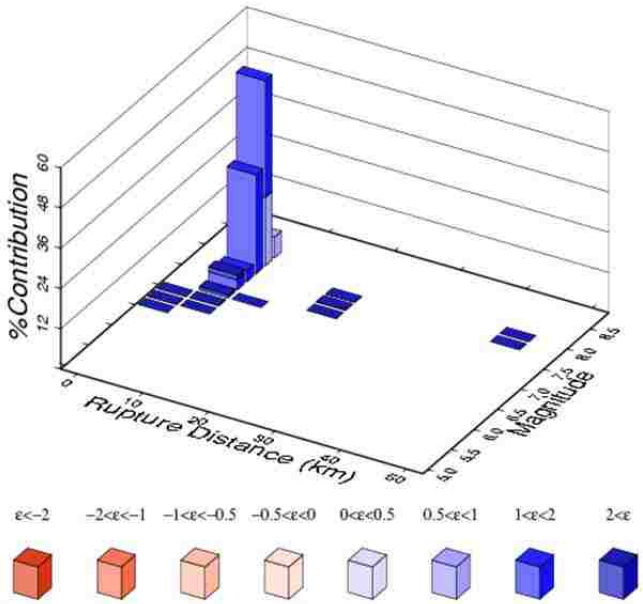

T_n = 10.00 s

Appendix II Ground Motion Sets

Ground Motion Set 1: JW0F00500 T_{cms} = *0.500 sec*

$\bar{M}_{seis}$= *7.5889* $\bar{R}_{seis}$= *3.0085* $\bar{\varepsilon}$ = *1.3870*

	RSN	Filename	M_{seis}	R_{seis}	Component[2]	SF_{GM}
1	1479	CHICHI/TCU034-E.at2	7.62	35.69	000	2.0747
2	2114	DENALI/ps10047.at2	7.90	0.18	047	3.4356
3	1282	CHICHI/HWA033-N.at2	7.62	49.31	090	3.9765
4	848	LANDERS/CLW-TR.at2	7.28	19.74	090	1.7868
5	1198	CHICHI/CHY029-N.at2	7.62	10.97	090	2.6612
6	1258	CHICHI/HWA005-W.at2	7.62	43.17	180	3.8005
7	986	NORTHR/0638-285.at2	6.69	12.92	285	3.0705
8	1504	CHICHI/TCU067-E.at2	7.62	0.64	000	2.3380
9	1487	CHICHI/TCU047-N.at2	7.62	35.00	090	2.5198
10	1504	CHICHI/TCU067-N.at2	7.62	0.64	090	1.7838
11	900	LANDERS/YER270.at2	7.28	23.62	270	3.6346
12	322	COALINGA/H-CAK270.at2	6.36	23.78	270	3.1455
13	825	CAPEMEND/CPM000.at2	7.01	8.20	000	1.2659
14	313	CORINTH/COR--L.at2	6.60	10.27	000	3.0644
15	1158	KOCAELI/DZC180.at2	7.51	13.60	180	3.0154
16	1512	CHICHI/TCU078-E.at2	7.62	0.00	000	2.2682
17	1493	CHICHI/TCU053-E.at2	7.62	5.97	000	2.9986
18	316	WESTMORL/PTS225.at2	5.90	16.54	225	3.2959
19	183	IMPVALL/H-E08140.at2	6.53	3.86	140	2.6044
20	1508	CHICHI/TCU072-N.at2	7.62	7.03	090	1.9574

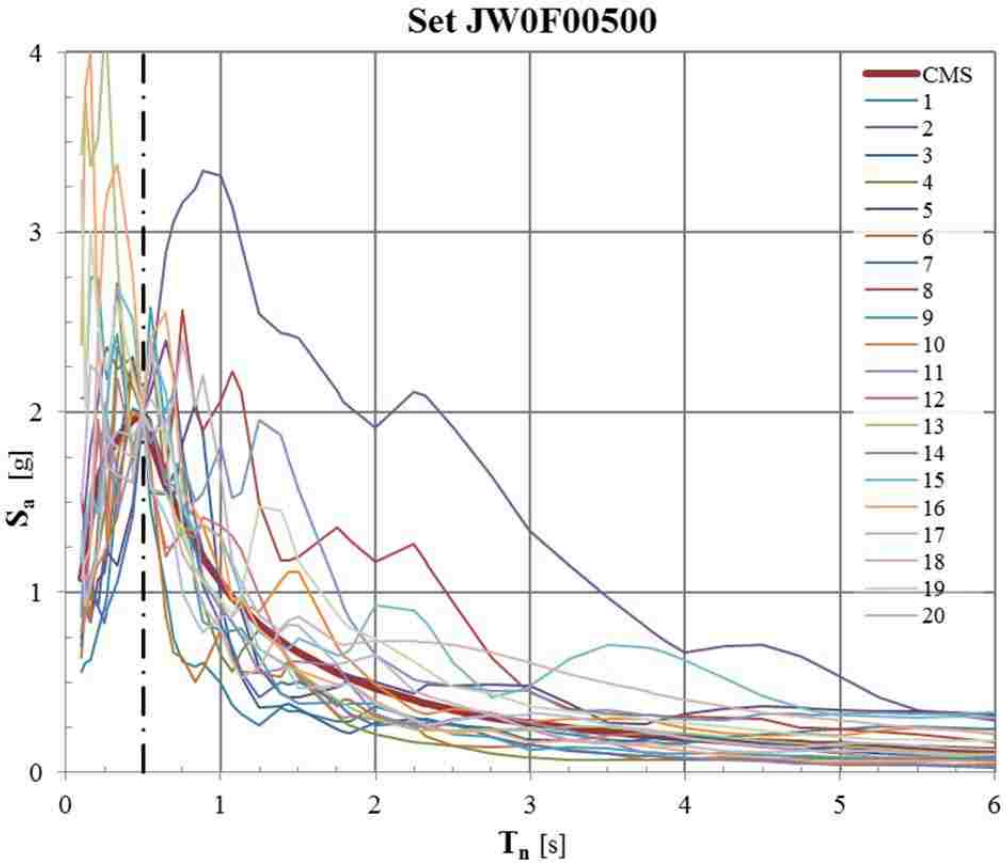

[2] *For programming and data processing components labeled with cardinal direction were relabeled using numerical values with East corresponding to 000°. Where components are denoted by longitudinal or transverse, longitudinal was labeled as 000°.*

Ground Motion Set 2: JW0F00646 T_{cms} = *0.646 sec*

$\bar{M}_{seis}$= *7.6281* $\bar{R}_{seis}$= *3.0247* $\bar{\varepsilon}$ = *1.3766*

	RSN	Filename	M_{seis}	R_{seis}	Component[2]	SF_{GM}
21	1087	NORTHR/TAR090.at2	6.69	0.37	090	0.8430
22	778	LOMAP/HDA255.at2	6.93	24.52	255	2.1810
23	1425	CHICHI/TAP032-E.at2	7.62	93.15	000	3.7134
24	1198	CHICHI/CHY029-E.at2	7.62	10.97	000	2.5637
25	1493	CHICHI/TCU053-E.at2	7.62	5.97	000	3.7175
26	1158	KOCAELI/DZC270.at2	7.51	13.60	270	2.6800
27	1487	CHICHI/TCU047-N.at2	7.62	35.00	090	2.2812
28	1505	CHICHI/TCU068-E.at2	7.62	0.32	000	2.0394
29	1491	CHICHI/TCU051-N.at2	7.62	7.66	090	3.4204
30	1317	CHICHI/ILA013-W.at2	7.62	81.71	180	2.9553
31	1524	CHICHI/TCU095-E.at2	7.62	45.15	000	2.8976
32	1158	KOCAELI/DZC180.at2	7.51	13.60	180	2.5214
33	170	IMPVALL/H-ECC092.at2	6.53	7.31	092	3.2285
34	1187	CHICHI/CHY015-W.at2	7.62	38.14	180	2.7653
35	1508	CHICHI/TCU072-E.at2	7.62	7.03	000	1.2597
36	1085	NORTHR/SCE288.at2	6.69	5.19	281	2.6714
37	1508	CHICHI/TCU072-N.at2	7.62	7.03	090	1.7510
38	1194	CHICHI/CHY025-N.at2	7.62	19.09	090	3.9255
39	949	NORTHR/ARL090.at2	6.69	3.30	090	2.5814
40	777	LOMAP/HCH180.at2	6.93	27.33	180	2.5724

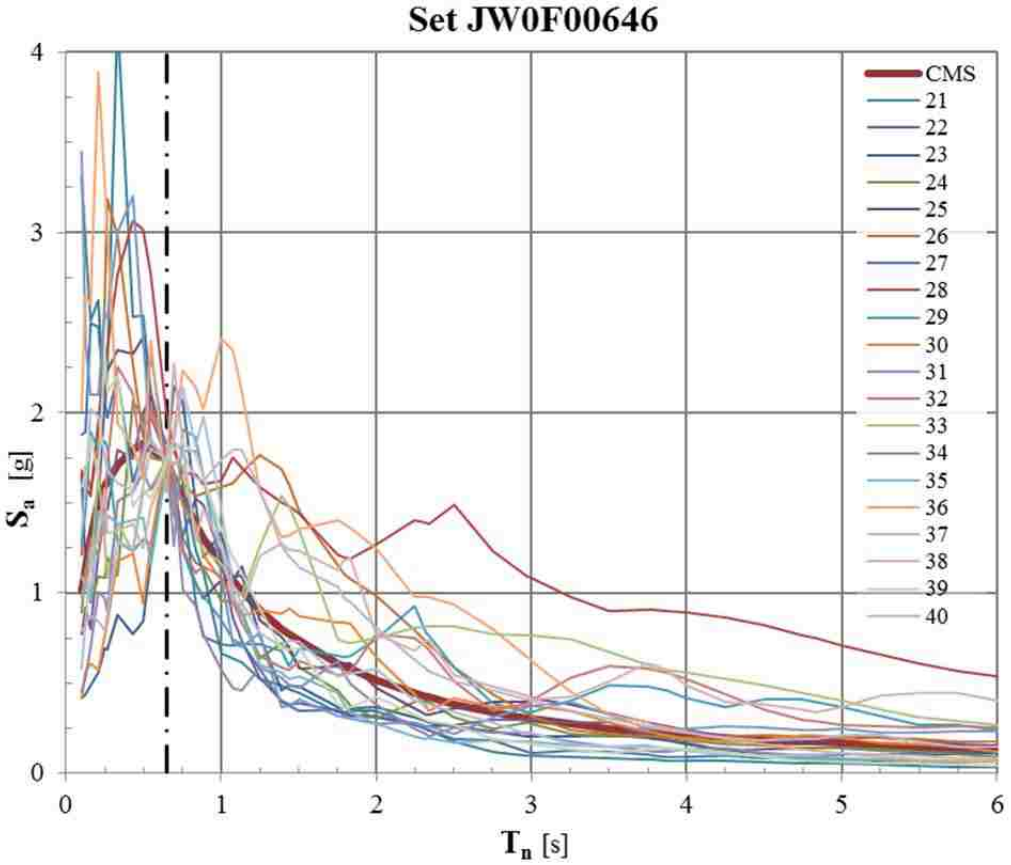

Ground Motion Set 3: JW0F00834 T_{cms} = *0.834 sec*

$\bar{M}_{seis}$= *7. 6722* $\bar{R}_{seis}$= *3. 6722* $\bar{\varepsilon}$ = *1. 3611*

	RSN	Filename	M_{seis}	R_{seis}	Component[2]	SF_{GM}
41	1246	CHICHI/CHY104-N.at2	7.62	18.04	090	2.5272
42	1147	KOCAELI/ATS000.at2	7.51	68.09	000	2.6664
43	1541	CHICHI/TCU116-N.at2	7.62	12.40	090	3.5703
44	2114	DENALI/ps10047.at2	7.90	0.18	047	1.5667
45	1513	CHICHI/TCU079-N.at2	7.62	10.97	090	1.9848
46	1541	CHICHI/TCU116-E.at2	7.62	12.40	000	3.9397
47	1509	CHICHI/TCU074-N.at2	7.62	13.46	090	2.0969
48	1425	CHICHI/TAP032-E.at2	7.62	93.15	000	3.8514
49	721	SUPERST/B-ICC000.at2	6.54	18.20	000	3.0670
50	963	NORTHR/ORR360.at2	6.69	20.10	360	1.2853
51	1317	CHICHI/ILA013-W.at2	7.62	81.71	180	3.3015
52	180	IMPVALL/H-E05140.at2	6.53	1.76	140	2.5863
53	729	SUPERST/B-IVW360.at2	6.54	23.85	360	3.2970
54	1508	CHICHI/TCU072-E.at2	7.62	7.03	000	1.0687
55	1602	DUZCE/BOL000.at2	7.14	12.02	000	1.9491
56	1504	CHICHI/TCU067-E.at2	7.62	0.64	000	1.8089
57	900	LANDERS/YER270.at2	7.28	23.62	270	3.7548
58	1198	CHICHI/CHY029-E.at2	7.62	10.97	000	3.3062
59	1549	CHICHI/TCU129-E.at2	7.62	1.84	000	2.1211
60	1492	CHICHI/TCU052-N.at2	7.62	0.66	090	1.5280

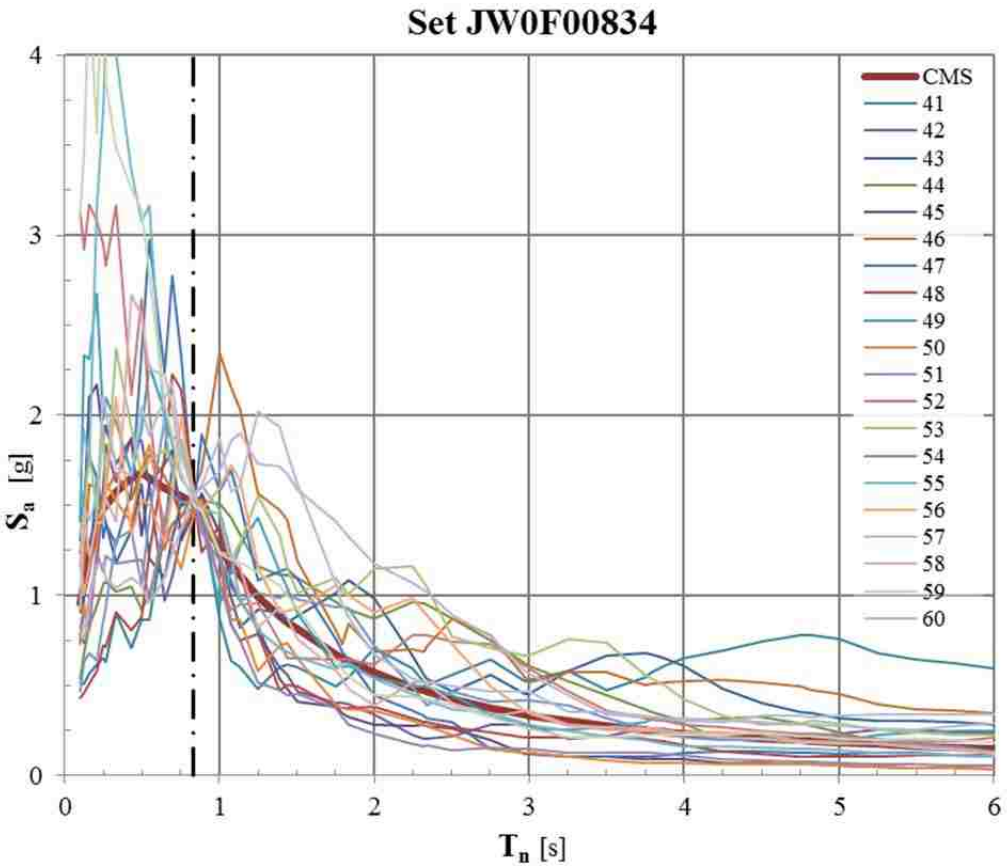

Ground Motion Set 4: JW0F01077 T_{cms} = *1.077 sec*

$\bar{M}_{seis}$= *7.7122* $\bar{R}_{seis}$= *3.0729* $\bar{\varepsilon}$ = *1. 3402*

	RSN	Filename	M_{seis}	R_{seis}	Component[2]	SF_{GM}
61	1194	CHICHI/CHY025-E.at2	7.62	19.09	000	3.0808
62	1489	CHICHI/TCU049-N.at2	7.62	3.78	090	3.8331
63	1549	CHICHI/TCU129-E.at2	7.62	1.84	000	2.3346
64	900	LANDERS/YER270.at2	7.28	23.62	270	3.0669
65	1492	CHICHI/TCU052-N.at2	7.62	0.66	090	1.0895
66	1193	CHICHI/CHY024-E.at2	7.62	9.64	000	3.6827
67	1504	CHICHI/TCU067-E.at2	7.62	0.64	000	1.3706
68	1515	CHICHI/TCU082-E.at2	7.62	5.18	000	3.6888
69	1505	CHICHI/TCU068-E.at2	7.62	0.32	000	1.3178
70	2114	DENALI/ps10047.at2	7.90	0.18	047	1.3946
71	1419	CHICHI/TAP017-E.at2	7.62	97.69	000	3.2638
72	1494	CHICHI/TCU054-N.at2	7.62	5.30	090	3.8080
73	779	LOMAP/LGP090.at2	6.93	3.88	090	2.8509
74	1508	CHICHI/TCU072-E.at2	7.62	7.03	000	1.7974
75	1166	KOCAELI/IZN090.at2	7.51	30.74	090	3.3470
76	723	SUPERST/B-PTS225.at2	6.54	0.95	225	1.3364
77	776	LOMAP/HSP000.at2	6.93	27.67	000	1.4559
78	1203	CHICHI/CHY036-E.at2	7.62	16.06	000	2.7584
79	864	LANDERS/JOS000.at2	7.28	11.03	000	2.7693
80	738	LOMAP/NAS180.at2	6.93	70.90	180	3.5528

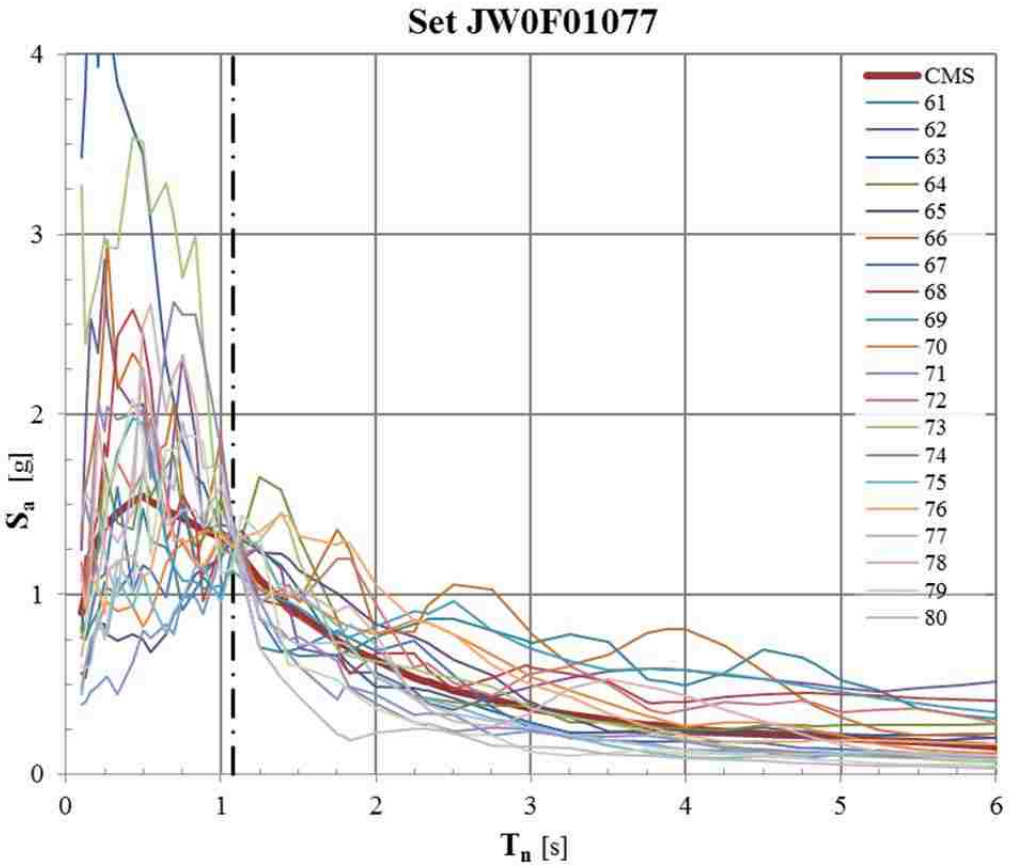

Ground Motion Set 5: JW0F01391 T_{cms} = *1.391 sec*

$\bar{M}_{seis}$=*7. 7458* $\bar{R}_{seis}$= *3. 0922* $\bar{\varepsilon}$ = *1. 3200*

	RSN	Filename	M_{seis}	R_{seis}	Component[2]	SF_{GM}
81	143	TABAS/TAB-TR.at2	7.35	1.79	090	2.7426
82	1494	CHICHI/TCU054-N.at2	7.62	5.30	090	3.8660
83	1045	NORTHR/WPI046.at2	6.69	2.11	046	1.3295
84	1504	CHICHI/TCU067-E.at2	7.62	0.64	000	2.1487
85	1492	CHICHI/TCU052-N.at2	7.62	0.66	090	0.9814
86	1515	CHICHI/TCU082-N.at2	7.62	5.18	090	3.1935
87	1500	CHICHI/TCU061-E.at2	7.62	17.19	000	3.7472
88	1491	CHICHI/TCU051-E.at2	7.62	7.66	000	3.7949
89	1505	CHICHI/TCU068-N.at2	7.62	0.32	090	1.2400
90	170	IMPVALL/H-ECC092.at2	6.53	7.31	092	2.2377
91	1411	CHICHI/TAP005-E.at2	7.62	105.45	000	3.5812
92	1505	CHICHI/TCU068-E.at2	7.62	0.32	000	1.2896
93	779	LOMAP/LGP090.at2	6.93	3.88	090	2.1722
94	1166	KOCAELI/IZN090.at2	7.51	30.74	090	3.5019
95	900	LANDERS/YER270.at2	7.28	23.62	270	2.0665
96	171	IMPVALL/H-EMO270.at2	6.53	0.07	270	2.0443
97	1147	KOCAELI/ATS090.at2	7.51	68.09	090	2.3253
98	2114	DENALI/ps10047.at2	7.90	0.18	047	1.4312
99	1231	CHICHI/CHY080-N.at2	7.62	0.11	090	1.1396
100	1048	NORTHR/STC180.at2	6.69	12.09	180	1.5658

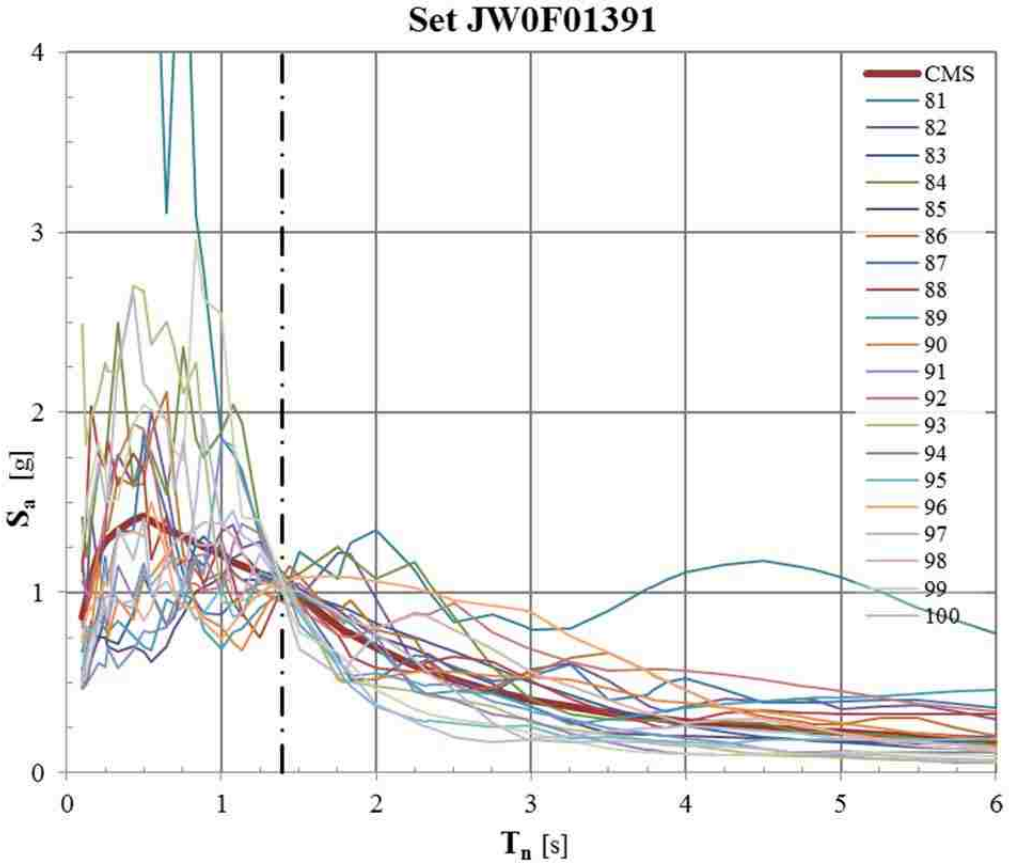

Ground Motion Set 6: JW0F01797 T_{cms} = *1.797 sec*

$\bar{M}_{seis}$=*7. 7735* $\bar{R}_{seis}$= *3.1082* $\bar{\varepsilon}$ = *1.2970*

	RSN	Filename	M_{seis}	R_{seis}	Component[2]	SF_{GM}
101	1329	CHICHI/ILA037-N.at2	7.62	81.70	090	2.5903
102	1509	CHICHI/TCU074-N.at2	7.62	13.46	090	2.6515
103	1504	CHICHI/TCU067-E.at2	7.62	0.64	000	1.5173
104	778	LOMAP/HDA165.at2	6.93	24.52	165	3.0341
105	1508	CHICHI/TCU072-N.at2	7.62	7.03	090	2.7318
106	1494	CHICHI/TCU054-N.at2	7.62	5.30	090	2.7783
107	2507	CHICHI03/CHY101-E.at2	6.20	24.40	000	2.9057
108	1551	CHICHI/TCU138-N.at2	7.62	9.79	090	2.3002
109	1492	CHICHI/TCU052-N.at2	7.62	0.66	090	0.9376
110	1546	CHICHI/TCU122-N.at2	7.62	9.35	090	3.9717
111	1495	CHICHI/TCU055-E.at2	7.62	6.36	000	3.8223
112	1529	CHICHI/TCU102-E.at2	7.62	1.51	000	1.5312
113	2114	DENALI/ps10047.at2	7.90	0.18	047	1.3570
114	1528	CHICHI/TCU101-E.at2	7.62	2.13	000	3.9278
115	1505	CHICHI/TCU068-E.at2	7.62	0.32	000	1.3654
116	1500	CHICHI/TCU061-N.at2	7.62	17.19	090	3.8292
117	900	LANDERS/YER270.at2	7.28	23.62	270	3.3964
118	1501	CHICHI/TCU063-N.at2	7.62	9.80	090	2.8290
119	1505	CHICHI/TCU068-N.at2	7.62	0.32	090	1.1520
120	1193	CHICHI/CHY024-N.at2	7.62	9.64	090	2.9059

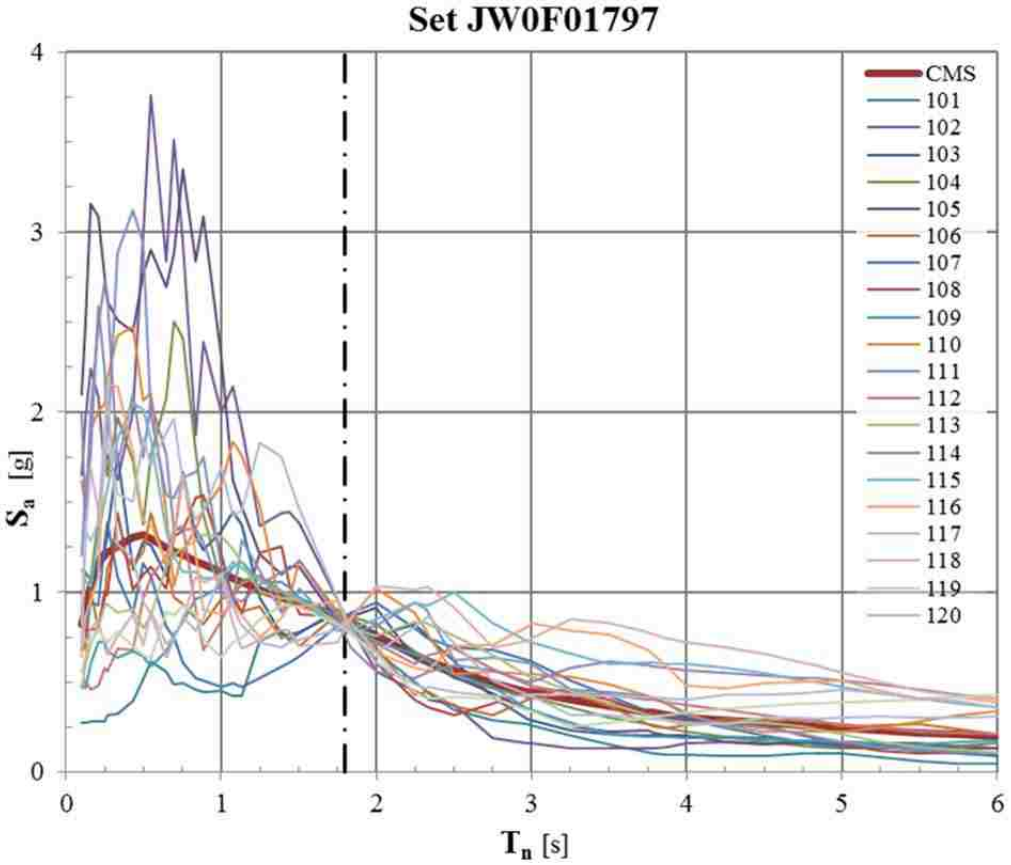

Ground Motion Set 7: JW0F02321 T_{cms} = *2.321 sec*

$\bar{M}_{seis}$=*7. 7907* $\bar{R}_{seis}$= *3.1177* $\bar{\varepsilon}$ = *1.2779*

	RSN	Filename	M_{seis}	R_{seis}	Component[2]	SF_{GM}
121	1111	KOBE/NIS000.at2	6.90	7.08	000	3.4387
122	1500	CHICHI/TCU061-E.at2	7.62	17.19	000	3.9649
123	1114	KOBE/PRI090.at2	6.90	3.31	090	3.3798
124	1508	CHICHI/TCU072-N.at2	7.62	7.03	090	3.3420
125	2114	DENALI/ps10047.at2	7.90	0.18	047	1.1242
126	1492	CHICHI/TCU052-N.at2	7.62	0.66	090	1.0454
127	1501	CHICHI/TCU063-N.at2	7.62	9.80	090	1.9829
128	1505	CHICHI/TCU068-E.at2	7.62	0.32	000	0.9409
129	3548	LOMAP/LEX090.at2	6.93	3.22	090	2.3016
130	1491	CHICHI/TCU051-N.at2	7.62	7.66	090	3.2146
131	1542	CHICHI/TCU117-N.at2	7.62	25.44	090	2.5212
132	2114	DENALI/ps10317.at2	7.90	0.18	317	2.4085
133	1490	CHICHI/TCU050-N.at2	7.62	9.51	090	3.1880
134	1529	CHICHI/TCU102-E.at2	7.62	1.51	000	1.5693
135	806	LOMAP/SVL360.at2	6.93	23.92	360	3.0614
136	1526	CHICHI/TCU098-N.at2	7.62	47.67	090	3.9737
137	721	SUPERST/B-ICC090.at2	6.54	18.20	090	2.6281
138	1495	CHICHI/TCU055-N.at2	7.62	6.36	090	2.9877
139	1505	CHICHI/TCU068-N.at2	7.62	0.32	090	1.8615
140	1533	CHICHI/TCU106-N.at2	7.62	14.99	090	2.4366

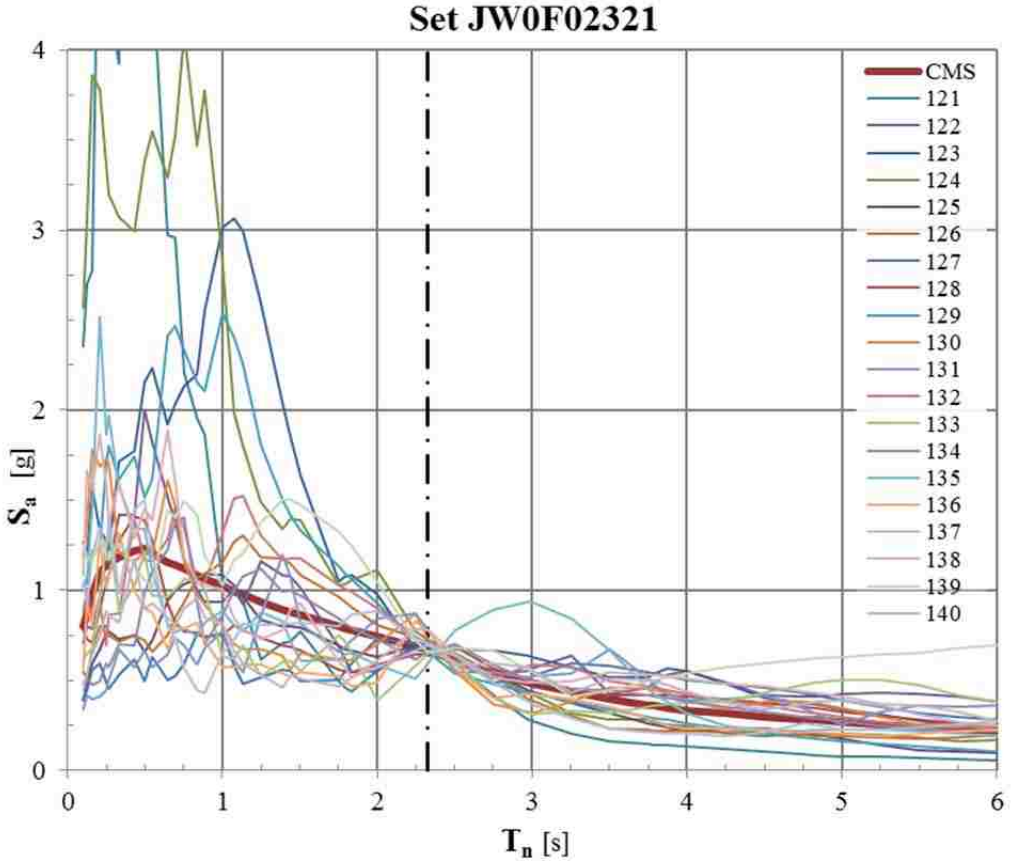

Ground Motion Set 8: JW0F02997 T_{cms} = *2.997 sec*

$\bar{M}_{seis}$= *7.8038* $\bar{R}_{seis}$= *3.1245* $\bar{\varepsilon}$ = *1.2607*

	RSN	Filename	M_{seis}	R_{seis}	Component[2]	SF_{GM}
141	1508	CHICHI/TCU072-N.at2	7.62	7.03	090	3.9330
142	1492	CHICHI/TCU052-N.at2	7.62	0.66	090	1.4488
143	721	SUPERST/B-ICC090.at2	6.54	18.20	090	3.8058
144	1629	STELIAS/059v2279.at2	7.54	80.00	279	3.0397
145	1505	CHICHI/TCU068-E.at2	7.62	0.32	000	0.9909
146	1494	CHICHI/TCU054-N.at2	7.62	5.30	090	3.4900
147	1501	CHICHI/TCU063-N.at2	7.62	9.80	090	1.8577
148	1550	CHICHI/TCU136-W.at2	7.62	8.29	180	3.3640
149	1515	CHICHI/TCU082-N.at2	7.62	5.18	090	2.9968
150	1482	CHICHI/TCU039-E.at2	7.62	19.90	000	2.8058
151	1488	CHICHI/TCU048-E.at2	7.62	13.55	000	3.6268
152	1533	CHICHI/TCU106-N.at2	7.62	14.99	090	2.3187
153	1510	CHICHI/TCU075-E.at2	7.62	0.91	000	1.6879
154	778	LOMAP/HDA165.at2	6.93	24.52	165	3.8963
155	1528	CHICHI/TCU101-E.at2	7.62	2.13	000	3.7646
156	1180	CHICHI/CHY002-W.at2	7.62	24.98	180	2.8093
157	803	LOMAP/WVC000.at2	6.93	8.48	000	3.7577
158	1045	NORTHR/WPI046.at2	6.69	2.11	046	1.4428
159	1477	CHICHI/TCU031-E.at2	7.62	30.18	000	3.4175
160	1262	CHICHI/HWA011-N.at2	7.62	49.29	090	3.7837

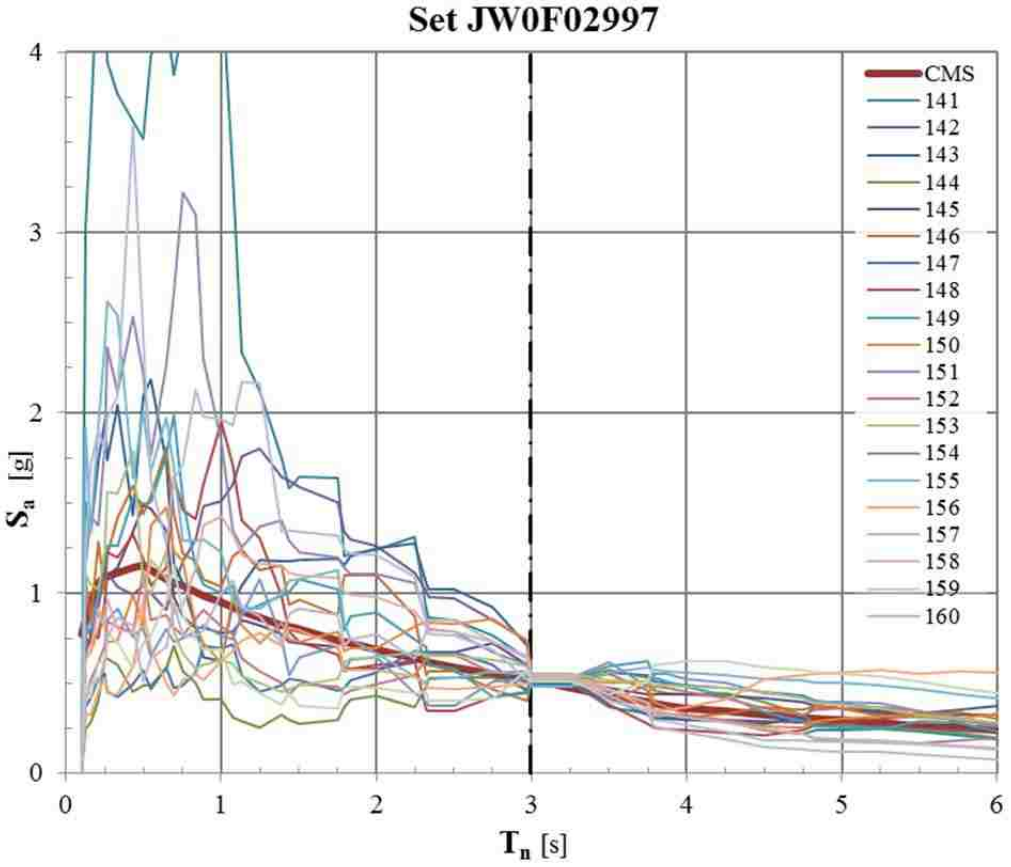

Ground Motion Set 9: JW0F03871 T_{cms} = *3.871 sec*

$\bar{M}_{seis}$= *7.8113* $\bar{R}_{seis}$= *3.1280* $\bar{\varepsilon}$ = *1.2543*

	RSN	Filename	M_{seis}	R_{seis}	Component[2]	SF_{GM}
161	1120	KOBE/TAK000.at2	6.90	1.46	000	2.0950
162	1505	CHICHI/TCU068-N.at2	7.62	0.32	090	1.5474
163	1482	CHICHI/TCU039-E.at2	7.62	19.90	000	2.8889
164	806	LOMAP/SVL360.at2	6.93	23.92	360	3.0750
165	1519	CHICHI/TCU087-E.at2	7.62	7.00	000	3.6200
166	1527	CHICHI/TCU100-E.at2	7.62	11.39	000	3.4843
167	1528	CHICHI/TCU101-E.at2	7.62	2.13	000	2.7547
168	1548	CHICHI/TCU128-E.at2	7.62	13.15	000	2.2793
169	1605	DUZCE/DZC180.at2	7.14	6.58	180	2.1173
170	1538	CHICHI/TCU112-E.at2	7.62	27.50	000	1.9631
171	2114	DENALI/ps10047.at2	7.90	0.18	047	1.7478
172	1492	CHICHI/TCU052-E.at2	7.62	0.66	000	1.2292
173	1517	CHICHI/TCU084-N.at2	7.62	11.24	090	3.6797
174	1502	CHICHI/TCU064-E.at2	7.62	16.62	000	2.7843
175	879	LANDERS/LCN260.at2	7.28	2.19	260	1.2656
176	1505	CHICHI/TCU068-E.at2	7.62	0.32	000	0.9314
177	1495	CHICHI/TCU055-N.at2	7.62	6.36	090	2.2470
178	1310	CHICHI/ILA004-W.at2	7.62	86.61	180	3.4162
179	1482	CHICHI/TCU039-N.at2	7.62	19.90	090	2.3553
180	1515	CHICHI/TCU082-N.at2	7.62	5.18	090	2.4194

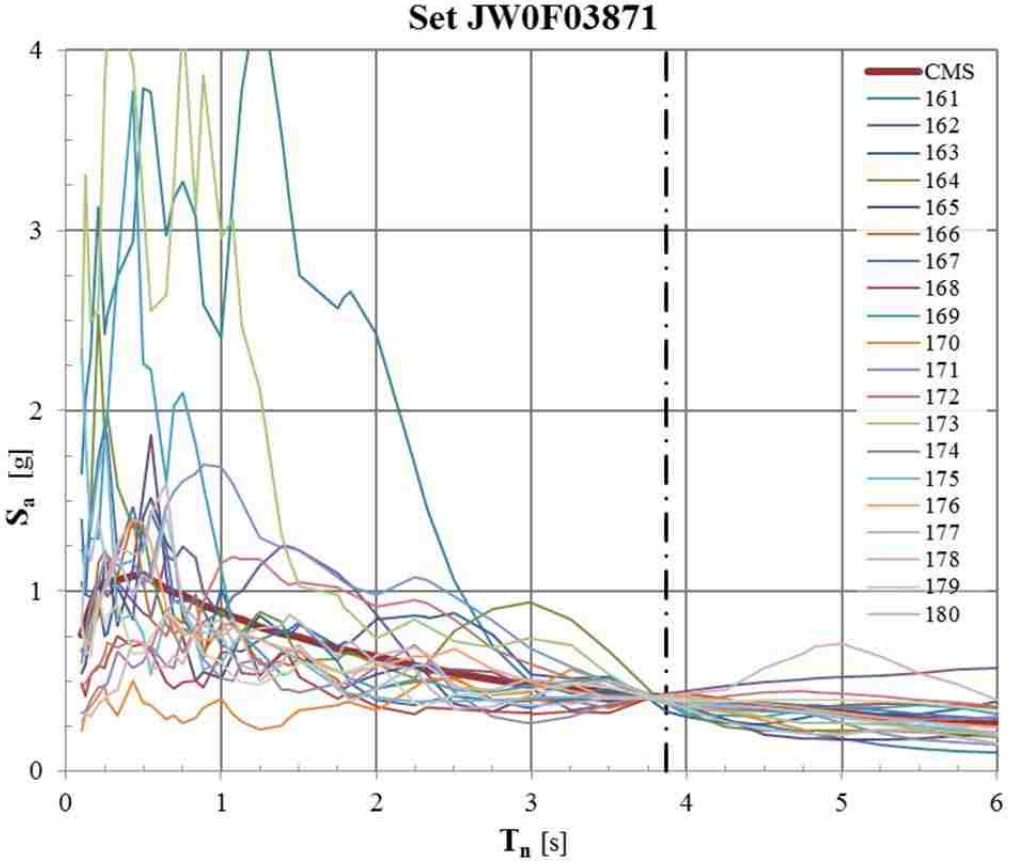

Ground Motion Set 10: JW0F05000 T_{cms} = 5.000 sec

$\bar{M}_{seis}$= 7.8079 $\bar{R}_{seis}$= 3.1400 $\bar{\varepsilon}$ = 1.2553

	RSN	Filename	M_{seis}	R_{seis}	Component[2]	SF_{GM}
181	1492	CHICHI/TCU052-N.at2	7.62	0.66	090	2.1065
182	1553	CHICHI/TCU141-W.at2	7.62	24.21	180	1.5525
183	1479	CHICHI/TCU034-E.at2	7.62	35.69	000	3.0362
184	1527	CHICHI/TCU100-E.at2	7.62	11.39	000	3.7775
185	1505	CHICHI/TCU068-N.at2	7.62	0.32	090	1.0126
186	1505	CHICHI/TCU068-E.at2	7.62	0.32	000	0.9572
187	1494	CHICHI/TCU054-N.at2	7.62	5.30	090	3.8145
188	1538	CHICHI/TCU112-N.at2	7.62	27.50	090	3.9127
189	1550	CHICHI/TCU136-N.at2	7.62	8.29	090	2.9015
190	1492	CHICHI/TCU052-E.at2	7.62	0.66	000	0.9059
191	1548	CHICHI/TCU128-E.at2	7.62	13.15	000	2.1695
192	1554	CHICHI/TCU145-W.at2	7.62	35.34	180	3.2410
193	1484	CHICHI/TCU042-E.at2	7.62	26.32	000	3.7491
194	1491	CHICHI/TCU051-E.at2	7.62	7.66	000	3.9391
195	1488	CHICHI/TCU048-E.at2	7.62	13.55	000	3.2935
196	143	TABAS/TAB-TR.at2	7.35	1.79	090	0.9185
197	1491	CHICHI/TCU051-N.at2	7.62	7.66	090	3.1173
198	779	LOMAP/LGP000.at2	6.93	3.88	000	1.7245
199	1233	CHICHI/CHY082-N.at2	7.62	36.11	090	3.5621
200	2114	DENALI/ps10047.at2	7.90	0.18	047	2.1499

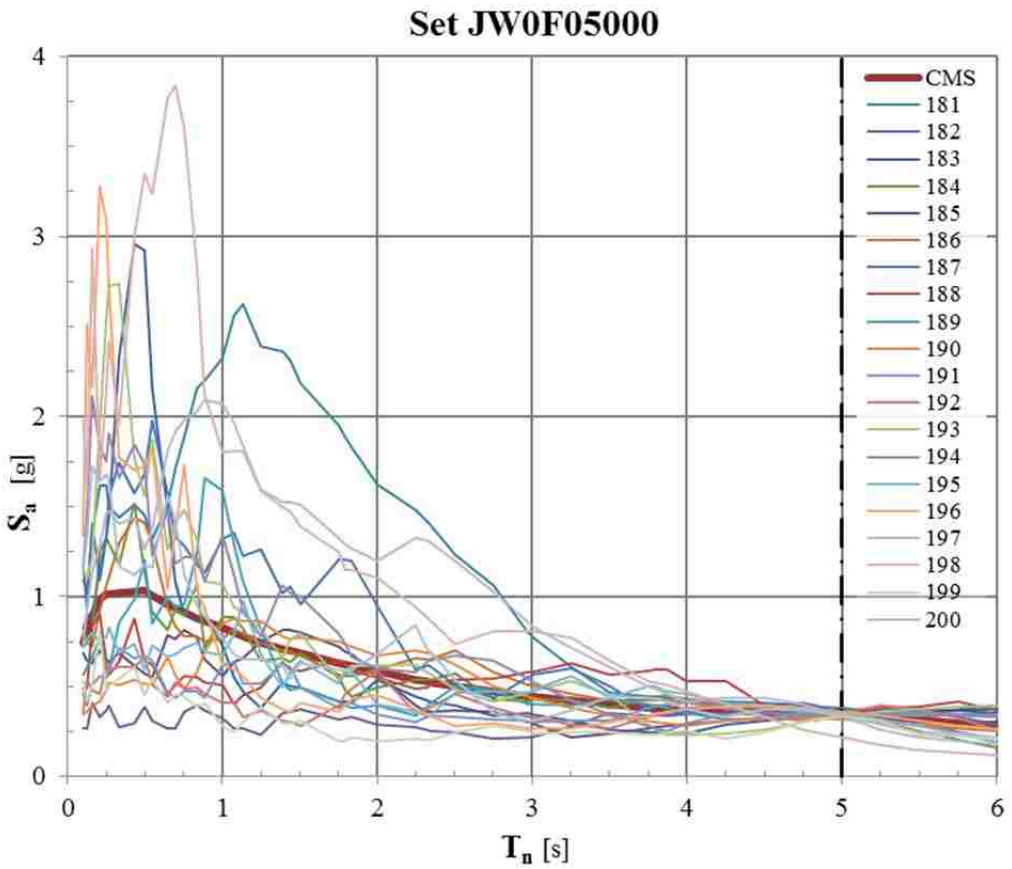

Appendix III Analysis Results

Median Ductility Demand

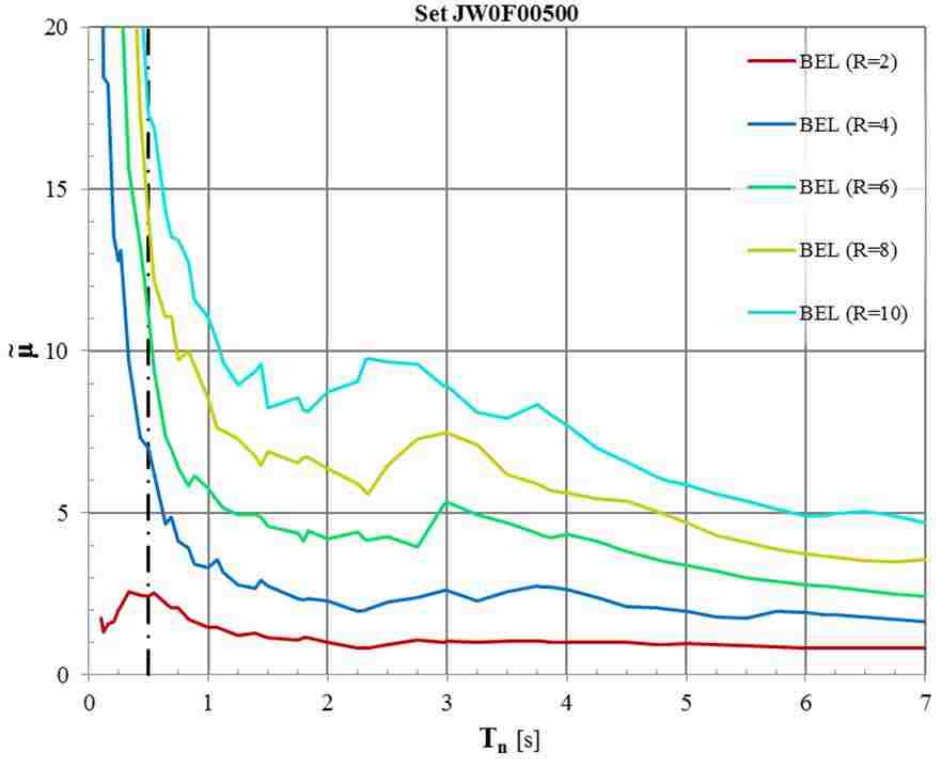
Set JW0F00500
BEL (R=2)
BEL (R=4)
BEL (R=6)
BEL (R=8)
BEL (R=10)
μ̃
T_n [s]

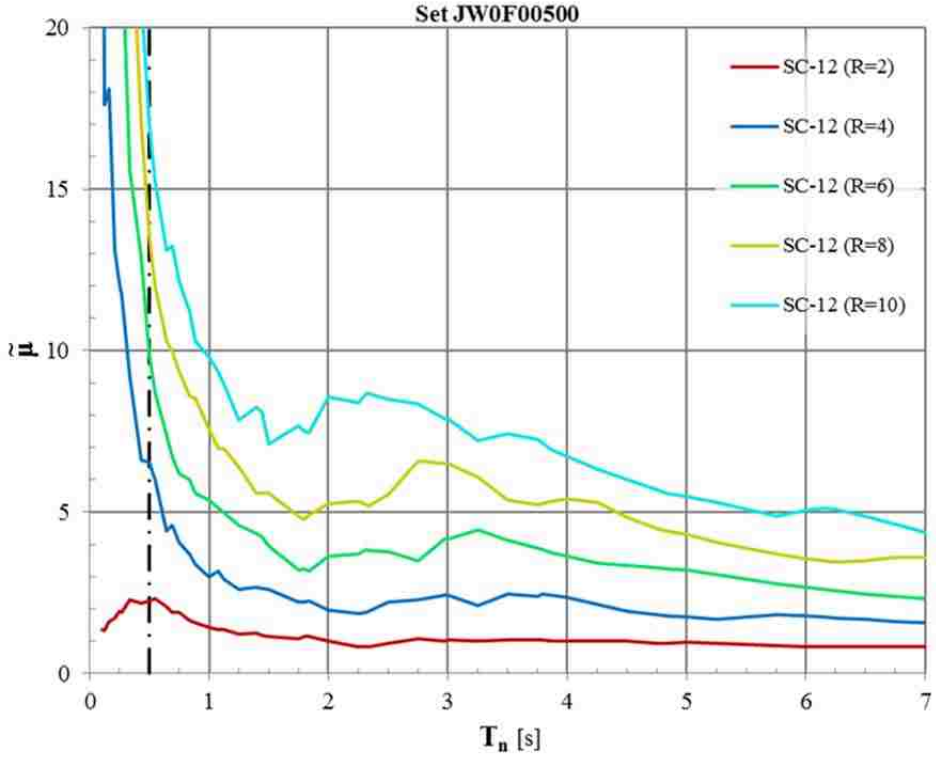
Set JW0F00500
SC-12 (R=2)
SC-12 (R=4)
SC-12 (R=6)
SC-12 (R=8)
SC-12 (R=10)
μ̃
T_n [s]

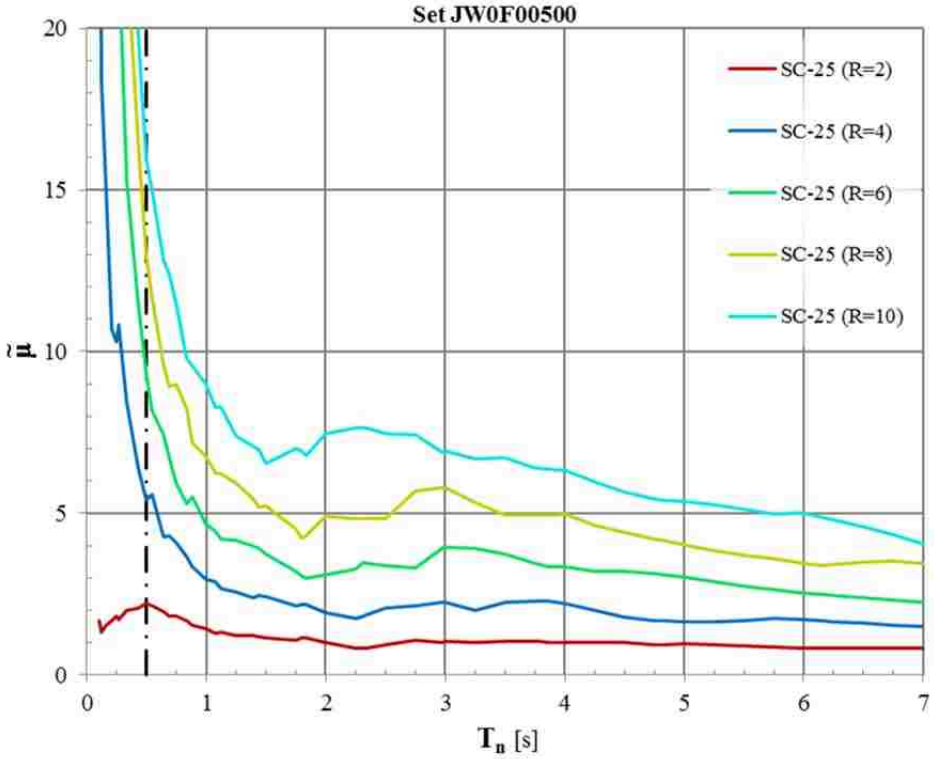
Set JW0F00500
SC-25 (R=2)
SC-25 (R=4)
SC-25 (R=6)
SC-25 (R=8)
SC-25 (R=10)
μ
T_n [s]

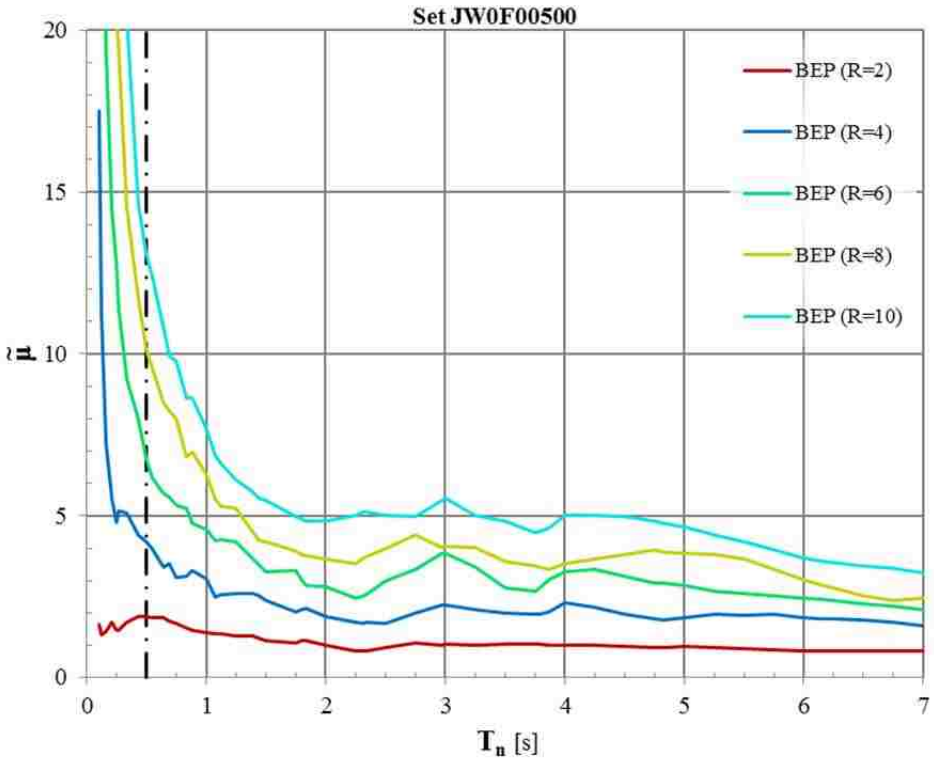
Set JW0F00500
BEP (R=2)
BEP (R=4)
BEP (R=6)
BEP (R=8)
BEP (R=10)
μ
T_n [s]

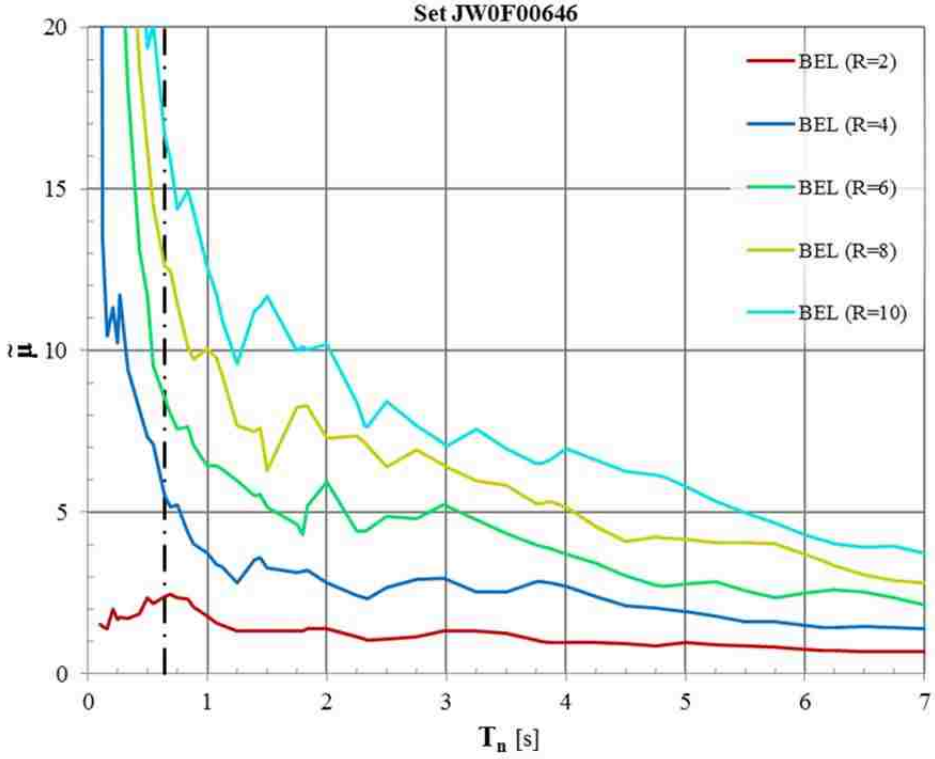
Set JW0F00646
BEL (R=2)
BEL (R=4)
BEL (R=6)
BEL (R=8)
BEL (R=10)
μ
T_n [s]

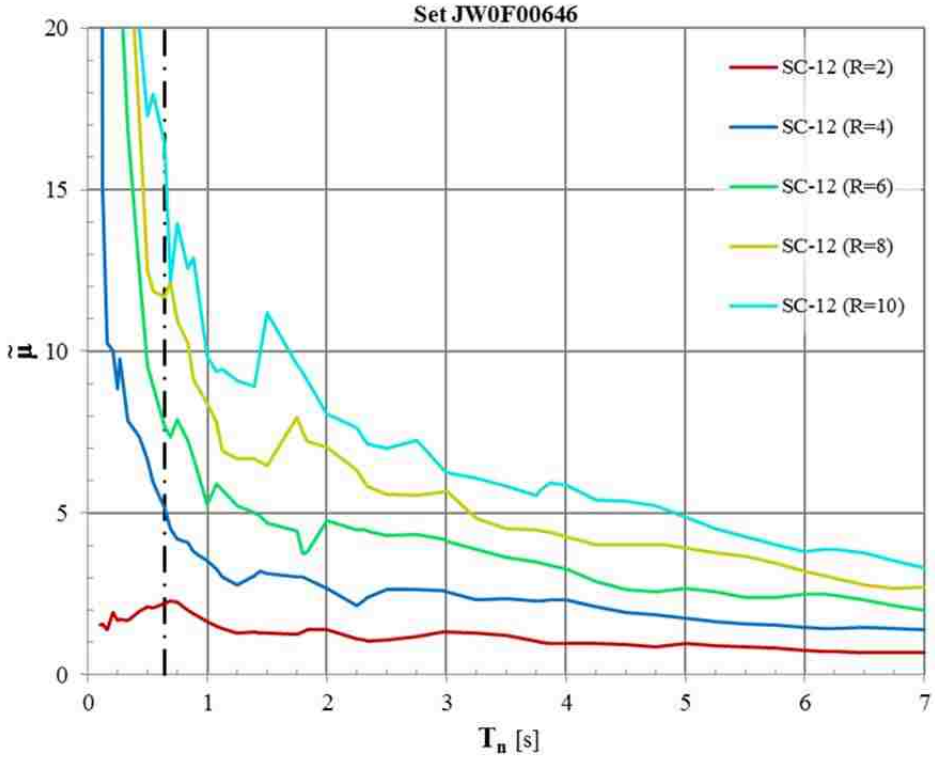
Set JW0F00646
SC-12 (R=2)
SC-12 (R=4)
SC-12 (R=6)
SC-12 (R=8)
SC-12 (R=10)
μ
T_n [s]

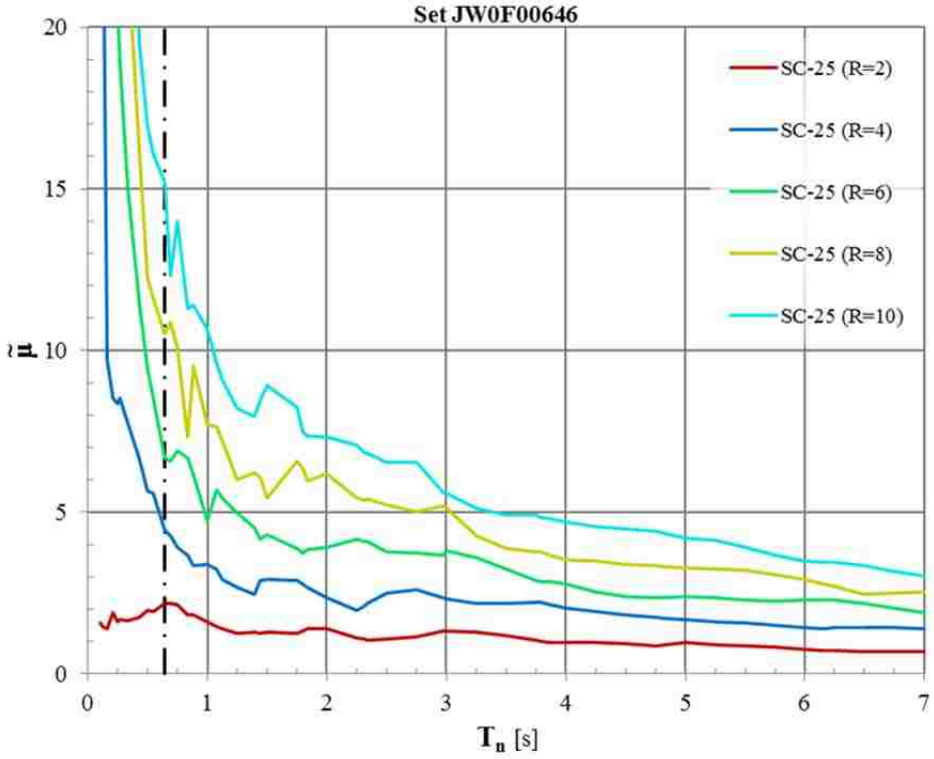
Set JW0F00646
SC-25 (R=2)
SC-25 (R=4)
SC-25 (R=6)
SC-25 (R=8)
SC-25 (R=10)
μ
T_n [s]

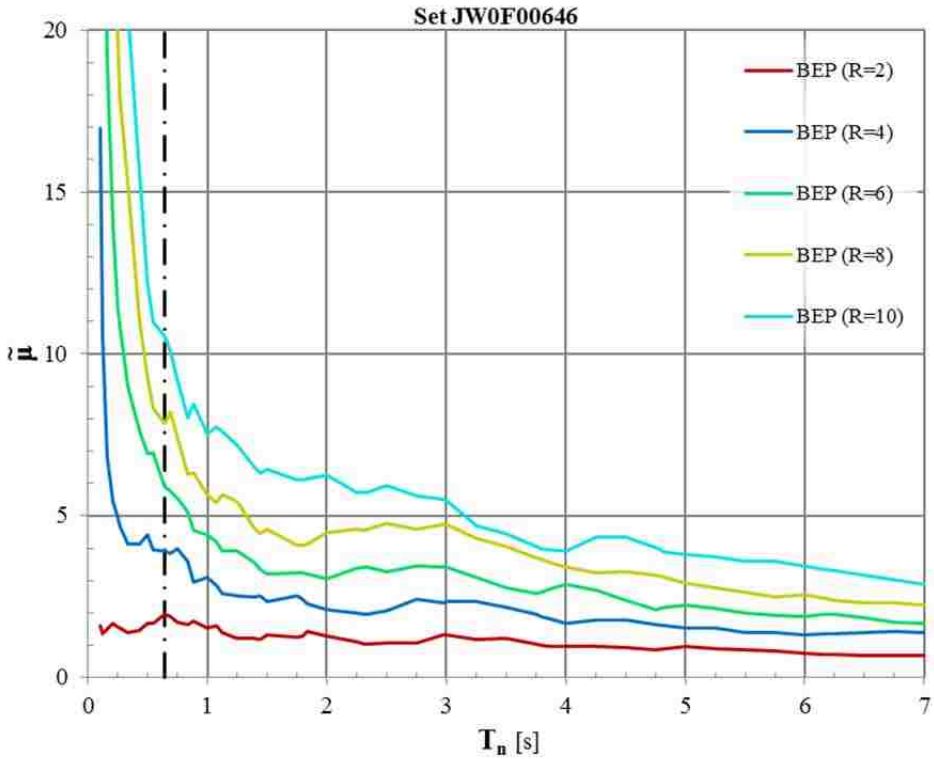
Set JW0F00646
BEP (R=2)
BEP (R=4)
BEP (R=6)
BEP (R=8)
BEP (R=10)
μ
T_n [s]

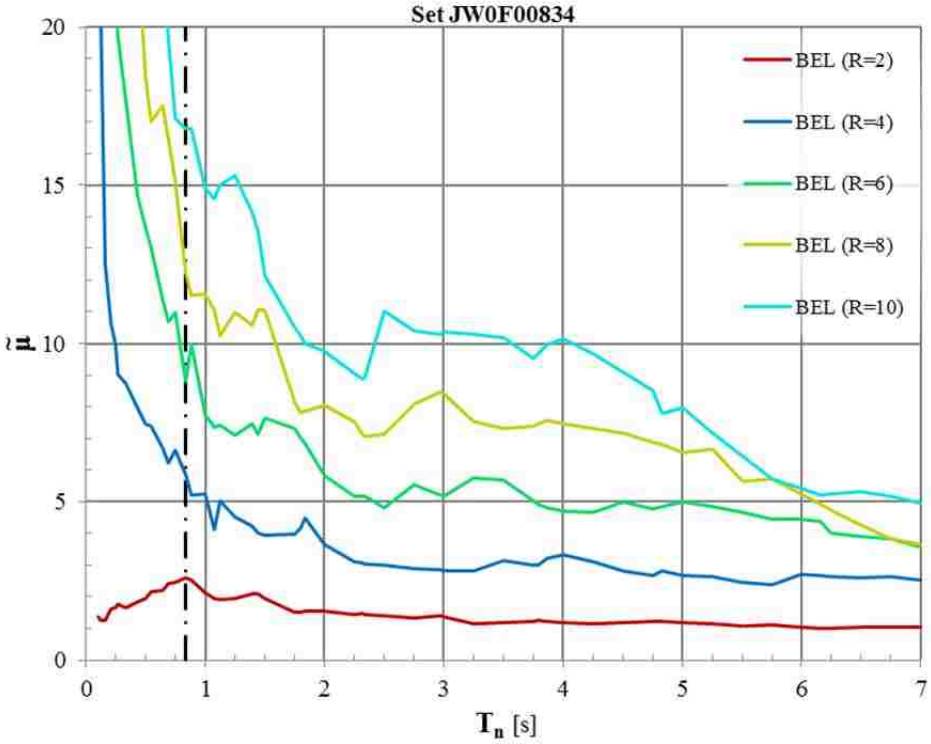
Set JW0F00834
BEL (R=2)
BEL (R=4)
BEL (R=6)
BEL (R=8)
BEL (R=10)
μ
T_n [s]

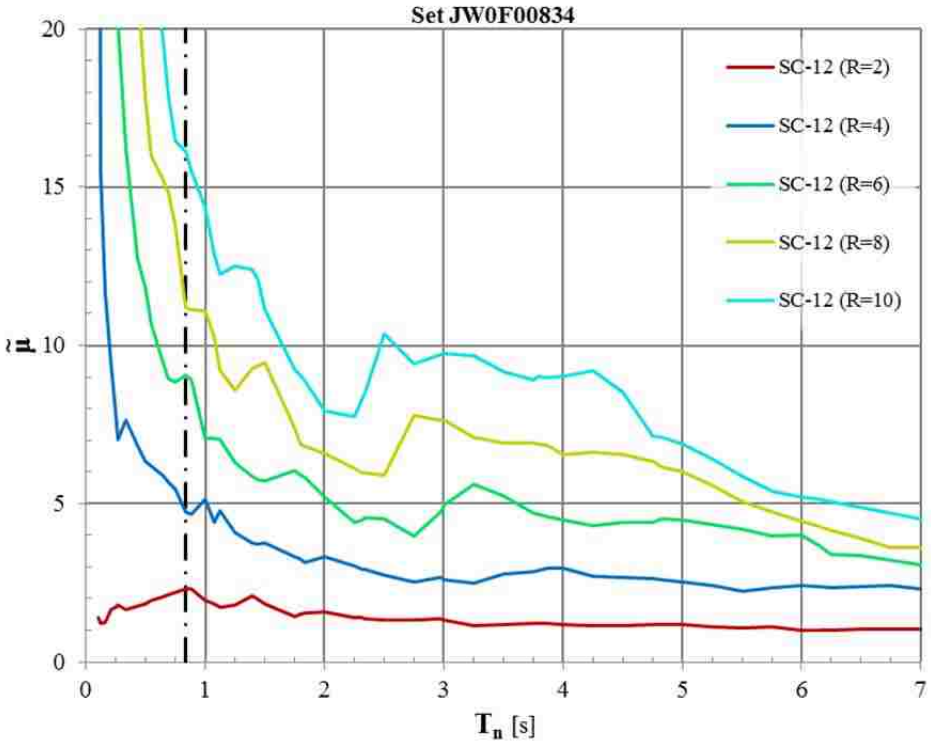
Set JW0F00834
SC-12 (R=2)
SC-12 (R=4)
SC-12 (R=6)
SC-12 (R=8)
SC-12 (R=10)
μ
T_n [s]

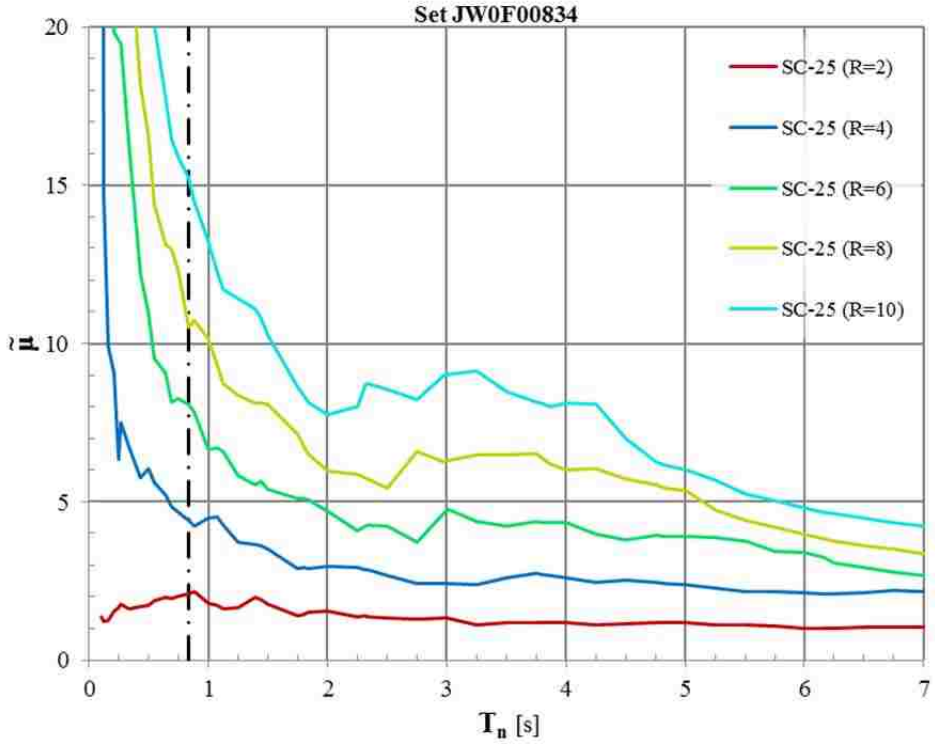
Set JW0F00834
SC-25 (R=2)
SC-25 (R=4)
SC-25 (R=6)
SC-25 (R=8)
SC-25 (R=10)
μ
T_n [s]

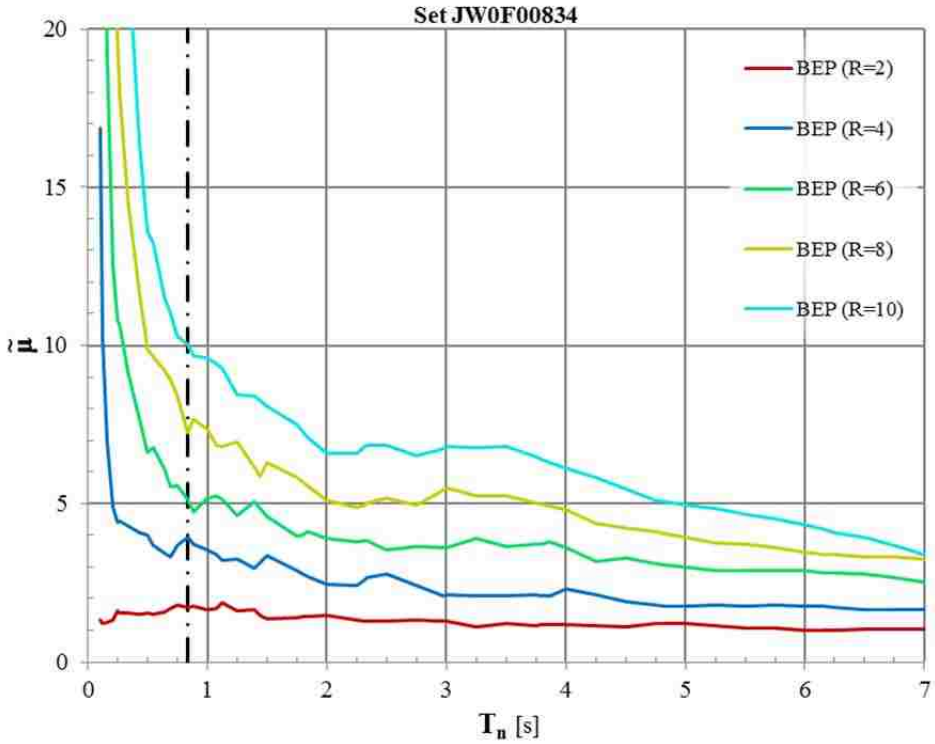
Set JW0F00834
BEP (R=2)
BEP (R=4)
BEP (R=6)
BEP (R=8)
BEP (R=10)
μ
T_n [s]

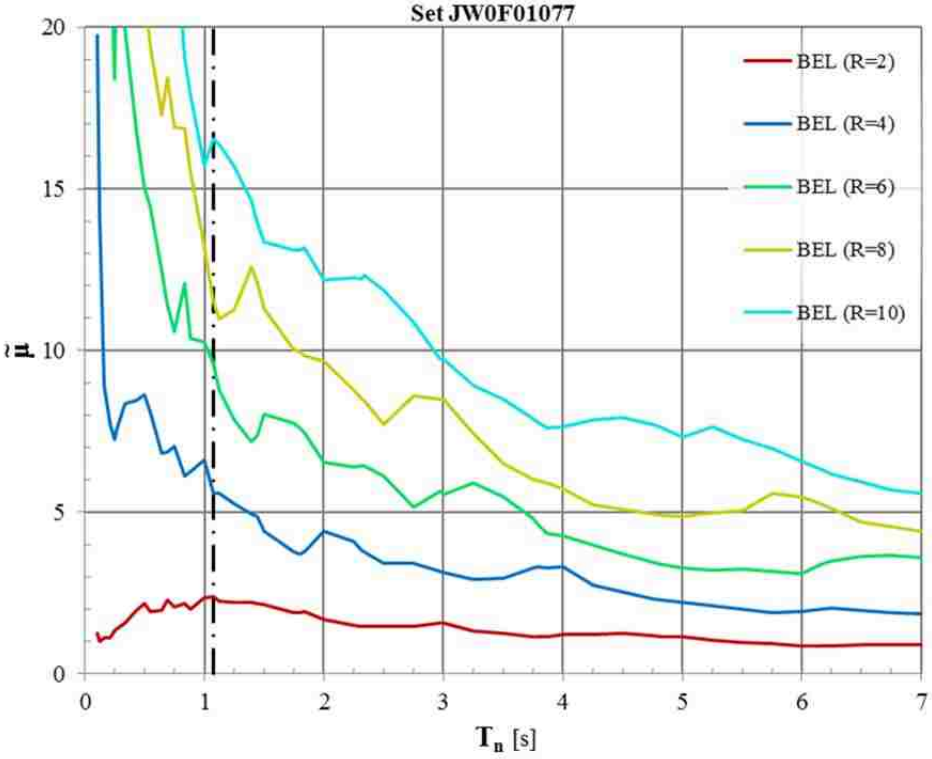
Set JW0F01077
BEL (R=2)
BEL (R=4)
BEL (R=6)
BEL (R=8)
BEL (R=10)
μ
T_n [s]

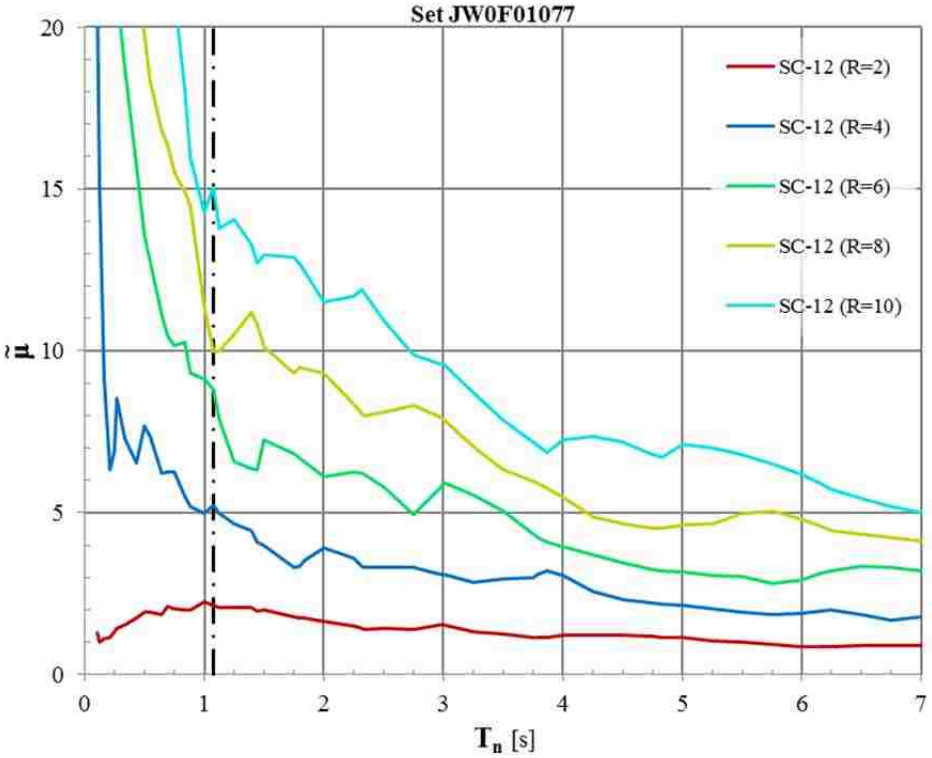
Set JW0F01077
SC-12 (R=2)
SC-12 (R=4)
SC-12 (R=6)
SC-12 (R=8)
SC-12 (R=10)
μ
T_n [s]

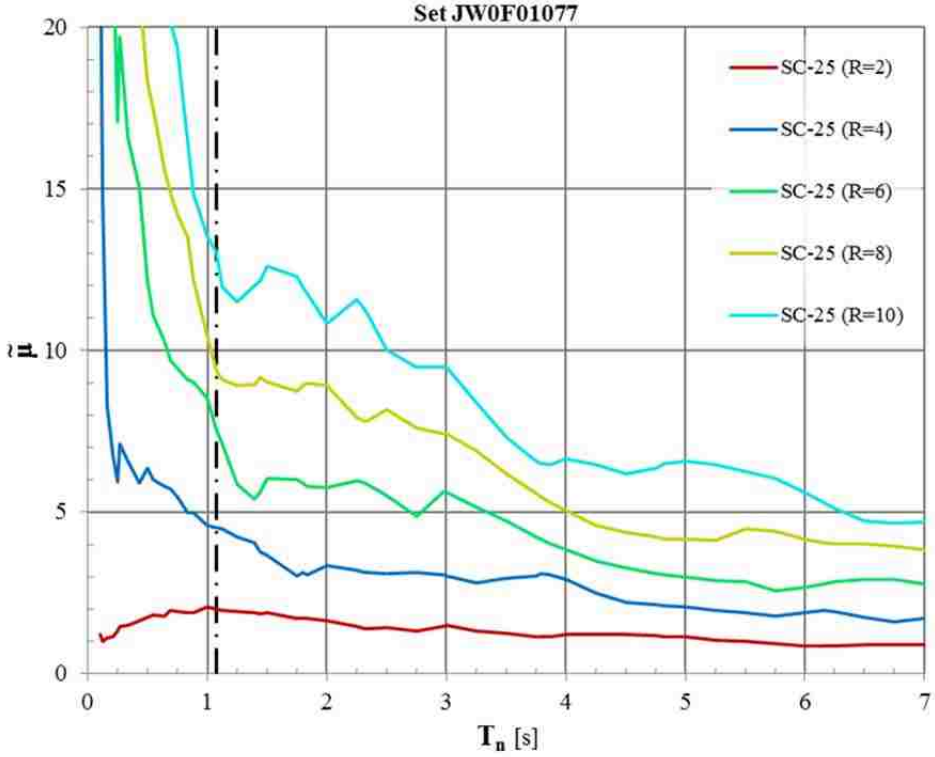
Set JW0F01077
SC-25 (R=2)
SC-25 (R=4)
SC-25 (R=6)
SC-25 (R=8)
SC-25 (R=10)
μ
T_n [s]

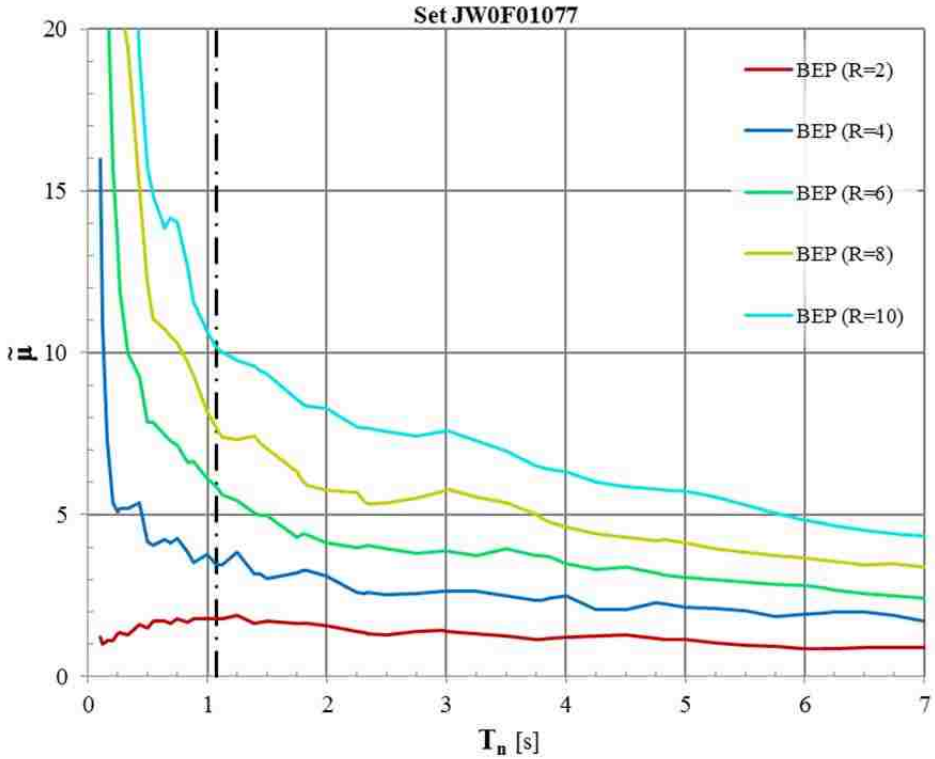
Set JW0F01077
BEP (R=2)
BEP (R=4)
BEP (R=6)
BEP (R=8)
BEP (R=10)
μ
T_n [s]

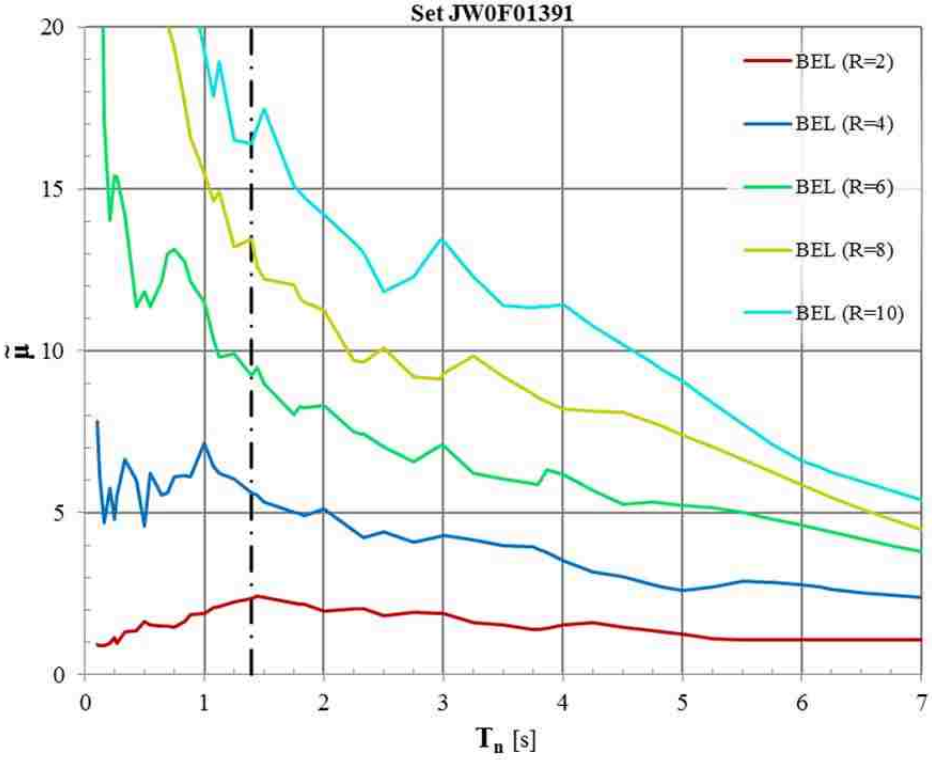
Set JW0F01391
BEL (R=2)
BEL (R=4)
BEL (R=6)
BEL (R=8)
BEL (R=10)
μ
0
5
10
15
20
0
1
2
3
4
5
6
7
T_n [s]

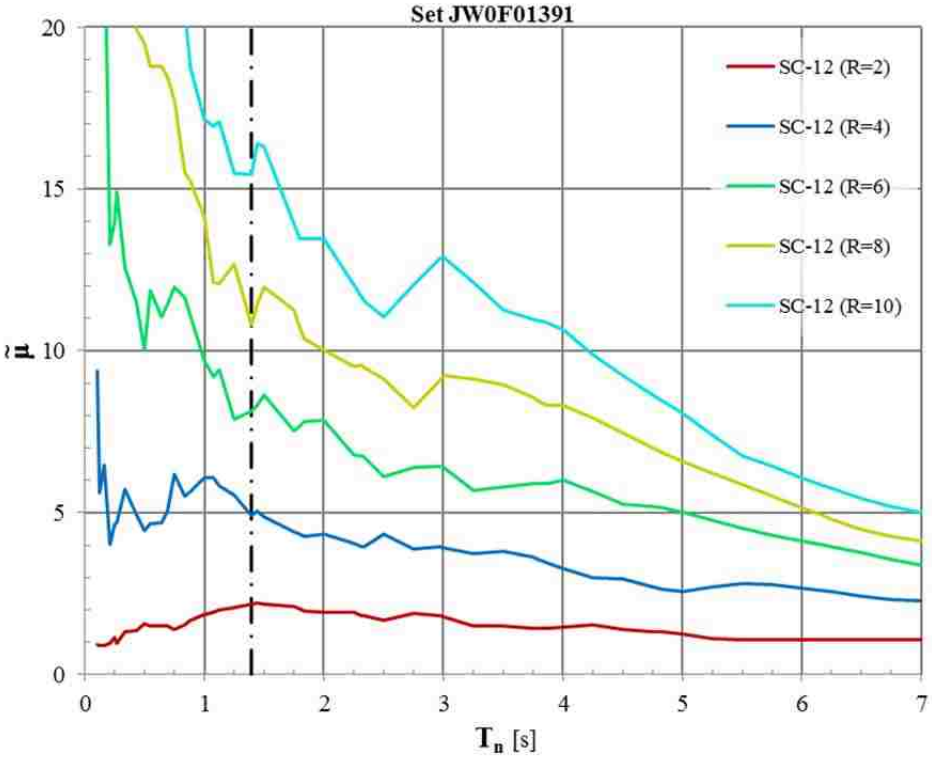
Set JW0F01391
SC-12 (R=2)
SC-12 (R=4)
SC-12 (R=6)
SC-12 (R=8)
SC-12 (R=10)
μ
0
5
10
15
20
0
1
2
3
4
5
6
7
T_n [s]

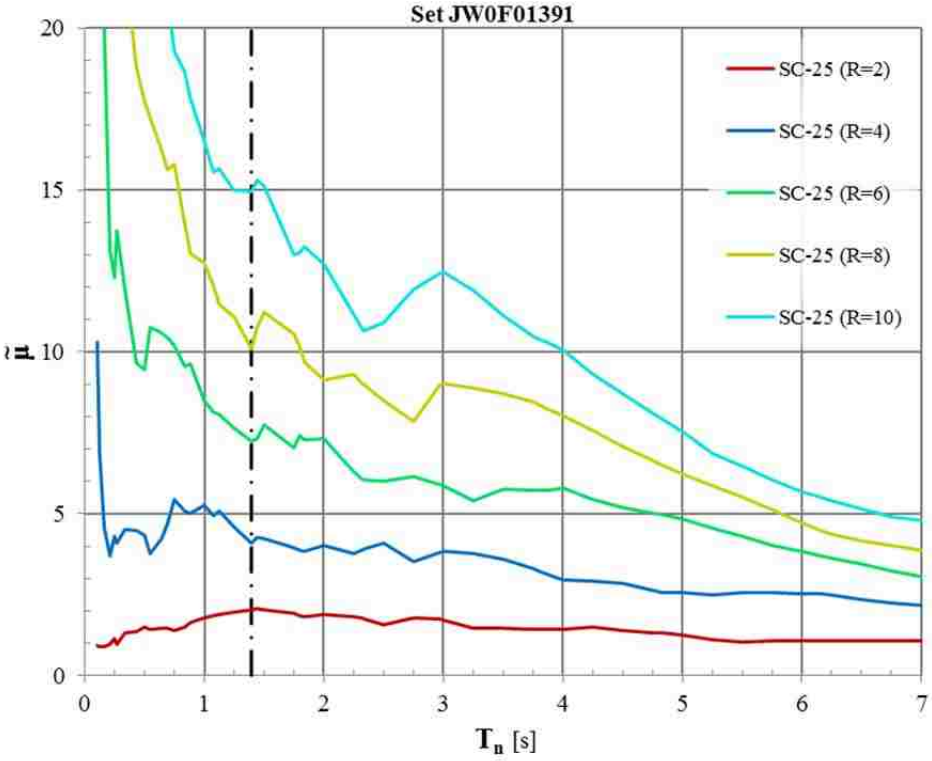
Set JW0F01391
SC-25 (R=2)
SC-25 (R=4)
SC-25 (R=6)
SC-25 (R=8)
SC-25 (R=10)
μ
0
5
10
15
20
0
1
2
3
4
5
6
7
T_n [s]

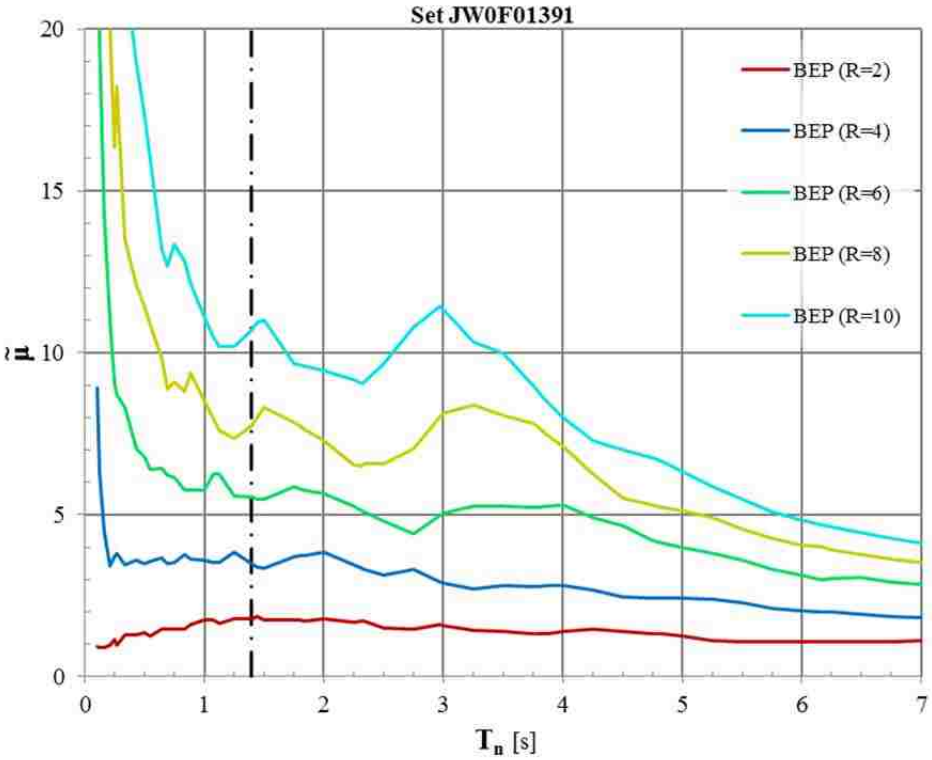
Set JW0F01391
BEP (R=2)
BEP (R=4)
BEP (R=6)
BEP (R=8)
BEP (R=10)
μ
0
5
10
15
20
0
1
2
3
4
5
6
7
T_n [s]

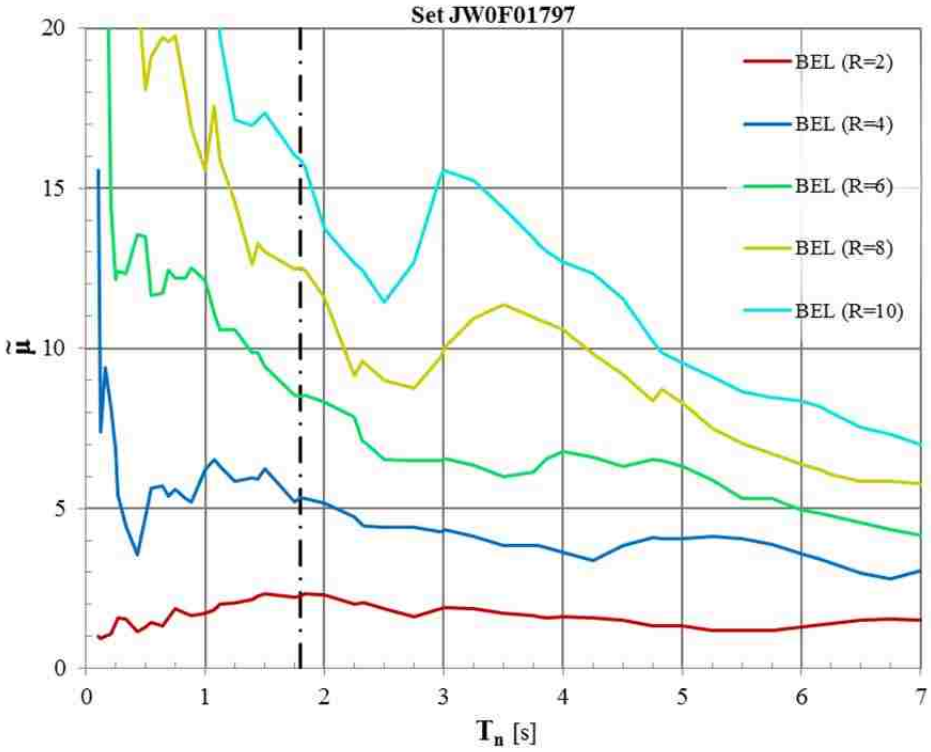
Set JW0F01797
BEL (R=2)
BEL (R=4)
BEL (R=6)
BEL (R=8)
BEL (R=10)
μ
0
5
10
15
20
0
1
2
3
4
5
6
7
T_n [s]

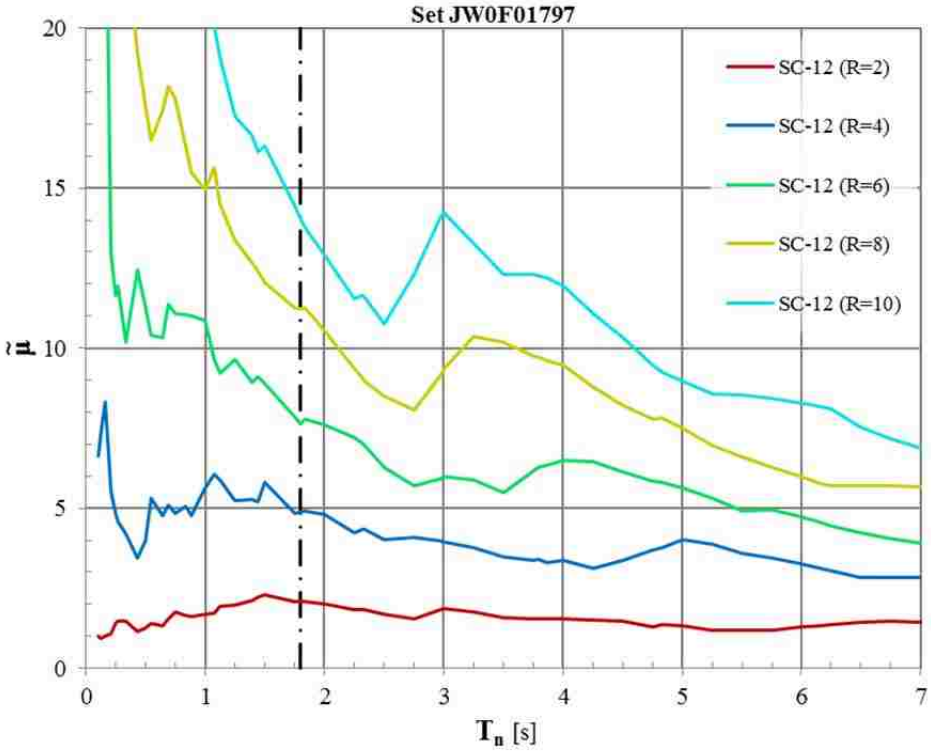
Set JW0F01797
SC-12 (R=2)
SC-12 (R=4)
SC-12 (R=6)
SC-12 (R=8)
SC-12 (R=10)
μ
0
5
10
15
20
0
1
2
3
4
5
6
7
T_n [s]

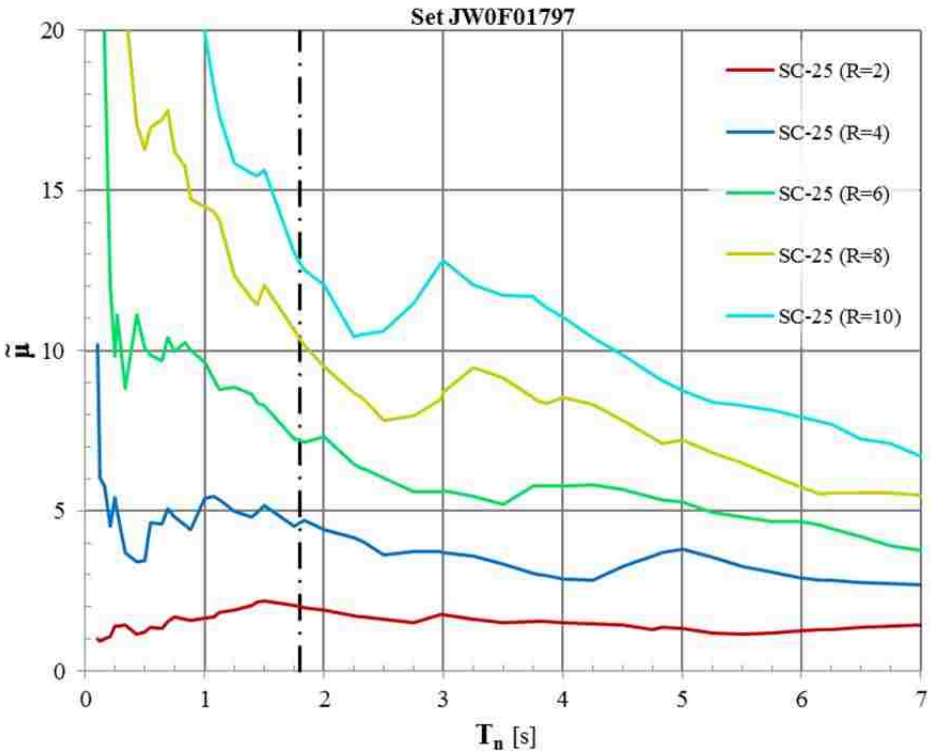
Set JW0F01797
SC-25 (R=2)
SC-25 (R=4)
SC-25 (R=6)
SC-25 (R=8)
SC-25 (R=10)
μ
T_n [s]

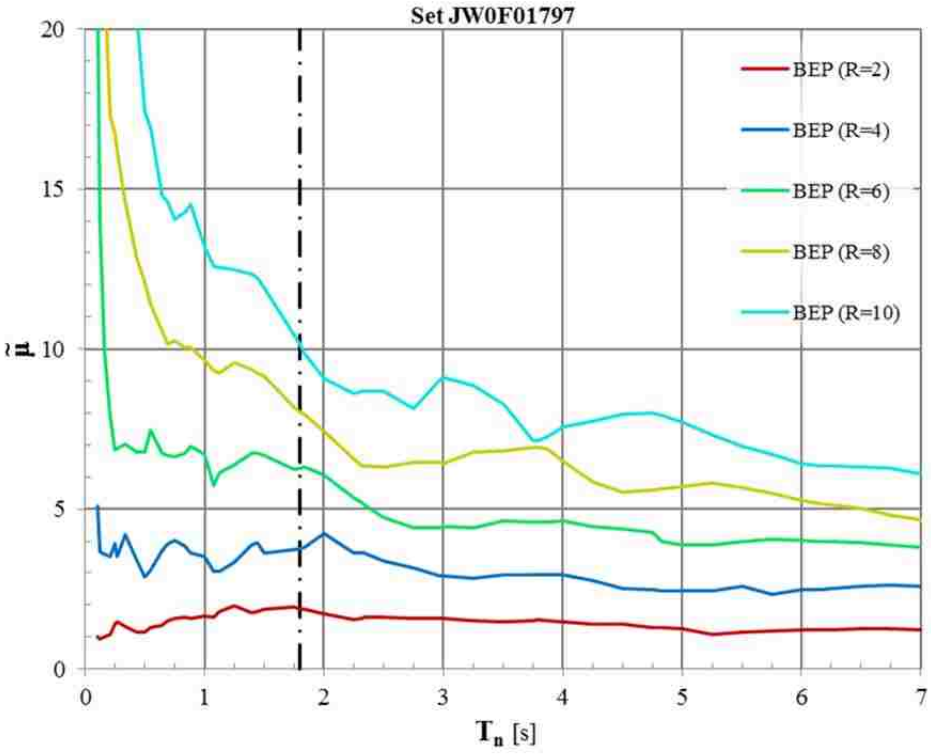
Set JW0F01797
BEP (R=2)
BEP (R=4)
BEP (R=6)
BEP (R=8)
BEP (R=10)
μ
T_n [s]

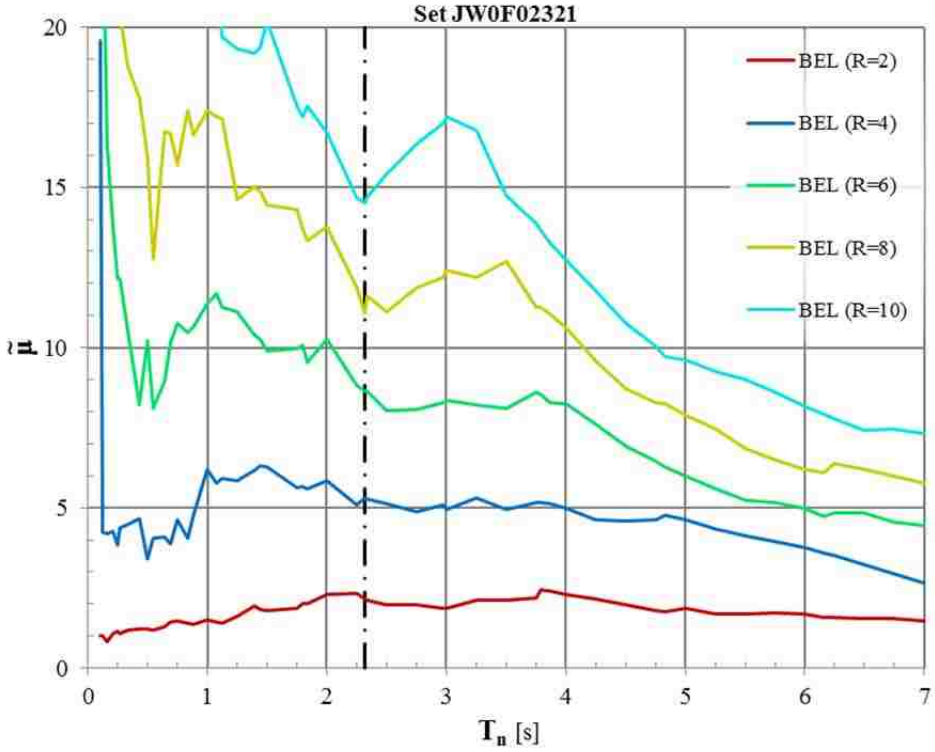
Set JW0F02321
BEL (R=2)
BEL (R=4)
BEL (R=6)
BEL (R=8)
BEL (R=10)
μ
20
15
10
5
0
0
1
2
3
4
5
6
7
T_n [s]

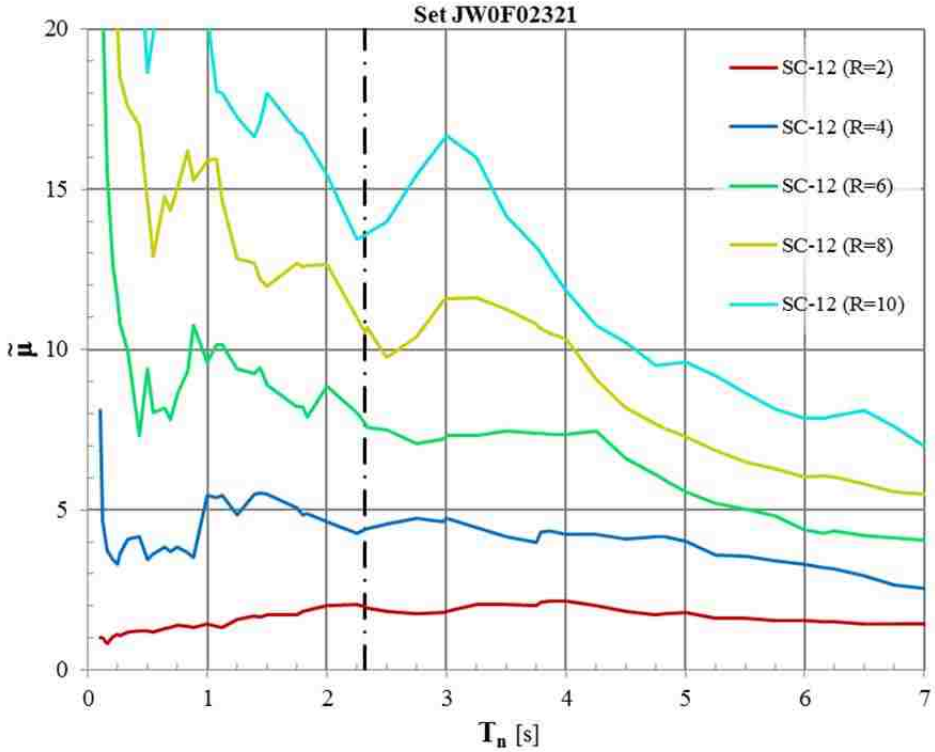
Set JW0F02321
SC-12 (R=2)
SC-12 (R=4)
SC-12 (R=6)
SC-12 (R=8)
SC-12 (R=10)
μ
20
15
10
5
0
0
1
2
3
4
5
6
7
T_n [s]

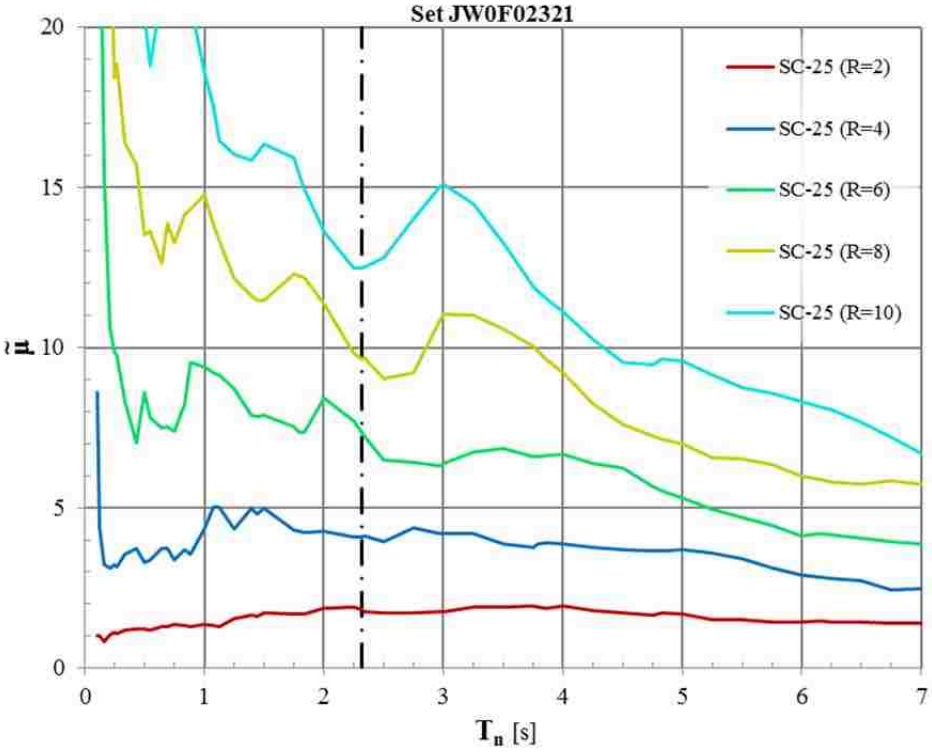
Set JW0F02321
SC-25 (R=2)
SC-25 (R=4)
SC-25 (R=6)
SC-25 (R=8)
SC-25 (R=10)
μ
T_n [s]

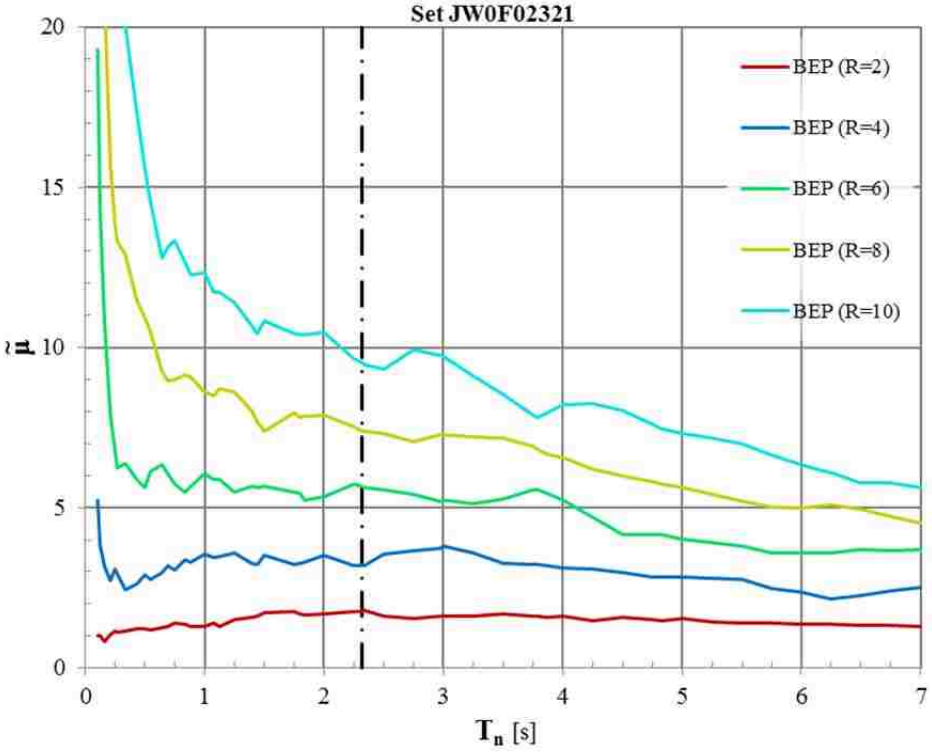
Set JW0F02321
BEP (R=2)
BEP (R=4)
BEP (R=6)
BEP (R=8)
BEP (R=10)
μ
T_n [s]

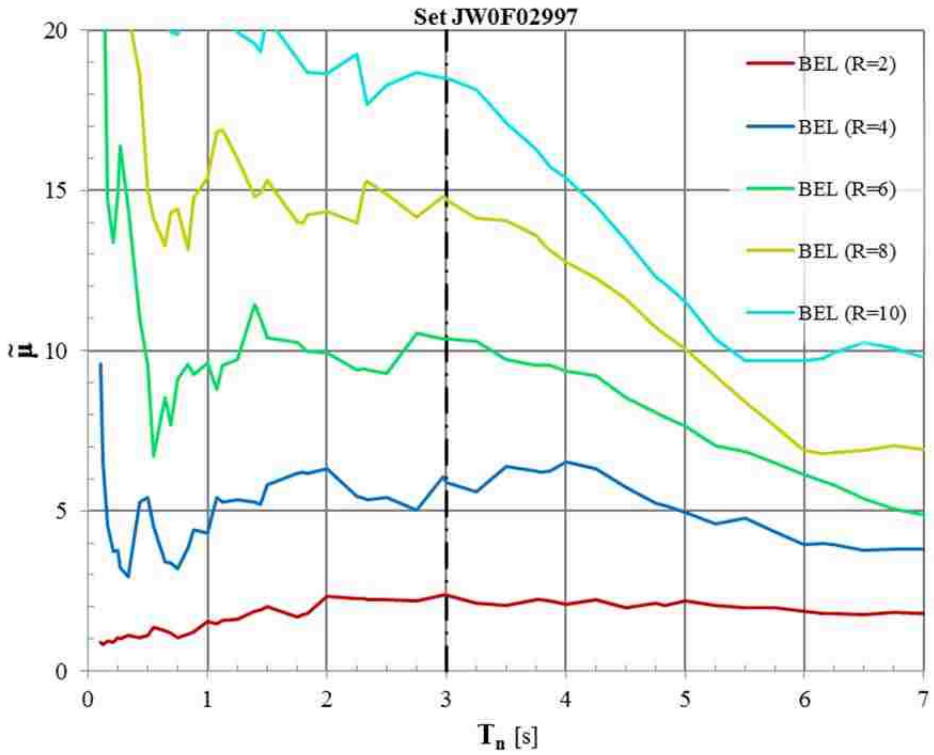
Set JW0F02997
BEL (R=2)
BEL (R=4)
BEL (R=6)
BEL (R=8)
BEL (R=10)
μ
0
5
10
15
20
0
1
2
3
4
5
6
7
T_n [s]

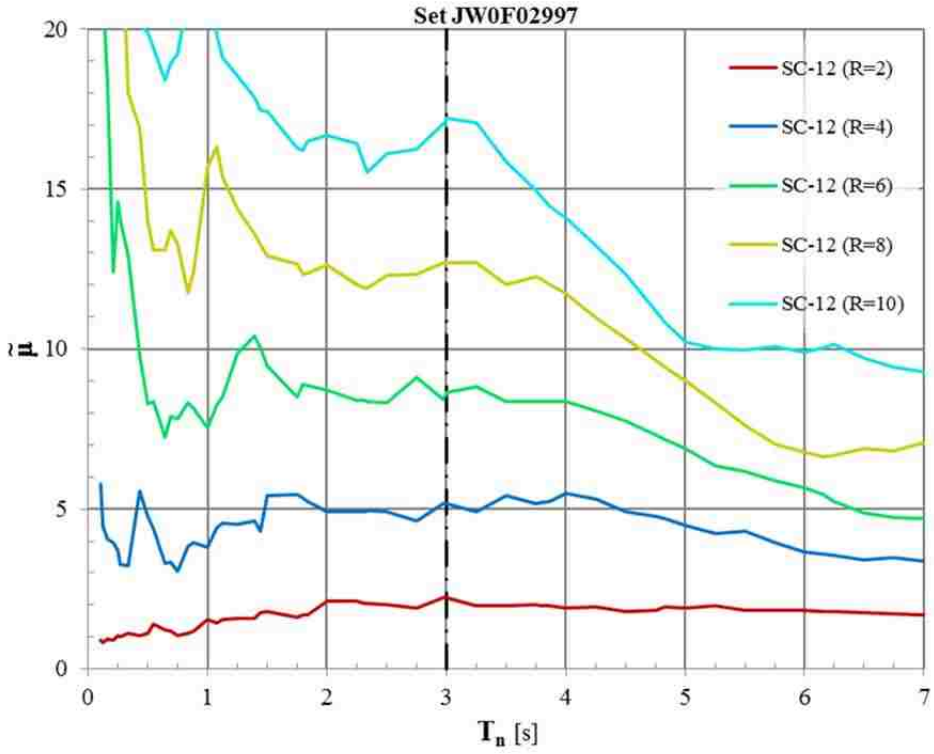
Set JW0F02997
SC-12 (R=2)
SC-12 (R=4)
SC-12 (R=6)
SC-12 (R=8)
SC-12 (R=10)
μ
0
5
10
15
20
0
1
2
3
4
5
6
7
T_n [s]

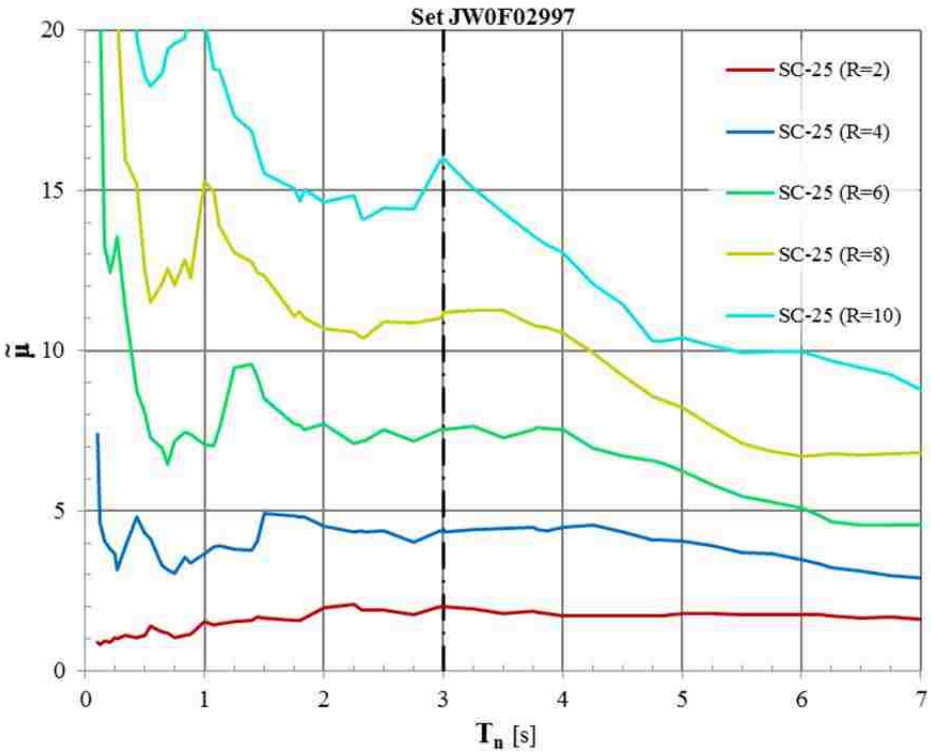
Set JW0F02997
SC-25 (R=2)
SC-25 (R=4)
SC-25 (R=6)
SC-25 (R=8)
SC-25 (R=10)
μ
0
5
10
15
20
0
1
2
3
4
5
6
7
T_n [s]

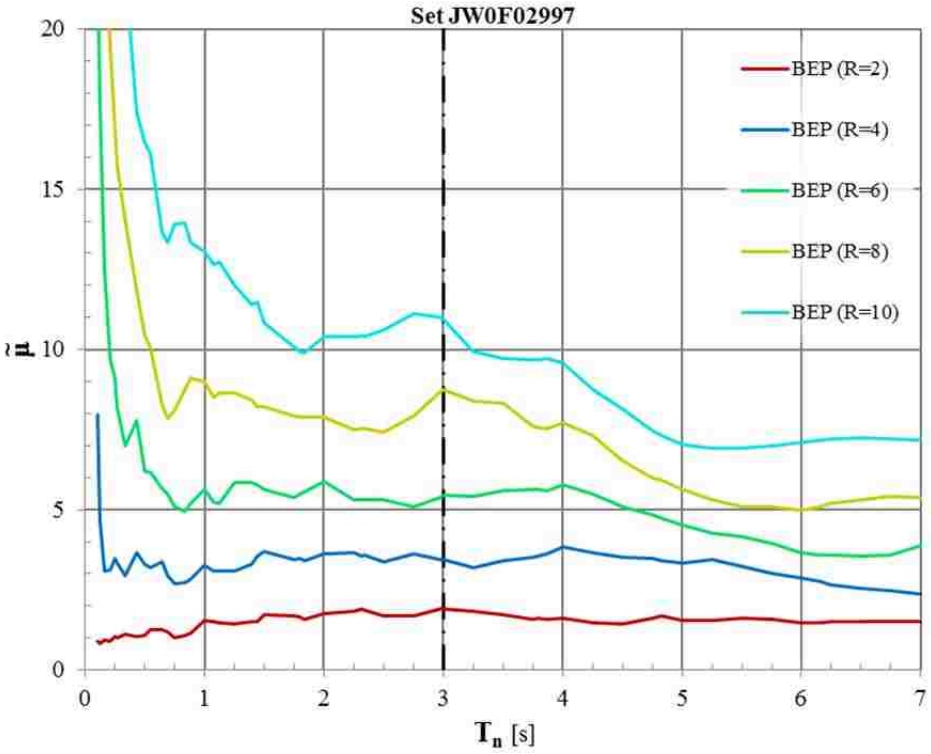
Set JW0F02997
BEP (R=2)
BEP (R=4)
BEP (R=6)
BEP (R=8)
BEP (R=10)
μ
0
5
10
15
20
0
1
2
3
4
5
6
7
T_n [s]

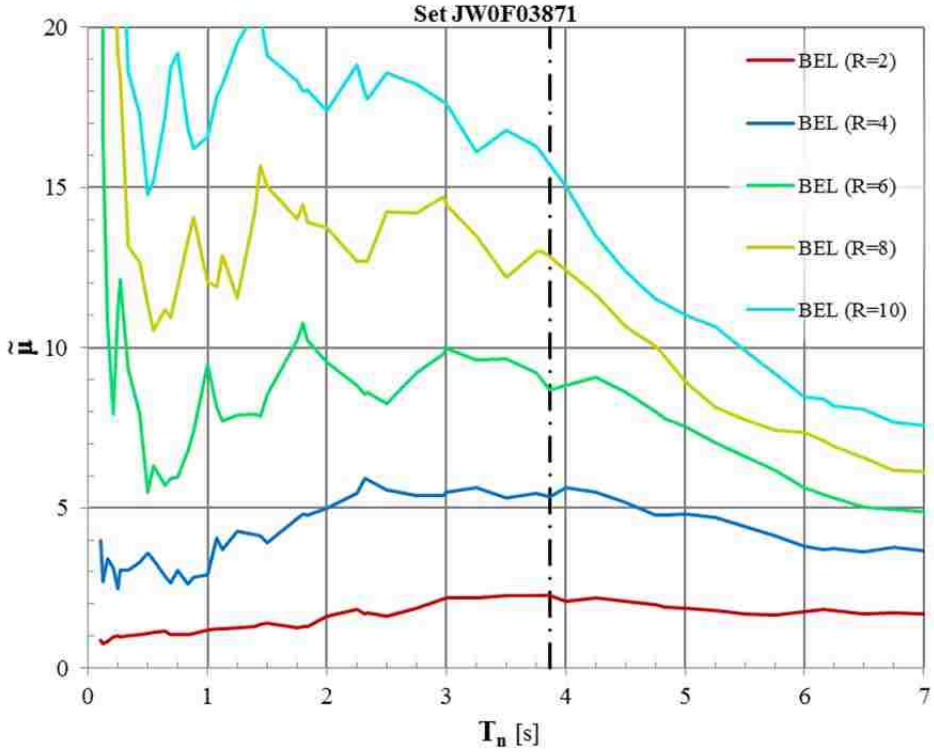
Set JW0F03871
BEL (R=2)
BEL (R=4)
BEL (R=6)
BEL (R=8)
BEL (R=10)
μ
0
5
10
15
20
0
1
2
3
4
5
6
7
T_n [s]

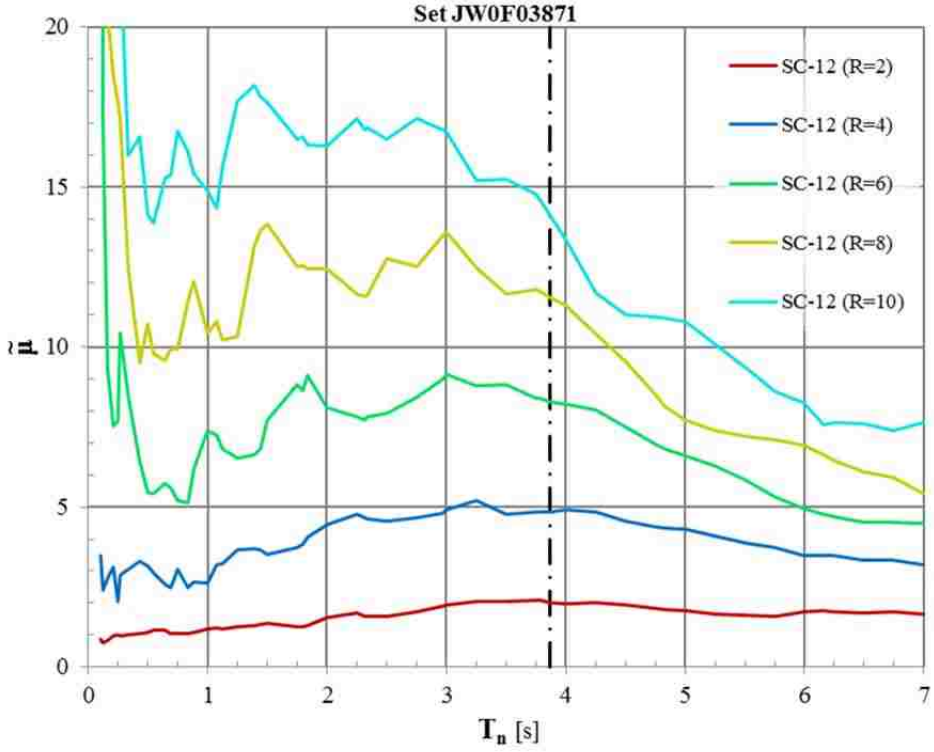
Set JW0F03871
SC-12 (R=2)
SC-12 (R=4)
SC-12 (R=6)
SC-12 (R=8)
SC-12 (R=10)
μ
0
5
10
15
20
0
1
2
3
4
5
6
7
T_n [s]

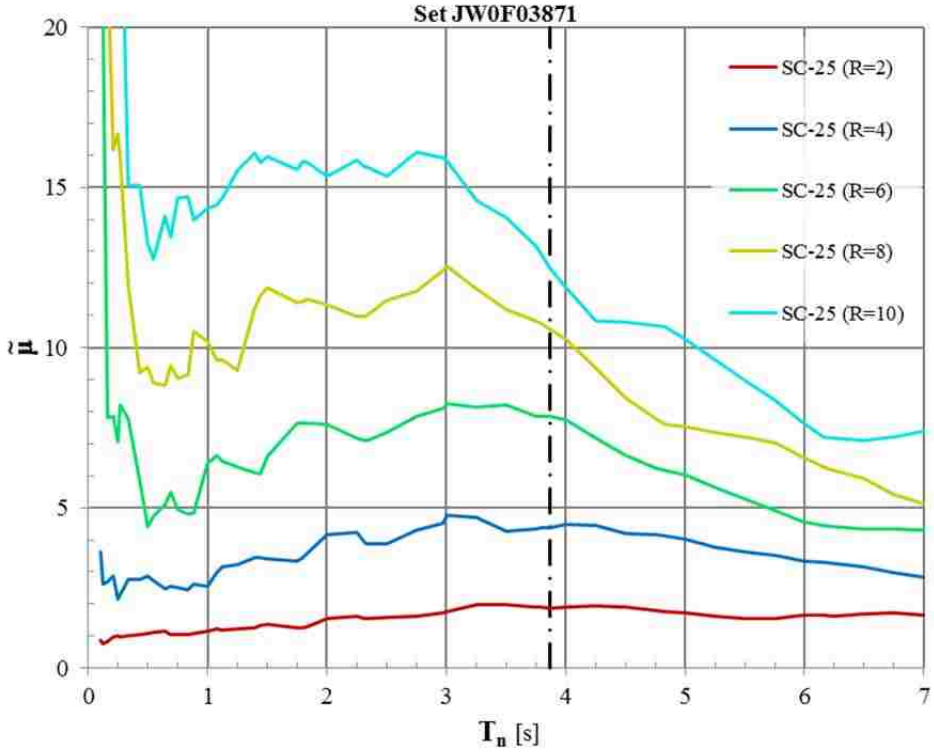
Set JW0F03871
SC-25 (R=2)
SC-25 (R=4)
SC-25 (R=6)
SC-25 (R=8)
SC-25 (R=10)
μ
0
5
10
15
20
0
1
2
3
4
5
6
7
T_n [s]

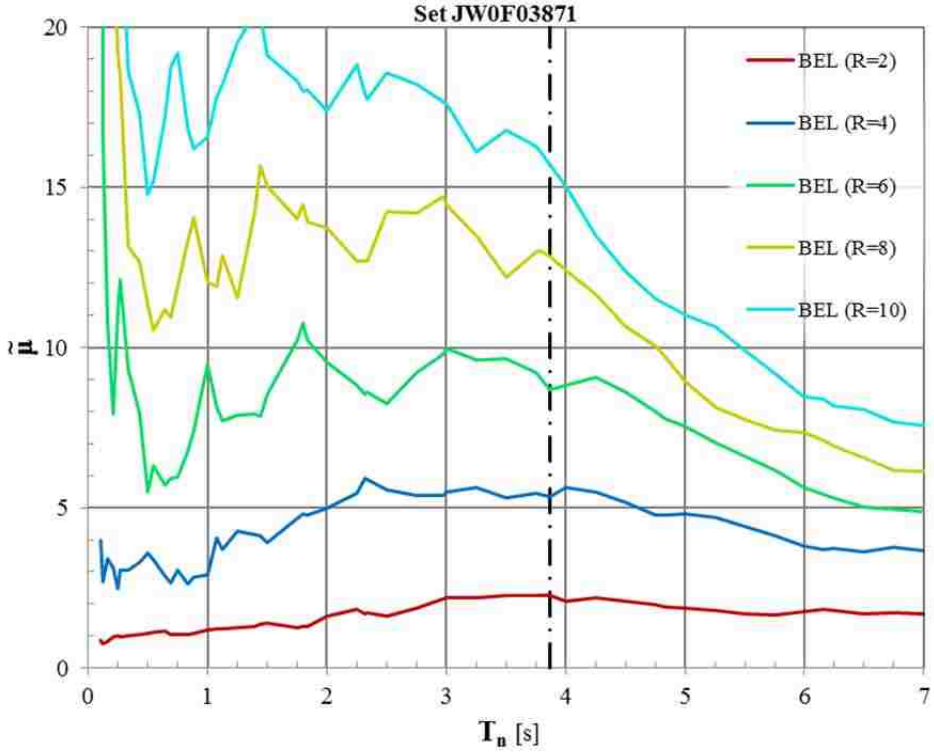
Set JW0F03871
BEL (R=2)
BEL (R=4)
BEL (R=6)
BEL (R=8)
BEL (R=10)
μ
0
5
10
15
20
0
1
2
3
4
5
6
7
T_n [s]

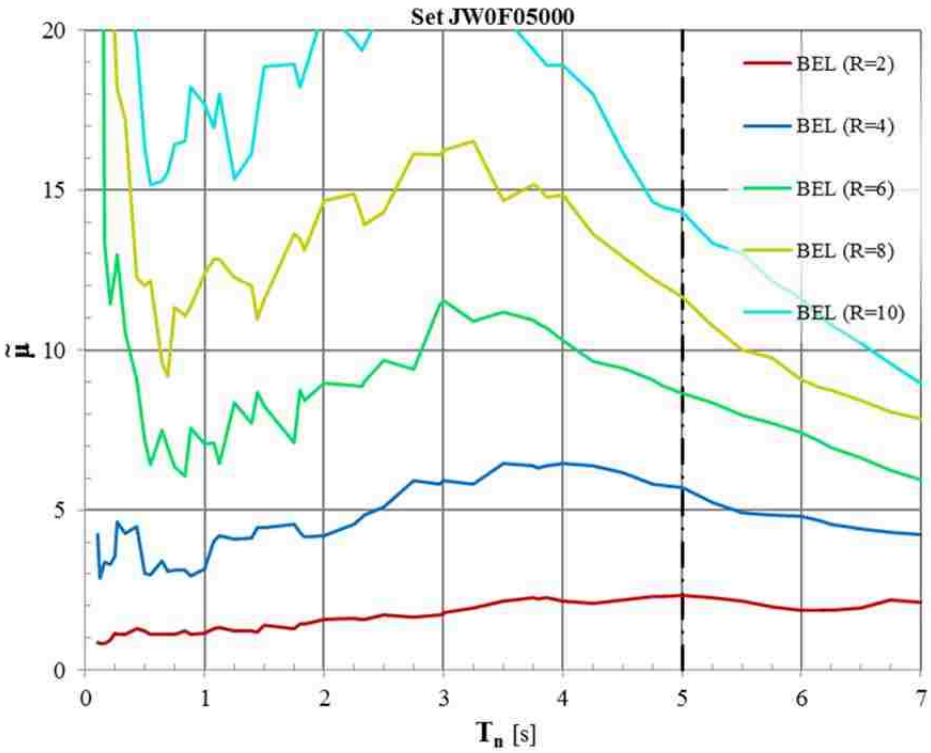
Set JW0F05000
BEL (R=2)
BEL (R=4)
BEL (R=6)
BEL (R=8)
BEL (R=10)
μ
0
5
10
15
20
0
1
2
3
4
5
6
7
T_n [s]

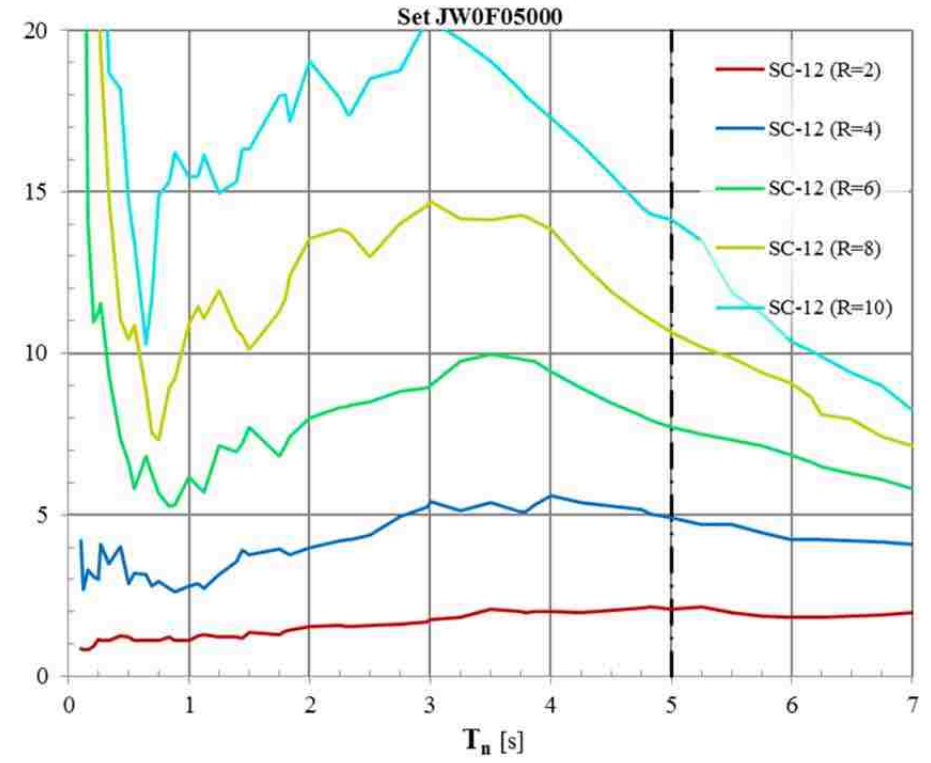
Set JW0F05000
SC-12 (R=2)
SC-12 (R=4)
SC-12 (R=6)
SC-12 (R=8)
SC-12 (R=10)
0
5
10
15
20
0
1
2
3
4
5
6
7
T_n [s]

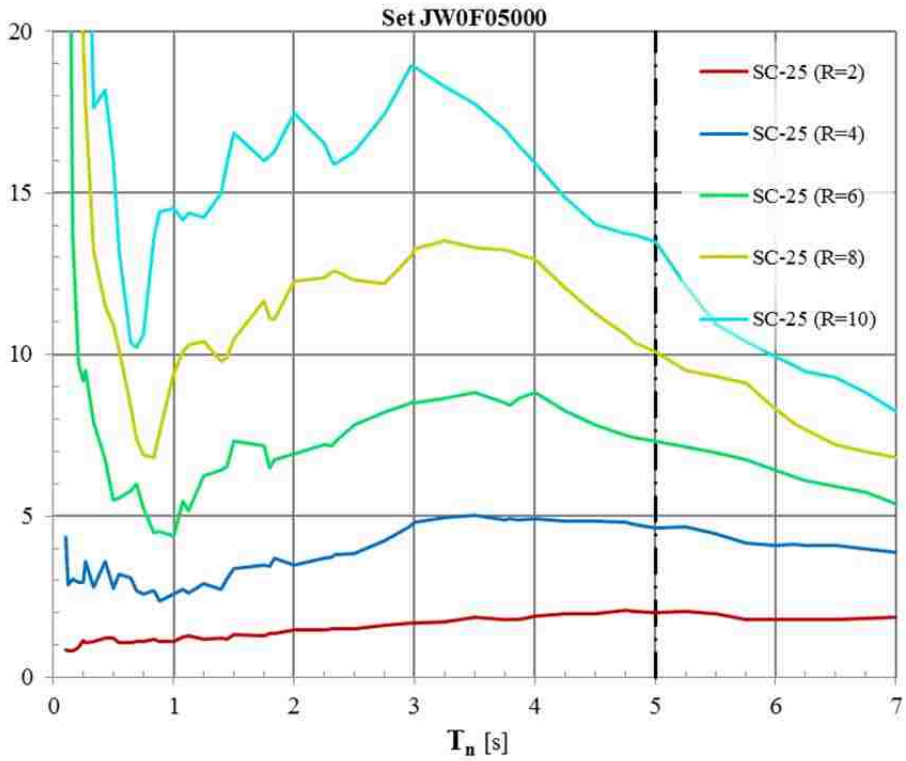
Set JW0F05000
SC-25 (R=2)
SC-25 (R=4)
SC-25 (R=6)
SC-25 (R=8)
SC-25 (R=10)
20
15
10
5
0
0
1
2
3
4
5
6
7
T_n [s]

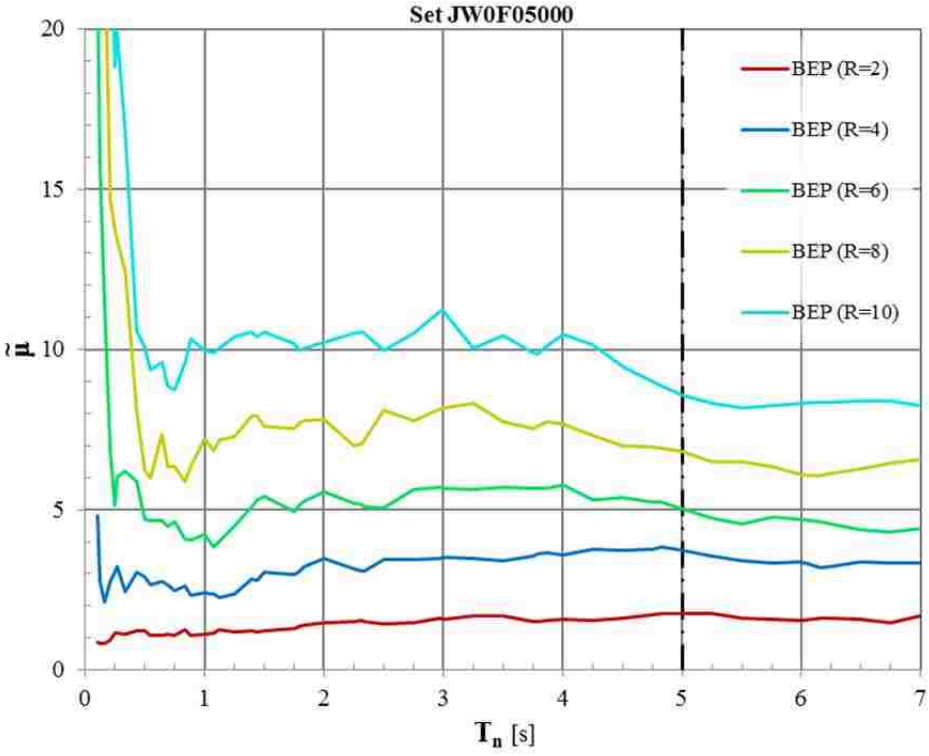
Set JW0F05000
BEP (R=2)
BEP (R=4)
BEP (R=6)
BEP (R=8)
BEP (R=10)
20
15
10
5
0
0
1
2
3
4
5
6
7
T_n [s]

APPENDIX IV VITA

Jonathan Paul Williams was born in Summit, New Jersey on August 27, 1984 to parents Linda and Raymond Williams Jr. Jonathan grew up in Westfield, New Jersey and graduated from Westfield Senior High School in June of 2002.

Jonathan completed his undergraduate studies at the Pennsylvania State University where he received his Bachelor of Architectural Engineering degree with an emphasis in building structural systems, and an Architectural Studies minor. He graduated from the Pennsylvania State University in 2008.

Following graduation Jonathan worked on a independent design-build project with a local architect where he managed the project from conceptual design through construction. In 2009 he founded Latitude Design & Research Corporation which provides consulting and professional, structural and architectural engineering services. Jonathan is a registered professional engineer in the state of New Jersey.

While growing his business Jonathan began attending Lehigh University. He will receive his Master of Science in Structural Engineering degree in September of 2017.